UNIVERSITY OF MISKOLC
FACULTY OF MECHANICAL ENGINEERING


# PROCESS CONTROL DURING LASER TRANSFORMATION HARDENING

***Ph.D. THESIS***

**REZA ROWSHAN**
*MECHANICAL ENGINEER*

Mechanical Engineering Sciences Ph.D. Program
Production Processes Subprogram
Mechanical Technology Part Program

Head of Ph.D. Program:
**DR. ISTVÁN PÁCZELT**
*Member of Hungarian Academy of Science*
*Doctor of Engineering Science*

Head of Ph.D. Subprogram:
**DR. ILLÉS DUDÁS**
*Doctor of Engineering Science*

Head of Ph.D. Part Program:
**DR. MIKLÓS TISZA**
*Doctor of Engineering Science*

Ph.D. Scientific Advisor:
**DR. MÁRIA KOCSIS BAÁN**
*Associate Professor*

Miskolc, Hungary

2007

**REZA ROWSHAN**

# Ph.D. Thesis

**MISKOLC**

**2007**

## ACKNOWLEDGEMENTS

First and foremost I would like to thank my parents for their endless love and continued support in my Master degree, as well as this advanced degree. If not for their support I would not have been able to attend the university at full-time and continue my education.

I am deeply indebted to my Ph.D. Scientific Advisor, Dr. Mária Kocsis Baán, for guiding me patiently, helping me work through my problems and spending time for the critical review of my work.

I would also like to sincerely thank Prof. Miklós Tisza for providing help throughout my studies as a Ph.D. student, his great enthusiasm and accepting me as a colleague at the Department of Mechanical Technology with continuous support.

Thanks are also extended to the Department of Mechanical Technology and the Laboratory stuff for their time and assistance in this work.

Also, I would like to thank the Bay Zoltán Institutes in Budapest and Miskolc for their great support in all the experiments we have done for my work.

My very special thanks to my wife, Orsolya Csernik, for her profound love, patience, understanding, and unconditional support throughout the development of this Dissertation. I would not have been able to complete this work without her support.

# Témavezető ajánlása

## Rowshan Reza „Process Control During Laser Transformation Hardening” című Ph.D. értekezéshez

Az anyagtudomány és az anyagtechnológiák elmúlt évtizedekben tapasztalt rendkívül dinamikus fejlődésén belül is kiemelt jelentőséggel bír a felületi illetve felületközeli rétegek szerkezetének, minőségének, s ennek révén tulajdonságainak megváltoztatására irányuló eljárások széles körének kifejlesztése és rohamos elterjedése.

A korszerű felülettudomány és felülettechnológia új és komplex szemléletmódú, interdiszciplináris szakterületté mindössze néhány évtizede formálódott: magában foglal minden mérnöki tevékenységet - a tervezéstől a gyártáson át a minőségellenőrző vizsgálatok és a felhasználás körülményeinek és következményeinek vizsgálatáig - amely a műszaki felületek optimális tulajdonságkombinációjának biztosításával az ipari termékek, szerkezeti és gépalkatrészek élettartamát, felhasználói tulajdonságait kedvezően befolyásolhatja.

A korszerű felületmódosító eljárások – a nagy energia-sűrűségű lézer és elektronsugár-technológiák, plazma-eljárások - bonyolultsága, jelentős költség-igénye, továbbá az anyag és réteg-kombinációk végtelen száma indokolja, hogy a korábbi „trial and error” módszert egyre inkább a tudatos anyag-és technológia tervezés, a folyamatok modellezése révén lehetővé váló folyamat-optimalizálás váltsa fel.

A lézeres felületedzés és bevonatolás témaköreiben a Miskolci Egyetem Gépészmérnöki Karának Mechanikai Technológiai Tanszékén közel 10 éve folyik kutatási együttműködés a BAYATI kutató intézettel, számos TDK és diplomaterv (köztük külföldi és Erasmus-ösztöndíjas hallgatók munkái) keretében elsősorban a technológiai paraméterek optimális megválasztásának sokoldalú problémáira irányulva.

Rowshan Reza a kezdetektől, diákként kapcsolódott be ebbe a kutató munkába és PhD hallgatóként, majd oktatóként, konzulensként is folyamatosan meghatározó jelentőségű, érdemi feladatokat látott el ebben. Munkáját a nagyfokú önállóság, innovativitás mellett a kiemelkedő lényeglátás és igényesség jellemzi.

Kutatásai során folyamatosan, nagy rendszerező és átfogó gondolkodásra, szintetizálásra való képességgel tanulmányozta a szakirodalmat, végzett ipari kísérleteket és továbbfejlesztette, bővítette a SYSWELD program-csomag alkalmazására épülő VEM modellezési lehetőségeket. Kezdetben az egyedi nyomvonalak lézeres felületedzése során megvalósuló hőmérséklet-eloszlás 2D és 3D-s modellezését, a rétegmélység és a technológiai paraméterek összefüggéseit vizsgálta, számításait kísérleti mérésekkel támasztva alá. A későbbiekben a hőkezelési technológiák leírásában szokásos hőfok-idő diagrammok tetszőlegesen kiválasztott pontokra érvényes adatsorait vetette össze a kezelés eredményeként létrejött szövetszerkezettel és a felületi tulajdonságokkal. Számos vonatkozásban elemezte modelljeinek helytállóságát – eltérő energia-eloszlási modellekkel, eltérő abszorpciós adatokkal végzett számításokat, eltérő anyagminőségeken, egyedi és átlapolódó nyomvonalakra. Megismerte a lézeres felületmódosítás ipari gyakorlatban való elterjedését akadályozó problémákat – az optimális paraméter-tartományok meghatározásának növekvő igényét, illetve a nem állandósult állapotok, a bonyolult geometriák okozta szabályozási bizonytalanságok és az ezekből adódó, a felületi réteg szerkezeti inhomogenitását előidéző hatások (ismételt hőhatás, elő- és túlmelegedés, megeresztődés, edző hatású hűlés elmaradása) okozta nehézségeket. Számos olyan területen is végzett modellezési feladatokat (pl. hegesztés,

keramikus anyagok kötései), amelyek, ha nem is kapcsolódtak közvetlenül PhD témájához – s így a disszertációban sem jelennek meg – bővítették látókörét, mélyítették ismereteit és fokozták kreatív gondolkodását.

Rowshan Reza rendszeresen beszámolt kutatási eredményeiről különböző nemzetközi és hazai fórumokon, rendezvényeken, eleget téve a Sályi István Gépészeti Tudományok Doktori Iskola publikációs követelményeinek.

Értekezését nagyfokú gondossággal készítette, angol nyelven. Szövegezése jól érthető, elvi megfontolásait és eredményeit megfelelő, a megértést és az áttekinthetőséget segítő illusztrációkkal támasztja alá. Tézisei a PhD cím elnyeréséhez szükséges kívánalmakat messzemenően kielégítik.

Miskolc, 2007. 02. 23.

Kocsisné dr. Baán Mária
témavezető

# CONTENTS

# ÖSSZEFOGLALÓ

Számos szerkezeti anyag tulajdonságait változtathatjuk meg előnyösen a megfelelő hőkezelési eljárás alkalmazásával. A hőkezelési módszerek közül az elmúlt évtizedekben a felületkezelés került a figyelem középpontjába, mert ez az eljárás lehetőséget kínál a stratégiailag fontos anyagokkal való takarékosságra, illetőleg differenciált, optimális felületi és tömbi tulajdonságokkal rendelkező alkatrészek létrehozására.

Edzhető ötvözetek, különösen a szénacélok, gyengén ötvözött acélok és öntöttvasak esetében a legvonzóbb lehetőségeknek a lokalizált edzési technikákat alkalmazását tekinthetjük. Ebben az esetben a teljes alkatrész hevítése helyett (ahogy azt a teljes átedzés során tesszük), csak a felületi réteget austenitesítjük és edzzük. Ezáltal a tömbi tulajdonságok, különösen a szilárdság és a szívósság, változatlanok maradnak, és az alkatrészek torzulásának lehetősége a minimálisra csökken.

A lézeres felületedzés, amely a lézersugarat hőforrásként használja - hasonlóan más lokalizált edzési eljárásokhoz, mint például a lángedzés, az indukciós edzés és az elektronsugaras edzés - az acél felületét célzottan hőkezeli egy bizonyos mélységben, amíg az eléri az ausztenitesítési hőmérsékletet, majd edző hatású hűtést alkalmaz a martenzites állapot elérése érdekében.

A lézeres felületedzés során elengedhetetlen, hogy megfelelő széntartalommal rendelkező, elegendő mennyiségű ausztenitet érjünk el a hevítés során, figyelembe véve a magas hevítési sebességet és elkerülve a felület megolvadását.

Jelen tézisben, egy végeselemes szoftvert – a SYSWELD-et – használtam numerikus eszközként arra, hogy megvizsgáljam a lézeres felületedzési eljárásokhoz kapcsolódó problémákat. Három dimenziós modelleket fejlesztettem ki az acélok egyedi nyomvonalakon történő lézeres felületedzésére, melyek révén előre jelezhetjük a hőeloszlást, a fázisátalakulásokat és az elérhető keménységet a munkadarab tetszőleges pontjaiban, tetszőleges időben.

Annak érdekében, hogy megfelelő kapcsolatot teremtsünk a bemeneti és kimeneti paraméterek között, ezen szimulációk hőmérséklet-számítási eredményeit használtam a lézeres felületedzés optimális paraméter-tartományának működési tartományainak meghatározására kvázi-statikus állapotok esetén.

Kifejlesztettem egy új optimális hőmérséklet szabályozási stratégiát a lézeres felületedzési folyamatokra a Rendszer Interfész Nyelvezet (SIL) felhasználásával a végeselemes szoftverben.

A módszer révén úgy kívánjuk szabályozni a bevitt lézerenergiát, hogy egy állandó hőmérséklet intervallumot, vagy akár egy állandó hőmérsékletet érjünk el a munkadarab bármely kijelölt pontján, tekintet nélkül a folyamat állapotára és a geometria összetettségére.

Ez a stratégia bizonyítottan megoldást jelent azon kritikus nehézségek leküzdésére, melyek a lézeres felületedzés során jelentkeznek, mint például a tranziens állapotok és a geometria összetettsége.

Nagy felületek lézersugárral történő felületedzése úgy valósítható meg, ha a felületedzett nyomvonalak átlapolódnak, ami a lézeres felületedzés problémáját még összetettebbé teszi. Egymástól különböző távolságokban levő, egymást követő lézer nyomvonalakat modelleztem azon célból, hogy az átlapolódás jelenségét nagyobb részletességgel vizsgálhassam. Számos szimuláció eredményeként a hőeloszlást és a fázisátalakulásokat elemeztem, figyelembe véve a megeresztési hatásokat és a keménység eloszlást. A keménységeloszlás eredményeinek elemzése hozzájárulhat ahhoz, hogy megtaláljuk az optimális folyamat paramétereket és a kívánt távolságot az átlapolt lézer nyomvonalak között.

# SUMMARY

The properties of many engineering materials may be favourably modified by application of a suitable heat treatment. Among heat treatment methods, surface treatment is a subject of consideration interest because it offers the chance to save strategic materials or to allow improved components with idealised surface and bulk properties.

When dealing with transformation hardenable alloys, in particular carbon steels, low alloy steels and cast irons, the option to harden using localised hardening techniques may be the most attractive. In this case, instead of heating the whole component (as in through hardening), only the surface is affected, so that the bulk properties, specifically the toughness, remain unaffected, and component distortion is minimised.

Laser Transformation Hardening (LTH) which involves the use of laser as a heat source, similarly to other localised hardening processes such as flame hardening, induction hardening and electron beam hardening, selectively heat treats the surface of the steel to a certain depth to reach austenitisation temperature and then to be quenched very rapidly to obtain martensite.

Critical factors in LTH are obtaining adequate amount of austenite with appropriate carbon content during heating, considering the high heating rate, and avoiding surface melting.

In this thesis, finite element code – SYSWELD – is used as a numerical tool to investigate the problems associated with LTH processes. Three dimensional models for single track LTH of steel have been developed that allow the prediction of the thermal distribution, phase transformations and the hardness attained at arbitrarily shaped intensity profile.

To establish appropriate relationship between the output and the input parameters, thermal results of these simulations were used to determine the LTH operating regions for quasi steady state conditions.

A new optimal temperature control strategy for LTH has been developed using System Interface Language (SIL) in the finite element code. The method is to control the input laser

energy to achieve a constant temperature interval, or even a constant temperature at any point of the workpiece.

This strategy proved to be the solution for overcoming the critical difficulties concerning LTH processes such as transient states and geometry complexities.

To harden large size surfaces by laser beam it is necessary to overlap the hardening passes that results in complexity of the LTH problem. Two successive laser tracks with different distances from each other were modelled to investigate the overlapping phenomenon in more details. Thermal distribution and phase transformation considering the tempering effects and the hardness analysis were the results of several simulations. Hardness results can assist the finding of the optimal process parameters and the required distance between overlapping laser tracks.

# LIST OF SYMBOLS

| | |
|---|---|
| $A$ | surface absorptivity |
| $A_1$ | $A_1$ temperature |
| $A_3$ | $A_3$ temperature |
| $A_{c3}$ | $A_{c3}$ temperature |
| $A_{cm}$ | $A_{cm}$ temperature |
| $A_{ij}$ | portion of phase $i$ transformed to phase $j$ in unit time |
| $a$ | thermal diffusivity ($mm^2\ s^{-1}$) |
| $b$ | constant of the martensite transformation process according to temperature |
| $\boldsymbol{C}$ | thermal inertia matrix |
| $C$ | carbon concentration, % |
| $C1$ | constant near to unity |
| $C_{HJ}$ | Hollomon and Jaffe composition dependent constant |
| $c$ | specific heat capacity ($J\ g^{-1}\ {}^oC^{-1}$) |
| $\overline{c}$ | specific heat of all phases ($J\ g^{-1}\ {}^oC^{-1}$) |
| $c_i$ | specific heat of phase $i$ ($J\ g^{-1}\ {}^oC^{-1}$) |
| $d$ | workpiece thickness (mm) |
| $e$ | natural constant |
| $F$ | heating and cooling rate as a functions of temperature ($^oC\ s^{-1}$) |
| $F'$ | heating and cooling rate as a functions of temperature ($^oC\ s^{-1}$) |
| $f_i$ | accumulation terms |
| $\overline{H}$ | enthalpy of all phases ($J\ kg^{-1}$) |
| $H_i$ | enthalpy of phase $i$ ($J\ kg^{-1}$) |
| $HV$ | Vickers hardness |
| $HV_{bainite}$ | Vickers hardness of bainite phase |

| | |
|---|---|
| $HV_{ferrite}$ | Vickers hardness of ferrite phase |
| $HV_i$ | Vickers hardness of a tempered structure at time $t_i$ |
| $HV_{martensite}$ | Vickers hardness of martensite phase |
| $HV_t$ | instantaneous Vickers hardness after tempering |
| $HV_{tempered}$ | Vickers hardness of tempered martensite |
| $HV_0$ | Vickers hardness of quenched martensite |
| $HV_{100}$ | Vickers hardness of 100% tempered martensite |
| $\boldsymbol{K}$ | thermal conductivity matrix |
| $k$ | thermal conductivity (W mm$^{-1}$ $^{o}$C$^{-1}$) |
| $\bar{k}$ | thermal conductivity of all phases (W mm$^{-1}$ $^{o}$C$^{-1}$) |
| $k_i$ | thermal conductivity of phase $i$ (W mm$^{-1}$ $^{o}$C$^{-1}$) |
| $K_{i\rightarrow j}$ | constants of reaction $i \rightarrow j$ |
| $K'_{i\rightarrow j}$ | constants of reaction $i \rightarrow j$ |
| $L_{ij}$ | latent heat of transformation |
| $M_f$ | martensite finish temperature ($^{o}$C) |
| $M_s$ | martensite start temperature ($^{o}$C) |
| $P$ | power (W) |
| $p$ | metallurgical phase proportion |
| $\bar{p}$ | phase proportion at equilibrium |
| $p_{eq}$ | phase proportion at equilibrium |
| $p_g$ | generalised time-temperature parameter |
| $p_{HJ}$ | Hollomon and Jaffe tempering parameter |
| $p_i$ | proportion of phase $i$ |
| $p^m$ | martensite phase proportion |
| $p_{tempered}$ | tempered structure proportion |
| $\dot{p}^m$ | martensite phase proportion as a function of time |
| $q$ | heat flux density (W mm$^{-2}$) |
| $q_c$ | convection heat flux (W mm$^{-2}$) |
| $q_G$ | Gaussian heat flux density (W mm$^{-2}$) |
| $q_0$ | maximum heat flux density (W mm$^{-2}$) |
| $q_{0new}$ | the new calculated maximum heat flux density (W mm$^{-2}$) |
| $\dot{Q}$ | rate energy per unit time (J s$^{-1}$ mm$^{-3}$) |
| $R$ (mm) | distance from a point of interest to heat source (thick plate case) |
| $r_b$ | beam radius (mm) |
| $r_i$ | segmental moving heat source radii (mm) |
| $r_0$ | Gaussian radius (mm) |
| $r'$ | distance from a point of interest to heat source (thin plate case) (mm) |
| $\boldsymbol{T}$ | table containing all the nodal temperatures |
| $T$ | temperature ($^{o}$C) |
| $T_{constant}$ | constant temperature ($^{o}$C) |
| $T_{max}$ | maximum temperature ($^{o}$C) |
| $T_p$ | peak temperature ($^{o}$C) |
| $TR$ | time delay (s) |
| $T_0$ | ambient temperature ($^{o}$C) |

| | |
|---|---|
| $T^0$ | prescribed initial temperature ($^oC$) |
| $\dot{T}$ | heating or cooling rate ($^oC\ s^{-1}$) |
| $\Delta T$ | allowable temperature deviation ($^oC$) |
| $t_b$ | time over which energy is injected at a point on surface (s) |
| $t_0$ | time taken for heat to diffuse over the source half width (s) |
| $v$ | velocity of heat source (mm $s^{-1}$) |
| $V$ | volume ($mm^3$) |
| $V_R$ | cooling rate in hardness calculations ($^oC\ s^{-1}$) |
| $x'$ | distance from a point of interest to heat source as a result of coordinate transformation (mm) |
| $x, y, z$ | rectangular coordinates fixed at workpiece (mm) |
| $\beta$ | convective heat transfer coefficient (W $mm^{-2}\ ^oC$) |
| $\Delta t$ | time interval between two temperatures (s) |
| $\delta$ | Stefan-Boltzmann constant |
| $\varepsilon$ | surface emissivity |
| $\rho$ | density (g $mm^{-3}$) |
| $\overline{\rho}$ | density of all phases (g $mm^{-3}$) |
| $\rho_i$ | density of phase $i$ (g $mm^{-3}$) |
| $\rho c$ | volume heat capacity (J $mm^{-3}\ ^oC^{-1}$) |
| $\tau$ | delay time as a function of temperature (s) |
| $\vartheta$ | local balances of the outgoing and incoming thermal flows in the volume element |
| $\psi$ | table containing all the residual nodal powers |

# 1. PREFACE

## 1.1 Introduction

To improve the surface properties of metallic engineering parts, several thermal surface treatment methods are available. Laser Transformation Hardening (LTH) is a method of producing hard, wear resistant patterns on discrete surface regions of components.

The use of lasers in the heat treatment of metals was first reported in Germany in the early 1960s [1] and followed some years later in the Russian literature [2]. In the mid 1960s researchers at US Steel [3] and in Japan [4] studied laser induced austenitisation and hardening of ferrous alloys. The first mathematical models of the heat flow during processing provided greater insight into the role of the process variables in determining the thermal cycle induced [5] and the geometry of the hardened region [6].

Although LTH was one of the first methods of laser based materials engineering to be industrialised, the process has never been exploited to its full potential. The reasons lie in a lack of knowledge concerning the process, the large number of more familiar surface hardening processes that are commercially available [7] and the high instruments cost. Extreme heating and cooling rates make this process to be considered as a complex engineering task. Recent important developments in the technology of the laser source, optics and software enable the process to be viewed more favourably against competing processes.

Finite element method as a numerical method and induced mathematical tool can describe most essential parts of the process. This technique can be suitable for finding the optimal process parameters for treating components of widely varying size and shape.

## 1.2 Overview of the Thesis

In Chapter 2 industrial laser machines and their different application fields are briefly introduced. Laser surface treatments are classified and laser transformation hardening is discussed in more details. Applications of LTH are described at the end of this chapter.

Theory of heat flow by deriving the analytical solutions taken from literature and introducing the numerical methods are demonstrated in Chapter 3.

Chapter 4 starts with discussion of the SYSWELD code's theoretical background. Input data of material for thermal and phase transformations calculations, and the methods of parameter fixing are illustrated in this chapter. Single track LTH processes are modelled and at the end the operating regions for quasi steady state conditions are shown.

The developed optimal control strategy for laser transformation hardening using System Interface Language (SIL) is contributed in Chapter 5. The applications of this strategy in different fields are discussed using finite element modelling examples. In this chapter the aim is to find the optimal process parameters of single track LTH for critical cases such as transient states and complex geometries.

The effects of the overlapping phenomenon on the microstructure of steels have been studied in Chapter 6. Numerical modelling of tempering and the method of data extraction needed as input parameters are demonstrated and controlled by experimental results. Finite element modelling of multi pass LTH, taking the tempering effects into consideration, has been established. Hardness distribution results show that the model is well dedicated to solve overlapping problems in LTH.

# 2. LASER TRANSFORMATION HARDENING: STATE OF THE ART

## 2.1 Introduction

Laser is the acronym of Light Amplification by Stimulated Emission of Radiation. The laser light is set to be coherent, highly monochromatic, and parallel. The parallelism, or low divergence, however, is what makes material processing possible. Since a parallel beam can be focused on a small spot, concentrating all the power of the beam on that spot. These characteristics of the laser light give the laser a unique feature, capable of applying it in various engineering fields.

The privilege of concentrating the power enhanced the laser beam application in various production processes such as cutting, drilling, welding and soldering, as well as heat treatment of surface layers (*Figure 2.1*).

The materials processing by laser are governed by $CO_2$, Nd:YAG and Excimer lasers. The $CO_2$ laser operates by electric excitation of an active lasing medium consisting of a mixture of helium, nitrogen and carbon dioxide. The $CO_2$ lasers have a wavelength of *10.6 μm*, and are available with powers up to *45 kW* [8], and can operate in either pulsed or continuous wave mode.

Such features promote the $CO_2$ lasers to play an important role in the industrial field, for example in cutting, welding and heat treatment of steels.

The Nd:YAG laser which stands for neodymium yttrium aluminium garnet is built up of rare ions that have sets of energy levels making them strong laser media. These energy levels are transitions in inner electron shells, allowing the Nd:YAG laser to operate in either pulsed

or continuous wave modes. In case of pulsed Nd:YAG, it contains flash lamps, while continuous wave Nd:YAG use continuous arc lamps. This laser emits in the near infrared light at 1.06 μm wavelength. In material processing, the Nd:YAG is used for welding, drilling, cutting [9] and surface treatment.

The Excimer laser is an electrically excited gas laser. The word Excimer is an abbreviation of the word "excited dimmer" which is an excited medium, composed of inert gas and a halogen in the laser resonant cavity such as argon with halogens like fluorine, having a wavelength range from *0.193* to *0.348 μm*. They only operate in a pulse mode that has a short duration of *0.01-0.5 μs*, and a peak power reaching up to *100 kW*. The Excimer processing is used to increase surface roughness in order to improve the adhesion properties or surface absorptivity, and is also used in surface treatment [10].

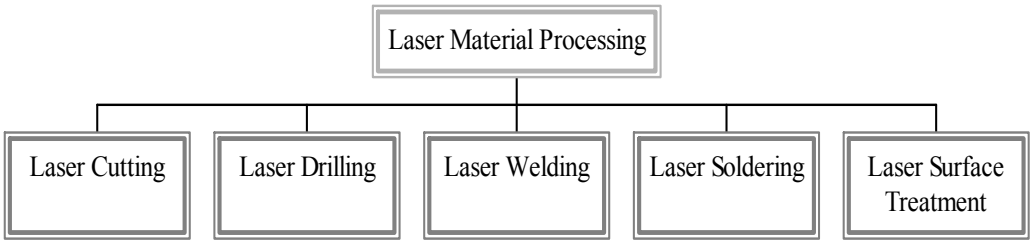


*Figure 2.1 Laser materials processing technologies*

The ability to achieve power densities up to $10^6$ *W/cm*$^2$ enables high power lasers to be applied within a variety of applications in several industrial sectors. In *Figure 2.2*, the beam parameters are combined to form power density and beam interaction time, so that the practical operating regimes for various types of laser processing can be defined [11].

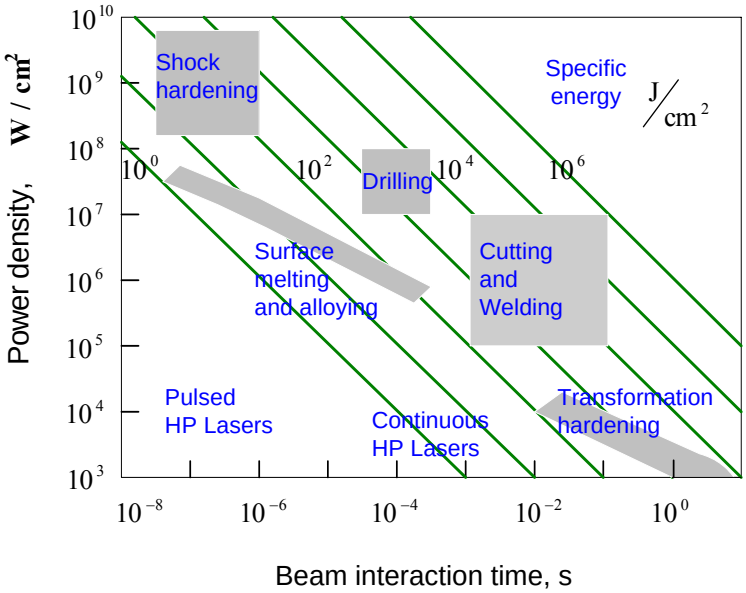


*Figure 2.2 Operating regimes for various methods of laser material processing* [11]

## 2.2 Laser Surface Treatments

High power lasers provide a source of energy, hence a method of heating materials, which can be accurately controlled. The development and industrial application of lasers in materials processing such as drilling, cutting and welding have progressed rapidly.

With the continuous laser of high output, surface treatment technology is rapidly growing with the identification of new and improved processing methods. Nowadays, surface treatment is a subject of consideration interest because it offers the chance to save strategic materials or to allow improved components with idealised surface and bulk properties.

The basic physics of laser surface treatment is simply heat generation by laser interaction with the surface of an absorbing material and subsequent cooling either by heat conduction into the interior, or by thermal radiation at high temperatures from the surface of the material. It belongs to the group of short time hardening processes which are characterised by the extremely rapid heating and cooling. Laser surface treatments can be subdivided into those which make modification via heating the surface without melting and those with melting the surface of the materials. Further classification of laser surface treatments is shown in *Figure 2.3*.

Advantages of laser heat treatment can be categorised from different points of view:

- considering limited energy consumption and its consequences:
  - savings in energy compared to conventional surface heat treatment procedures as heating is restricted to only a shallow layer of a small volume, localised only to the required area;
  - due to minimal energy input, small deformations and/or dimensional changes of the workpiece after heat treatment;
  - no need for or minimal final machining of the parts by grinding;
- considering environmental aspects:
  - hardened surface is achieved due to self-quenching of the overheated surface layer through heat conduction into the cold bulk of the material;
  - since heat treatment is done without any agents for quenching, the procedure is a clean one with no need to clean and wash the workpiece after heat treatment;
- considering flexibility and productivity of the process:
  - the energy input can be adapted over a wide range by changing laser source power, with focusing lenses having different focuses, or different degrees of defocus (the position of the lens focus with respect to the workpiece and/or laser beam);
  - capability of switching the laser beam between workstations by simple optical devices at atmospheric environment;
  - the optical system can be adapted to the shape or complexity of the product by means of different shapes of lenses and mirrors;
  - it is possible to heat-treat extremely small or large parts with complex shapes including small bores as well as treating inaccessible areas;
  - the directing of the beam over the workpiece surface is made with computer support;
  - laser heat treatment is convenient for individual or mass production of parts;
  - reproducibility and reliability of quality of the treated surface layer with accurately controlled depth and width of the layer;
  - high level of suitability for production line incorporation and automation of the procedure.

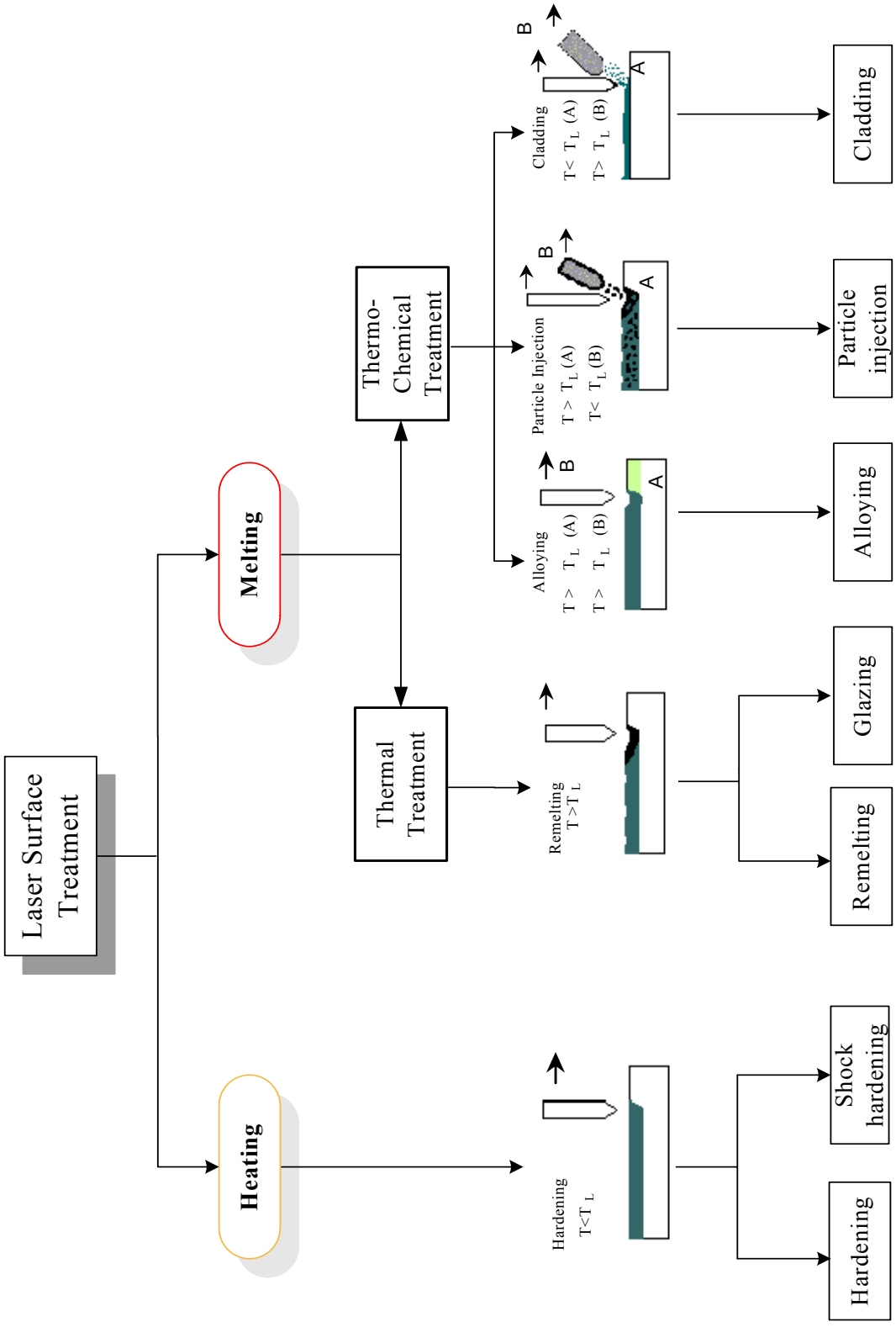


*Figure 2.3 Classification of laser surface treatments*

The use of laser for heat treatment can have the following difficulties:

- non homogeneous energy distribution in the laser beam;
- very narrow temperature field ensuring the aimed microstructural changes;
- adjustment of kinematics conditions of the workpiece and/or laser beam to different product shapes;
- poor absorptivity of the laser light in interacting with the metallic material surface.

## 2.3 Laser Transformation Hardening (LTH)

In laser transformation hardening, which involves using a laser as a heat source, the beam energy is applied to harden a surface with the rest of the component acting as a heat sink avoiding surface melting. Laser transformation hardening similar to other localised hardening processes such as flame hardening, induction hardening and electron beam hardening, selectively heat treats the surface of the steel to reach austenitisation temperature to the required depth and then quenched very rapidly to obtain martensite. These processes are usually applicable if it is not required to harden an entire part, the reason is that wear or high stress is localised, hence only well defined small areas need to be hard. Also it is advantageous to have most of a component tough and ductile, whereas martensite is very hard and brittle.

Laser transformation hardening competes with many established methods of surface treatment. This is one reason why its uptake has been relatively slow: a very good technical and economic case must be made before an existing process is replaced. *Table 2.1* summarises the principal features of laser hardening and its competing techniques. The advantages and drawbacks of laser hardening can best be summarised by comparing the process with these competing techniques [7].

*Table 2.1 Comparison of LTH with competing methods of hardening*

| **Parameter** | **Laser** | **Induction Hardening** | **Carburising** | **Flame** | **Electron beam** |
|---|---|---|---|---|---|
| **Max. treatment depth, mm** | 1.5 | 5 | 3 | 10 | 1 |
| **Distortion** | Very low | Medium | Medium | High | Very low |
| **Flexibility** | High | Low | Medium | High | Medium |
| **Precision** | High | Medium | Medium | Low | High |
| **Operator skill** | Medium | Medium | Medium | High | Medium |
| **Environment impact** | Low | Low | High | Medium | Low |
| **Quenchant required** | No | mostly | Yes | Yes | No |
| **Material flexibility** | High | Medium | Low | Medium | High |

## 2.4 Mechanism of Laser Transformation Hardening

The hardening of steel is due to the temperature dependent transformation of the crystal structure of iron and changes in carbon solubility, associated with these transformations. In surface hardening, however, the heating period and the holding, if there is any, of the process cycle is much shorter than those of bulk hardening. This is particularly true for laser

transformation hardening where heating to the austenitisation temperature occurs within seconds or even fractions of a second.

The four most important criteria for LTH can be summarised as:

- The temperature for the zone being hardened must reach well into austenitisation zone.
- Between the heating and cooling cycle, the substrate should be maintained at the austenitisation temperature long enough for carbon diffusion.
- There should be enough mass ratios between the treated layer and the bulk so that the cooling rate by self quenching is such that it could satisfy the critical quenching rate requirement.
- Surface of the workpiece heated by laser beam should not reach the melting temperature.

The phase transformation induced by LTH for steels take the following steps:

- Formation of austenite from pearlite-ferrite (hypoeutectoid steels) or pearlite-cementite (hypereutectoid steels) aggregate structure,
- Martensite transformation from austenite.

### 2.4.1 Austenite Formation Mechanism

The basic reaction taking place during the heating period of steel by laser, is the phase transformation of the bcc $\alpha$-solid solution to fcc $\gamma$- solid solution. This occurs by nucleation and growth of the new phase in the matrix of the initial phase. In slow heating, under equilibrium circumstances the process will start at $A_1$ (*723 °C*) temperature in a carbon steel and will be complete at the $A_3$ ($A_{cm}$) line. However when the heating rate is high, the system is far from equilibrium condition and the $A_{c3}$ line will tend to be displaced upward to higher temperatures (*Figure 2.4*).

The high heating rates associated with LTH, combined with the need to allow sufficient time above $A_{c3}$ line to form homogeneous austenite, necessitate high peak temperature. Therefore LTH parameters are usually designed to give peak temperatures well above those employed in conventional hardening to ensure austenitisation, but not high enough to initiate surface melting.

The relatively short period, in which the temperature of the layer is above austenitisation temperature, can lead to incomplete austenitisation as the time for carbon diffusion may be insufficient. Therefore the carbon distribution in the substrate has an essential influence on the generated spatial distribution of microstructures and the resulting hardening profiles.

In general terms, the transformation process from the pearlite-ferrite (or cementite) aggregate to austenite (starting at $A_{c1}$ temperature) occurs in the following four stages:

*Stage 1*: The initial microstructure remains untransformed. During this period embryos for austenite nuclei are formed.

*Stage 2*: Austenite nuclei occur at the interface between ferrite and cementite, simultaneously growing into both ferrite and carbide.

*Stage 3*: Residual carbides dissolve during this period.

*Stage 4*: Carbon atoms diffuse further in the austenite, until homogeneous distribution of equilibrium carbon content is achieved.

It is clear that austenite nuclei must have an approximately eutectoid composition when they are formed just above the $A_1$ temperature. They must also form at a cementite-ferrite interface. Here austenitic embryos readily acquire carbon atoms, to become austenite nuclei.

After austenite nuclei form at the ferrite-cementite interface, two new interfaces (austenite-ferrite and austenite-cementite) occur. The process of austenitic growth is such that the austenite-ferrite and austenite-cementite interfaces move respectively into the ferrite and the cementite. The rate of austenite growth will depend on the rate of solution of carbide and ferrite, and also the rate of diffusion of the carbon atoms in the austenite.

The difference of the carbon concentration in austenite and ferrite at their interface is much less than at the austenite-cementite interface. The rate of austenite growth towards ferrite greatly exceeds the rate of growth towards cementite. Hence ferrite always disappears before cementite, for austenitisation of the eutectoid steel. At the instant when the ferrite disappears, the residual carbide still exits, and this continues to dissolve further in austenite. Furthermore, when the residual carbide has dissolved completely, the distribution of carbon in austenite is not homogeneous. The carbon concentration at cementite sites exceeds the carbon concentration at ferrite sites. Subsequently the distribution of carbon atoms in the austenite becomes increasingly homogeneous, by the diffusion of carbon atoms.

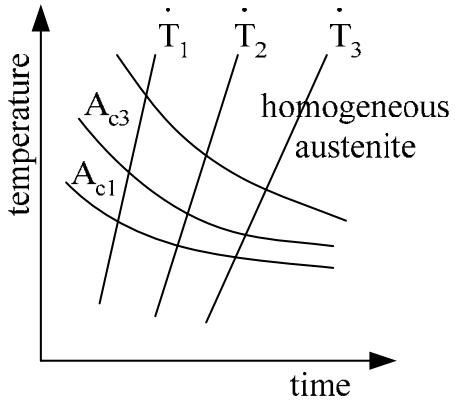


*Figure 2.4 Austenitisation diagram of a hypoeutectic steel*

The factors which affect austenite transformation can be summarised as follows:

*Temperature*: Both nucleation and growth rates increase with increasing temperature. Larger temperatures lead to an earlier disappearance of ferrite and also to a high volume fraction of residual carbide and a lower average concentration of carbon in austenite at the instant when ferrite disappears.

*Carbon content in steels:* An increase in carbon content in steels leads to an increase in the rate of austenite growth. When the carbon content is higher, the time needed for the ferrite to disappear becomes smaller and the time needed for dissolution of carbide becomes larger.

*Initial metallographic structure:* Austenitisation is strongly dependent on the shape and distribution of carbide in the initial structure. Fine carbides produce ferrite-carbide interfaces with large surface area. This increases the opportunity for nucleus formation. Hence lamellar and needle-shape carbides yield more rapid austenitisation than is obtained with nodular carbides.

### 2.4.2 Martensite Formation Mechanism

Martensitic transformation is a diffusionless $\gamma \rightarrow \alpha$ transformation which results in single phase martensite. The major step of the transformation of austenite to martensite is the rearrangement of the γ-lattice into the α-lattice. Considering that the martensitic transformation occurs without diffusion with extremely rapid cooling, the carbon atoms solved in the γ-austenite can not precipitate, that is they remain in the transforming lattice, which results in an oversaturated solid solution. It also leads to significant deformation of the lattice. This deformation is greater in the direction of one of the axes than in the other two directions. This distorts the lattice of martensite to a tetragonal lattice. The great lattice deformation caused by the excess carbon atoms in the martensite lattice results in the great hardness of the martensitic microstructure. This lattice distortion leads to high lattice stresses, providing the theoretical background for martensitic hardening, which results in the greatest hardness of the steels [12].

Therefore, martensite is a non equilibrium phase that forms when the cooling rate is fast enough to avoid the formation of pearlite and bainite. Considering the continues cooling curve of a steel, martensite can form at cooling rates faster than the lower critical cooling rate of the steel.

In LTH generally the cooling rates obtained from heat conduction into the substrate are high enough for martensite transformation even for steels with lower carbon content.

## 2.5 Applicability of Laser Transformation Hardening

### 2.5.1 Suitable Materials for Laser Transformation Hardening

Ferrous alloys, such as carbon–manganese, low alloy, tool, and martensitic stainless steels and cast irons are particularly suitable for laser hardening [7].

Low Carbon Steels (0.08% to 0.30% carbon) - Very rapid quenching is required to form martensite in low carbon steel. A shallow case depth of up to 0.5 mm can be achieved. The maximum hardness which can be reached is dependent upon the carbon content percentage in the steel.

Medium and High Carbon Steels (0.35% to 0.80% carbon) - These materials are better choices than low carbon steel because the higher the carbon content is, the higher can be the martensitic hardness. The maximum case depth without use of a water quench is around *1.0 mm*.

Alloy Steels - This is the most desirable type of steel to be used in the LTH process. The alloy elements – especially manganese, molybdenum, boron and chrome – aid in hardenability. These steels can be heat treated up to a 3 mm case depth and the maximum hardness, which can be achieved, is dependent upon the carbon content.

Tool Steels - These can also be treated easily by the LTH process. Results are similar to those achieved with alloy steels.

Martensitic Stainless Steel - Martensitic stainless steel can also be treated by the laser process. Though its microstructure does not readily display the hardened region, microhardness measurements clearly indicate high hardness.

In *Table 2.2* hardness values obtained by LTH of range of steels are given.

*Table 2.2 Surface hardness of laser transformation hardened steels* [7]

| STEEL TYPE | GRADE | C CONTENT WT % | HARDNESS, HV | REFERENCE |
|---|---|---|---|---|
| **Hypoeutectoid C-Mn** | AISI 1045 | 0.45 | 700 | [13] [14] |
| | AISI 1045 | 0.45 | 656 | [14] |
| | C 45 | 0.46 | 700 | [15] |
| | C60 | 0.62 | 875 | [15] |
| **Medium alloy** | 90 Mn Cr V 8 | 0.90 | 1000* | [15] |
| | 100 Cr 6 | 0.95 | 1000* | [15] |
| | X100CrMoV51 | 1.00 | 750 | [14] |
| **High alloy** | X155CrVMo121 | 1.55 | 850 | [15] |
| | X210Cr 12 | 2.09 | 950 | [15] |
| **Martensitic stainless** | AISI 440 | 0.61 | 585 | [16] |
| | AISI 410 | 0.12 | 560 | [17] |
| | AISI 410 | 0.23 | 560 | [18] |
| * Quenched in liquid nitrogen | | | | |

Pearlitic Cast Iron - All cast irons with pearlitic structures can be hardened by laser. The amount of pearlite present in cast irons determines their response to laser hardening. The greater the amount of pearlite is, the higher the hardenability becomes. Typical hardness values obtained after laser hardening are given in *Table 2.3*. Variations in composition and thermal conductivity also affect the response of cast irons to hardening. A high thermal conductivity means that the surface temperature remains relatively low, and surface melting is less likely. In contrast, high carbon content lowers the melting temperature, which limits the depth of hardening that can be achieved before surface melting occurs.

*Table 2.3 Surface hardness of transformation hardened cast irons* [7]

| CAST IRON TYPE | GRADE | HARDNESS, HV | REFERENCE |
|---|---|---|---|
| **Pearlitic grey** | ASTM 40 | 1000 | [19] [20] |
| | ASTM 40 | 700 | [21] |
| | Grade 17 GC | 850 | [22] |
| **Austenitic grey** | GGL 25 | 530 | [23] |
| **Pearlitic nodular** | GGG 60 | 950 | [24] |
| | GGG 40 | 650 | [24] |
| **Ferritic pearlitic (nodular)** | ASTM 80-55-06 | 960 | [19] [25] |
| | FCD 45A | 900 | [26] |
| **Alloyed** | Cr-Mo Alloyed | 900 | [24] |

## 2.5.2 Industrial Application of Laser Transformation Hardening

Laser hardening was introduced on an industrial scale in 1973. The automotive industry was among the first mass-production industries to exploit lasers for surface treatment. Laser heat treating was preferred because of low distortion, selective hardening and uniform shallow case depths. The advantage of reduced power requirement on shifting from furnace hardening to localized laser hardening proved very attractive to energy conscious industries [27]. Here some examples of industrial application of laser transformation hardening are introduced.

Increased front-end loads in cars due to addition of other equipment such as air-conditioning systems, pollution control devices and energy absorbing bumpers necessitated improving wear characteristics at the top and bottom of the bore. The laser makes a striped pattern with chosen width and depth corresponding to pre-determined regions of maximum mechanical stresses [28].

Chang [29] has established the technique of laser hardening of exhaust valves and valve guides for enhancing wear resistance. The use of unleaded gasoline has led to severe wear problems in exhaust valve seats and guides. The valve seat was hardened using a *2 kW* $CO_2$ laser to achieve a hardness of *55-60 HRC*, and the hardened depth was *0.5* to *0.76 mm*. Wear studies revealed that the wear rate of a laser hardened valve seat was reduced four times compared to that of an induction hardened valve seat. Distortion induced was three times less. The exhaust valve guide hardening was performed using a low power $CO_2$ laser of 400 W with a rotating copper mirror. The hardness achieved was in the range of *55-60 HRC* with a significantly reduced wear rate of around twelve times less than the unhardened valve guide.

In the case of surface hardening of gears, gear teeth flanks are usually hardened to increase their resistance to wear and fatigue. The thickness of the hardened layer should be such that it withstands the maximum contact stress without collapsing into the softer interior of the gear tooth. An excessive hardened depth will leave the tooth too brittle to withstand tensile stresses. The exact required value of case depth depends on the gear tooth form and the load. No hardening is required along the top of the tooth. The hardened area at the root of the tooth increases the fatigue resistance of the gear by forming compressive stresses, which offset the tensile stresses applied in service [30].

Carburized steel gears used in helicopters and other aircrafts are critical components. These high performance gears in helicopters operate under higher loads, speeds and surface temperatures than most industrial gears and are very much prone to pitting, scoring and tooth bending fatigue. The steels used for such gears have very high alloy contents and hence traditional or vacuum carburizing is not effective. For such steels, laser surface hardening is very effective in imparting the required properties for this high performance application.

Diesel engine crankshafts, pistons, gears, parking brake ratchets, valve seats and guides, truck axles, rocker arms and camshafts are typical applications where laser hardening could be employed [31].

In the automotive sector, quality is a very important factor in a customer's decision for a new vehicle. With respect to power train, quality indicates high fuel efficiency increased durability, smooth operation, low emission and low maintenance costs. In order to provide high quality the use of sophisticated surface modification in the production of power train components is required. In this respect the crankshaft is an excellent candidate for the application of laser hardening. High accuracy and increased lifetime are requirements of crankshafts. In a project conducted by Gassman et al. [32] on transformation hardening of bearings, the radii between the bearings and webs and a groove at the crankshaft journal were investigated using $CO_2$ and Nd:YAG laser radiation. The hardening of the bearing was done to increase wear resistance and laser treatment of the radii and the groove was aimed at increase fatigue resistance.

The gear box selector forks should have a hard and wear resistant surface for sliding contact between synchromesh gears but the bulk material, made of pearlitic, malleable iron should retain its ductility. Holtom [33] has given details of surface hardening of selector forks by a *2 kW* $CO_2$ laser at a company in U.K. In Europe, Fiat of Italy has laser hardening cylinder blocks and other engine components with *12 kW* $CO_2$ lasers [34].

Another example of laser heat treatment is hardening of piston ring groves, developed by Yanmar Diesel Engine Co. Ltd, Japan [35]. In a diesel engine, the abrasive wear created by a hard carbon deposit between the piston ring and the piston ring groove side face is a source of concern. Conventionally, the ductile cast iron pistons with a ring groove width of more than *5 mm* were treated by induction hardening. At Nippon steel in Japan, laser hardening was developed to anneal a very shallow layer approximately *3* micron on thin steel wire used for reinforcement of radial tires for cars. The purpose was to increase the bending strength [36].

Belev et al. [37] have studied the surface hardness and wear resistance of roll surfaces hardened by a high power dynamic laser and found an increase in hardness from *70 HRC* to *80-85 HRC* with considerable increase in wear resistance. Divinskii et al. [38] have studied the laser hardening of tractor-engine components. They have presented the operational regimes and the optical arrangement for the processing of damper components (disk, cover and rim) by using an industrial laser unit.

# 3. THEORY OF HEAT FLOW EQUATIONS

## 3.1 Introduction

The changes in microstructure and hence properties which occur when a heat source is applied to the surface of a solid material, depend strongly upon the thermal cycles experienced by each point within the material. Consequently a great deal of attention has been paid to making good predictive analysis, using both analytical and numerical methods, for a variety of different heat flow problems.

In this chapter, various theoretical analyses of heat flows in materials for moving heat source are reviewed.

## 3.2 Heat Flow Equations

The time dependent partial differential equation for transient heat flow in a three-dimensional solid in the Cartesian coordinate system (*x, y, z*) can be expressed as:

$$\nabla\left(k\nabla T\right)+\dot{Q}\{x,y,z,t\}=\rho c\frac{\partial T}{\partial t}, \qquad \textit{Eq. 3.1}$$

where $k$ is thermal conductivity, $T$ is temperature, $\dot{Q}$ is the rate of energy generation per unit time, $t$ is time, $\rho$ is the density and $c$ is the specific heat capacity.

For steady state condition, when all material parameters are considered to be constant and assuming that the materials are homogeneous and isotropic, heat flow equation can thus be simplified and written as:

$$\nabla^2 T+\frac{1}{k}\dot{Q}\{x,y,z,t\}=\frac{1}{a}\frac{\partial T}{\partial t}, \qquad \textit{Eq. 3.2}$$

where the parameter *a* is the thermal diffusivity and defined according to

$$a = \frac{k}{\rho c}. \qquad \textit{Eq. 3.3}$$

In most problems that occur in the theory of material processing, there is no additional heat input. The reminder of the workpiece acts as a heat sink and the value far from the origin is expected to tend to $T_0$, as in the case of cooling when $\dot{Q}\{x,y,z,t\}$ is zero, the *Eq. 3.2* further reduces to

$$\nabla^2 T = \frac{1}{a}\frac{\partial T}{\partial t}. \qquad \textit{Eq. 3.4}$$

## 3.3 Analytical Solutions of Heat Flow Equations for Moving Heat Sources

Rosenthal [39] adopted the quasi stationary state concept, in which if it is assumed that the workpiece is in steady motion parallel to the *x*-axis with velocity *v* and that all the material parameters are constant, the equation of heat conduction for the temperature *T* takes the relatively simple form

$$\nabla^2 T = \frac{v}{a}\frac{\partial T}{\partial x}. \qquad \textit{Eq. 3.5}$$

The point source model is a special solution of *Eq. 3.5*. The point source having power of *P* on the surface of a semi-infinite workpiece (see *Figure 3.1*), of which temperature is far away from $T_0$, gives rise to a temperature distribution given by

$$T = T_0 + \frac{AP}{2\pi kR} exp\left\{\frac{v}{2a}(x' - R)\right\}. \qquad \textit{Eq. 3.6a}$$

This equation is often referred to Rosenthal thick plate solution. *A* is the surface absorptivity of the workpiece and

$$R = \sqrt{x'^2 + y^2 + z^2} \qquad \textit{Eq. 3.6b}$$

where $x'$ is the result of coordinate transformation

$$x' = x - vt. \qquad \textit{Eq. 3.6c}$$

A restriction has to be made to *R* in *Eq. 3.6a*. If the physical state of the plate would undergo no change in the immediate vicinity of the heat source then *Eq. 3.6a* would give $T = \infty$ for $R = 0$, which is impossible. A closer approximation would be necessary in order to take the finite size of the heat source into account.

For a thin plate of a thickness *d*, the approximate solution is

$$T = T_0 + \frac{AP}{\sqrt{4\pi k\rho cvr'}\cdot d} exp\left\{\frac{v}{2a}(x' - r')\right\}, \qquad \textit{Eq. 3.7a}$$

where

$$r' = \sqrt{x'^2 + y^2}. \qquad \textit{Eq. 3.7b}$$

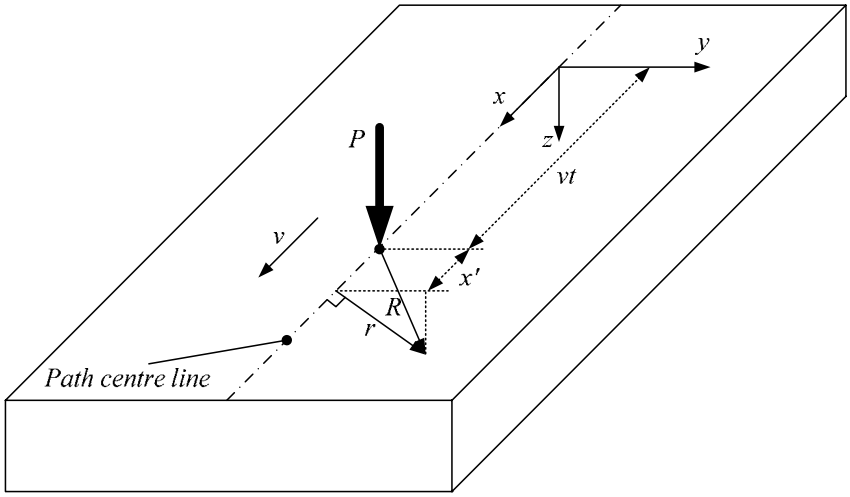


*Figure 3.1 Point source on the surface of a semi infinite workpiece*

The point source solution can be very useful in the construction of solutions to problems in which there is a specified incident intensity distribution. Point source solution can be used with specially shaped simple distributions of surface intensity.

Ion [40] approximated Rosenthal's solution by considering a fixed point in the *yz* plane ($x = 0$) and setting $x' = -vt$. Assuming that $r << vt$, for the point considered to be the distance from the path centre line is compared with the one moved by the heat source in unit time, the limiting solution for thick plate with instantaneous application of heat is

$$T = T_0 + \frac{AP}{2\pi kvt} exp\left\{-\frac{r^2}{4at}\right\}. \qquad \textit{Eq. 3.8}$$

The solution for a thin plate is

$$T = T_0 + \frac{AP}{vd\sqrt{4\pi k\rho ct}} exp\left\{-\frac{r^2}{4at}\right\}. \qquad \textit{Eq. 3.9}$$

The product $\rho c$ is the volume heat capacity ($J / m^3 K$) and the variable *r* is defined as the distance from the point of interest to the path centre line so that $r = \sqrt{y^2 + z^2}$.

The other special solution of the *Eq. 3.5* is the so called line source solution. Rykalin [41] modified Rosenthal's analysis by assuming that the heat is delivered from a line source. The line source solution can be obtained essentially in the same way as the point source. The differences are that the heat source has finite width in the *y* direction and it is infinitesimally thin in the *x* direction and the heat source moves along the *x* direction with high speed.

The modified solution for the temperature field in a semi-infinite, or in other words, thick plate case is:

$$T = T_0 + \frac{AP}{2\pi kv\sqrt{t(t+t_0)}} \exp\left\{-\frac{1}{4a}\left[\frac{z^2}{t} + \frac{y^2}{(t+t_0)}\right]\right\}, \qquad \textit{Eq. 3.10}$$

where

$$t_0 = \frac{r_b^2}{4a}. \qquad \textit{Eq. 3.11}$$

Here $t_0$ is the interaction time, the time taken for the heat to diffuse over the heat source half width $r_b$.

To overcome the infinite surface temperature caused by point and line source assumption, Ashby and Easterling [42] considered the width of the beam in both *x* and *y* directions. If the beam has radius $r_b$, the energy is injected at a given point on the surface over a time

$$t_b = C_1 \frac{r_b}{v}, \qquad \textit{Eq. 3.12}$$

where $C_1$ is a constant near unity. Heat diffuses inwards during this injection time, draining heat away from the surface, thereby limiting the surface temperature to a finite value. This can be allowed by replacing the real source in the plane $z = 0$ by an apparent source in the plane $z = z_0$ above the surface, so that

$$T = T_0 + \frac{AP}{2\pi k v \sqrt{t(t+t_0)}} \exp\left\{ -\frac{1}{4a}\left[ \frac{(z+z_0)^2}{t} + \frac{y^2}{(t+t_0)} \right] \right\}. \qquad \textit{Eq. 3.13}$$

Temperature distribution immediately below the centre of the beam $(y = 0)$ is then

$$T = T_0 + \frac{AP}{2\pi k v \sqrt{t(t+t_0)}} \exp\left\{ -\frac{1}{4a}\frac{(z+z_0)^2}{t} \right\}. \qquad \textit{Eq. 3.14}$$

In the limit of $t >> t_0$ which will be the case if the heat flow is quasi stationary

$$t = \frac{(z+z_0)^2}{4a}, \qquad \textit{Eq. 3.15}$$

and the peak temperature is

$$T_p = T_0 + \frac{2}{e\pi}\frac{AP}{\rho c v (z+z_0)}, \qquad \textit{Eq. 3.16}$$

where *e* is the natural constant. The depth at which a given peak $T_p$ is reached is

$$z + z_0 = \sqrt{\frac{2}{e\pi} \cdot \frac{AP}{\rho c v (T_p - T_0)}}. \qquad \textit{Eq. 3.17}$$

The parameter $z_0$ is determined by combining *Eq. 3.14* with the expiration of a peak surface temperature under a stationary beam of intensity $\frac{P}{\pi r_b^2}$ applied for a time $t_b$, produces a peak surface temperature $T_s$ given by

$$T_s = T_0 + \frac{2AP}{\pi^{3/2} r_b^2 k}\sqrt{a t_b}, \qquad \textit{Eq. 3.18}$$

with $z = 0$, *Eq. 3.16* gives

$$z_0^2 = \frac{\sqrt{\pi}}{e}\sqrt{\frac{a r_b}{C_1 v}} r_b. \qquad \textit{Eq. 3.19}$$

For the limit $t << t_0$,

$$t = \frac{(z+z_0)^2}{2a} \qquad \textit{Eq. 3.20}$$

and the peak temperature is

$$T_p = T_0 + \sqrt{\frac{2}{e}} \cdot \frac{AP}{\pi \rho c v r_b (z+z_0)}. \qquad \textit{Eq. 3.21}$$

The depth at which a given peak $T_p$ is reached is

$$z + z_0 = \sqrt{\frac{2}{e}} \cdot \frac{AP}{\pi \rho c v (T_p - T_0)}. \qquad \textit{Eq. 3.22}$$

Equating *Eq. 3.20* to *Eq. 3.18* gives $z_0$ in this limit as

$$z_0^2 = \frac{\pi}{e} \cdot \frac{ar_b}{C_1 v} . \qquad \textit{Eq. 3.23}$$

## 3.4 Numerical Methods

Until now various analytical solutions to the problem of heat flow in solids have been introduced. However in most cases of interest such analytical solutions might not be realistic. In situations where the thermo-physical properties are temperature dependent or for complicated geometries other methods should be used to describe the phenomena. Numerical solutions are suitable techniques for solving these problems. Primarily, because the development of computers of ever increasing speed which allow large calculations to be carried out, finite element method (FEM), finite difference method (FDM) and boundary element method (BEM) are techniques which are popular. Among the mentioned techniques, FEM is the most widespread numerical method for its flexibility to be applied for a wide range of problems.

Throughout this thesis, finite element method using SYSWELD code is the technique used for solving thermal and metallurgical processes.

Thermal problems accruing in any heat treatment processes that can be solved using the SYSWELD system may be divided into three categories:

- The first category concerns thermal problems at steady state involving constant thermo-physical properties.
- The second category concerns problems at transient (or non stationary) state with constant thermo-physical properties and boundary conditions, which can depend on time but not on temperature. Here the aim is to compute the temperature variation in the course of time starting from an initial state.
- Finally, the third category covers all the stationary or non stationary problems including non linearity e.g. heat transfer coefficient varying with temperature.

The major non linearity classes that can be handled with SYSWELD system cover the areas of conduction, convection and radiation at steady or transient state:

- non linearity of thermo-physical properties ( $k(T)$, $\rho(T)$, $c(T)$ ),
- problems of phase changes,
- non linearity of boundary conditions:
  - thermal heat as a function of wall temperature,
  - heat transfer coefficient as a function of wall temperature (forced or natural convection, etc), radiation in an infinite medium,
  - thermal radiation in a cavity (calculation of shape factors, grey body, etc),
  - thermal contact non linearities,
  - thermal coupling between a fluid and a structure in a pipe.

To these non linearities we can add particular modelling possibilities such as:

- simulation of the operation of a temperature regulator,
- modelling of heat sources of any form, including moving sources.

The finite element method, applied to the solution of non linear transient thermal problems to be solved, leads to the solving an equation of the type at each instant:

$$\psi = 0 , \qquad \textit{Eq. 3.24}$$

where $\psi$ represents a table containing all the residual nodal powers. Each component of $\psi$ represents the thermal unbalance at each node.

Generally, $\psi$ is expressed in the form

$$\psi = \vartheta - \phi - f_i \,, \qquad \textit{Eq. 3.25}$$

where $\vartheta$ represents all the thermal powers, supplied to the system (boundary conditions and sources of internal heat), $\phi$ expresses, in discrete form, the local balances of the outgoing and incoming thermal flows in the volume element, $f_i$ represents the accumulation terms. It is clear that all these quantities depend on the instant $t$ of computation and the temperature field at that instant.

In particular, it is possible to write $\phi$ and $f_i$ in the form:

$$\phi = \boldsymbol{K}\,\boldsymbol{T} \,, \qquad \textit{Eq. 3.26}$$

$$f_i = \boldsymbol{C}\dot{T} \,, \qquad \textit{Eq. 3.27}$$

where

$\boldsymbol{K}$ : thermal conductivity matrix,

$\boldsymbol{T}$ : table containing all the nodal temperatures,

$\boldsymbol{C}$ : thermal inertia matrix,

and $\dot{T} = \dfrac{\partial T}{\partial t}$.

For linear behaviour, matrices $\boldsymbol{K}$ and $\boldsymbol{C}$ are independent of the temperature. For non linear behaviour, *Eq. 3.24* should be solved at each instant, by the iterative method.

Taking $\psi_i$ as the residue resulting from the $i^{th}$ iteration, obtained with a temperature field of $T_i$, an improved solution could be obtained by writing:

$$\psi_{i+1} = \psi_i + (\frac{\partial \psi}{\partial T})_i \delta T_i = 0 \,, \qquad \textit{Eq. 3.28}$$

where $(\dfrac{\partial \psi}{\partial T})_i$ represents the tangent matrix resulting from the $i^{th}$ iteration.

Solution of the matrix equation, by an iterative or direct solver

$$\psi_i = (\frac{\partial \psi}{\partial T})_i \delta T_i \,, \qquad \textit{Eq. 3.29}$$

allows us to obtain a new approximation as

$$T_{i+1} = T_i + \delta T_i \,, \qquad \textit{Eq. 3.30}$$

then a new residue $\psi_{i+1}$ corresponding to $T_{i-1}$, and so on, till the residue obtained is better than the required precision.

# 4. THERMO-METALLURGICAL ANALYSIS OF LTH USING FINITE ELEMENT METHOD

## 4.1 Introduction

When surface of a material is rapidly heated by a moving laser source, rapid cooling will occur by heat conduction to the bulk of the material after the beam has passed. By properly selecting the process parameters:

- power of the laser beam,
- relative laser source-workpiece velocity (scanning rate),
- shape and dimension of the workpiece area on which the laser beam impinges (laser spot),
- power distribution in cross-section of the beam,

(all these results in a defined heating and cooling rate of the hardenable steel), phase transformations may be suitably controlled in order to allow hard martensite on the surface and at a given depth as an outcome of the treatment.

A lot of factors beside the just mentioned process parameters, influence the temperature distribution in the three dimensional workpiece as a consequence of the laser-material interaction including the absorption coefficient of the materials, the properties of the treated material (such as its thermal conductivity, specific heat and emissivity) and the shape and dimensions of the workpiece itself. When all these parameters are known, the thermal behaviour of the treated workpiece maybe analysed by means of analytical expressions

available in the literature, which have been discussed in section 3.2. Yet, these expressions, with few exceptions, come from idealised models of the heating process with restrictions in heat flow and workpiece dimension. As a consequence, they are not suitable for evaluation of edge and corner effects of the workpiece, which tends to concentrate the heat flow. In addition, most of the proposed models assume that the thermal properties of the metal do not vary with temperature. In reality heat diffusion is a three dimensional phenomenon, the dimensions of the workpiece can be comparable with that of laser spot and the thermal properties of the metals, especially its thermal conductivity, are temperature dependent. Moreover the majority of the developed models are devoted to study the process under quasi steady state conditions, while a fully time dependent model is necessary to investigate the thermal behaviour of the workpiece under realistic conditions.

In addition, sometimes it is necessary to implement complex patterns of laser spot, or to overlap hardening passes, or to take the presence of edges and other geometrical discontinuities of the workpiece into account.

As stated earlier, SYSWELD Finite Element Analysis Code is used to numerically simulate the laser transformation hardening processes. SYSWELD, developed by ESI Group, is a Finite Element Computer Code for determination of thermal, metallurgical and mechanical calculations of welding and heat treatments. The overall structure of this code can be found in SYSWELD Manuals [43].

## 4.2 Thermal Analysis

As in any phase transformation, during solid state phase transformations, certain amount of heat is produced or consumed due to the so-called latent heat of phase transformations. This effect causes changes of thermal conditions inside the part which have influences on the phase transformation speeds. To consider these influences of heat convection and solid state phase transformations, a coupled thermo-metallurgical analysis based on the enthalpy formulation is used. The modified heat conduction equation is

$$\bar{\rho}\frac{\partial \bar{H}}{\partial t} - \nabla(\bar{k}\nabla T) - q = 0, \qquad \textit{Eq. 4.1}$$

where

$\bar{\rho} = \sum_i p_i \rho_i$ is the density of phases with $\bar{\rho} = \rho(p_i, T)$,

$\bar{k} = \sum_i p_i k_i$ is the thermal conductivity of phases with $\bar{k} = k(p_i, T)$,

$\bar{H} = \sum_i p_i H_i$ is the enthalpy of phases with $\bar{H} = H(p_i, T)$

and $\sum_i p_i = 1$.

Moreover $p_i$ denotes the proportion of phase *i* and $\rho_i$, $k_i$ and $H_i$ are the density, thermal conductivity and the enthalpy of phase *i* at temperature *T* respectively, *q* represents the heat flux density.

Using the mixture laws for $\bar{\rho}$, $\bar{k}$, $\bar{H}$ and knowing that $\bar{c} = \sum_i \rho_i c_i$ is the specific heat of phases the modified heat equation is

$$\left(\sum_i p_i(\rho c)_i\right)\frac{\partial T}{\partial t} - \nabla\left(\left(\sum_i p_i k_i\right)\nabla T\right) - q + \sum_{i<j} L_{ij}(T)\cdot A_{ij} = 0, \qquad \textit{Eq. 4.2}$$

where $i$ and $j$ are indices of individual phases, $L_{ij}$ represents the latent heat of transformation of phase $i$ to $j$ at temperature $T$ and $A_{ij}$ is the portion of phase $i$ transformed to phase $j$ in unit time. The specific heat of phases $c_i$ is

$$c_i = \frac{\partial H_i}{\partial T} \qquad \textit{Eq. 4.3}$$

and $L_{ij}$ is calculated as a function of the phase enthalpies $H_i$ by (see *Figure 4.1*)

$$L_{ij} = H_j - H_i \,. \qquad \textit{Eq. 4.4}$$

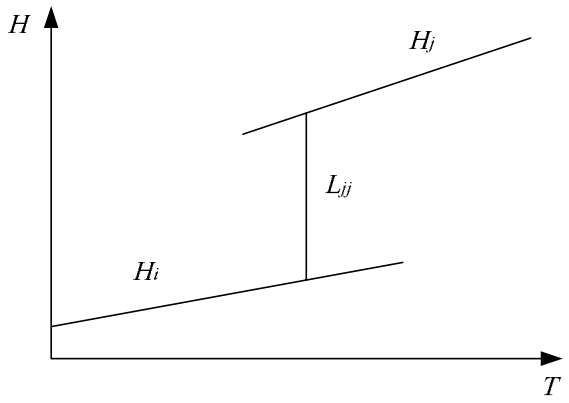


*Figure 4.1 Variation of enthalpies with temperature for i and j phases*

## 4.3 Phase Transformation Analysis

Due to a large variety of steel grades a general analysis of phase transformations and the accompanying effects is difficult. Different mathematical models have been proposed to describe the transformation kinetics. In case of steels, a distinction is normally made between two types of transformation, namely "diffusion type" and "diffusionless" or martensitic transformations.

### 4.3.1 Diffusion type Phase Transformation Model

The kinetics of "diffusion type" transformation, Leblond model, was initially introduced in SYSWELD and then generalisation of this model to include Johnson Mehl Avrami (JMA) type transformation kinetics was integrated in the SYSWELD code. The Leblond model approach requires determination of data from a Continuous Cooling Transformation (CCT) diagram, or dilatometric test used to construct the CCT diagrams. However in case of the JMA law, which gives phase proportion according to time at a constant temperature, direct determination of the parameters can be achieved using an Isothermal Transformation (TTT) diagram.

The diffusional phase transformation kinetics used in this work is the Leblond's model, of which a more detailed introduction will be given here.

The initial approach is of the phenomenological type, and the semi-empirical model is based on equations of the chemical kinetic type, rather than a totally empirical model based on direct introduction of CCT diagram data. This approach can be used to represent any type of transformations, whether by heating or cooling. The equation is generally written as follows:

$$\frac{dp}{dt} = \frac{\overline{p} - p}{TR}, \qquad \textit{Eq. 4.5}$$

where $p$ is the metallurgical phase proportion, $t$ is the time, $\overline{p}$ is interpreted as the equilibrium value and $TR$ is equivalent to the time delay which is a function of temperature and cooling rate. If $T$ is varied in time, the *Eq. 4.5* describes the fact that $p$ follows $\overline{p}$ after time delay $TR$.

In practice, a number of transformations can occur in the material. This signifies that the transformation rate for phase $i$ depends on the other metallurgical phases:

$$\frac{dp_i}{dt} = -\sum_{i \neq j} A_{ij} \ , \quad (j = 1, 2, ...., n), \qquad \textit{Eq. 4.6}$$

where $A_{ij}$ represents the quantity of phase $i$ transformed to phase $j$ per time unit. $A_{ij}$ can be given as

$$A_{ij} = (K_{i \to j} \cdot p_i) - (K'_{i \to j} \cdot p_j), \qquad \textit{Eq. 4.7}$$

where $K_{i \to j}$ and $K'_{i \to j}$ are constants of reaction $i \to j$, which can depend on the temperature $T$ and the cooling rate $\dot{T}$ under

$$K_{i \to j} = K(T) \cdot F(\dot{T}), \qquad \textit{Eq. 4.8}$$

$$K'_{i \to j} = K'(T) \cdot F'(\dot{T}). \qquad \textit{Eq. 4.9}$$

Considering the case of a single $1 \to 2$ transformation, such as austenitisation for example (phase 1 is the $\alpha$ phase, and phase 2 the $\gamma$ phase). The equations can then be written as follows:

$$\frac{p_2}{dt} = K_{1 \to 2} \cdot p_1 - K'_{1 \to 2} \cdot p_2 \qquad \textit{Eq. 4.10a}$$

so that, with $p_1 + p_2 = 1$;

$$\frac{p_2}{dt} = K_{1 \to 2} \cdot (K_{1 \to 2} - K'_{1 \to 2}) \cdot p_2 . \qquad \textit{Eq. 4.10b}$$

By identification with *Eq. 4.5*, we can write:

$$K_{1 \to 2} = \frac{\overline{p}_2}{TR} \qquad \textit{Eq. 4.10c}$$

and

$$-(K_{1 \to 2} + K'_{1 \to 2}) \cdot \overline{p}_2 = -\frac{\overline{p}_2}{TR}, \qquad \textit{Eq. 4.10d}$$

$$K'_{1 \to 2} = \frac{1}{TR} - K_{1 \to 2} . \qquad \textit{Eq. 4.10e}$$

Substituting *Eq. 4.10c* into *Eq. 4.10e* gives

$$K'_{1 \to 2} = \frac{1 - \overline{p}_2}{TR} . \qquad \textit{Eq. 4.10f}$$

Now we have to express $K_{1 \to 2}$ and $K'_{1 \to 2}$ as a function of $T$ and $\dot{T}$ as

$$K_{1 \to 2} = K(T) \cdot F(\dot{T}), \qquad \textit{Eq. 4.10g}$$

$$K'_{1 \to 2} = K'(T) \cdot F'(\dot{T}), \qquad \textit{Eq. 4.10h}$$

knowing that $F, F'$ are functions of temperature and $K, K'$ are functions of cooling rate.
Rearrangement of *Eq. 4.10e* gives

$$TR = \frac{1}{K_{1 \to 2} + K'_{1 \to 2}} \qquad \textit{Eq. 4.10i}$$

and substituting *Eq. 4.10h* in *Eq. 4.10g* follows

$$TR = \frac{1}{K(T)\cdot F(\dot{T}) + K'_{1\to 2}\cdot F'(\dot{T})}. \qquad \textit{Eq. 4.10j}$$

By introducing the phase proportion at equilibrium $p_{eq}$, as

$$K = \frac{p_{eq}(T)}{\tau(T)} \qquad \textit{Eq. 4.10k}$$

and

$$K' = \frac{1 - p_{eq}(T)}{\tau(T)}, \qquad \textit{Eq. 4.10l}$$

so that

$$\overline{p} = \frac{p_{eq}(T)\cdot F(\dot{T})}{p_{eq}(T)\cdot F(\dot{T}) + (1 - p_{eq})\cdot F'(\dot{T})}, \qquad \textit{Eq. 4.10m}$$

where $\tau$ is the delay time as a function of temperature only. In this manner *Eq. 4.10j* can be written as

$$TR = \frac{\tau(T)}{p_{eq}(T)\cdot F(\dot{T}) + (1 - p_{eq}(T))\cdot F'(\dot{T})}. \qquad \textit{Eq. 4.10n}$$

In case it is assumed that $F = F'$ then

$$TR = \frac{\tau(T)}{F(\dot{T})}. \qquad \textit{Eq. 4.10o}$$

Finally the transformation equation to be calibrated is

$$\frac{dp(T)}{dt} = \frac{p_{eq}(T) - p(T)}{\tau(T)} F(\dot{T}). \qquad \textit{Eq. 4.11}$$

Knowledge of functions $p_{eq}$, $\tau$, $F$ and $F'$ (if it is not equal to $F$) are therefore required for characterization of phase transformations.

In practice, an adjustment, involving comparison of the results of the CCT diagram with the predictions provided by the model, is required to obtain $p_{eq}$, $\tau$, $F$ and $F'$.

### 4.3.2 Martensitic Transformation Model

An expression for the amount of martensite, which fits experiments very well, is based on the assumption that as soon as the temperature drops below the $M_s$ temperature, there exists a linear relation between martensite growth and temperature decrease, $\dot{p}^m = -b\dot{T}$. This relation has to be corrected for the vanishing parent phase so that we end up with $\dot{p}^m = -(\overline{p} - p^m)b\dot{T}$. Integration from $M_s$ yields the Koistinen and Marburger equation:

$$p(T) = \overline{p}\left[1 - exp\left(-b\left(M_s - T\right)\right)\right], \quad \text{for} \quad T<M_s, \qquad \textit{Eq. 4.12}$$

where $\overline{p}$ represents the proportion obtained at an infinitely low temperature. $M_s$ and $b$ characterise initial transformation temperature, and evaluation of the transformation process according to temperature, respectively.

## 4.4 Numerical Determination of Hardness

Knowledge of the thermal and metallurgical history of a part is sufficient to predict its hardness at all points of the heat affected area. The hardness at any point in a given material depends on:

- the chemical composition of the material,
- the structure at the end of the thermal cycle for quenched and tempered structures,
- the cooling cycle to which the part was subjected (cooling rate),
- the grain size.

Empirical formulas taken from the literatures [44],[45],[46] have been implemented in numerical code for Vickers hardness calculations of martensite, bainite and ferrite structures in *Eq. 4.13-4.15*. These equations take the material's chemical composition, the final microstructure and the cooling rate at 700 °C ($V_R$) into account, while the grain size is neglected.

$$HV_{martensite} = 127 + 949C + 27Si + 11Mn + 8Ni + 16Cr + 21\log_{10}(V_R) \qquad \text{Eq. 4.13}$$

$$HV_{Bainite} = -323 + 185C + 330Si + 153Mn + 65Ni + 144Cr + 191Mo + \log_{10}(V_R)(89 + 53C - 55Si - 22Mn - 10Ni - 20Cr - 30Mo) \qquad \text{Eq. 4.14}$$

$$HV_{Ferrite} = 42 + 223C + 53Si + 30Mn + 12.6Ni + 7Cr + 1Mo + \log_{10}(V_R)(10 - 19Si + 4Ni + 8Cr + 130V) \qquad \text{Eq. 4.15}$$

In order to obtain valid results, the element proportions must be located within the following chemical composition ranges: 0.1 < C <0.5, Si < 1%, Mn < 2%, Ni ≤ 4%, Cr ≤ 3%, Mo≤ 1%, V < 0.2%, Cu < 0.5% and 0.01% < Al < 0.05%.

## 4.5 Material Data

In this thesis the unalloyed steel C45, MSZ 61(85), with chemical compositions shown in *Table 4.1*, was used because of the ample amount of data which is available on the behaviour of this steel. Where other steels show a different behaviour, transformation hardening of such steels may still be described by models similar to those presented here.

*Table 4.1 Chemical composition of C45 steel*

| C45 steel | | | | |
|---|---|---|---|---|
| C | Mn | Si | S | P |
| 0.45 | 0.65 | 0.40 | 0.020 | 0.02 |

### 4.5.1 Thermal Properties of Material

In general, for a finite element modelling it is necessary to specify the material properties, where they can be constant or temperature dependent.

The physical data used for laser transformation hardening in the models are plotted versus temperature in *Figures .4.2-4.5*. *Figures 4.2-4.3* show the thermal properties of phases as a function of temperature while *Figure 4.4* illustrates the mass density of phases versus

temperature. *Figure 4.5* shows the enthalpy shift during the $\gamma \rightarrow \alpha$ phase transformation. (In all figures standard SYSWELD notations are used, see more details in section 4.5.2)

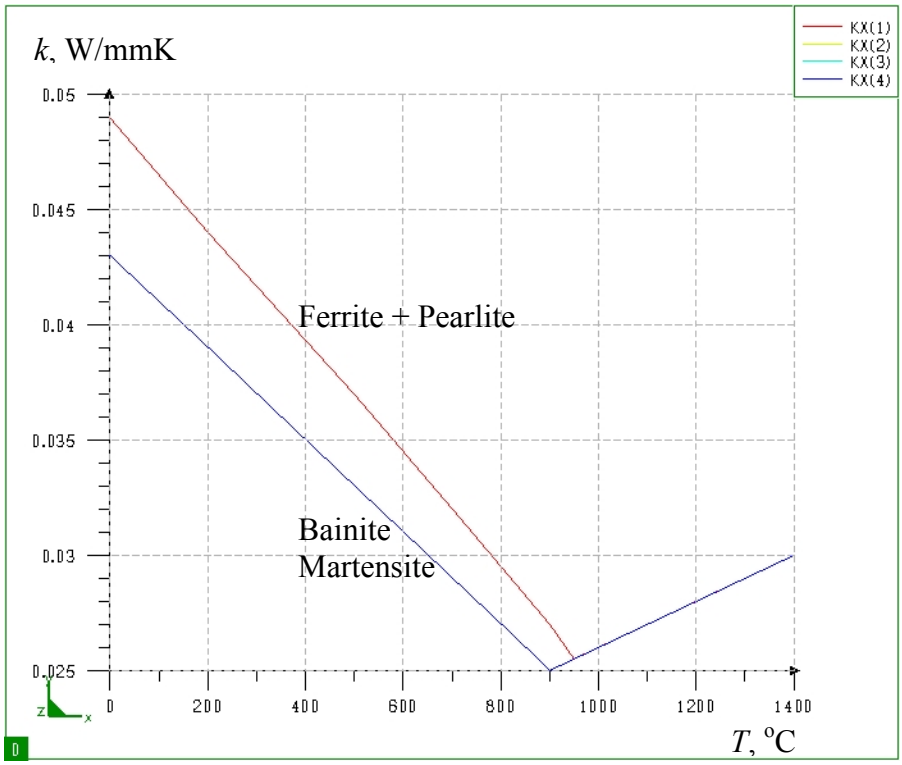


*Figure 4.2 Thermal conductivity as a function of temperature*

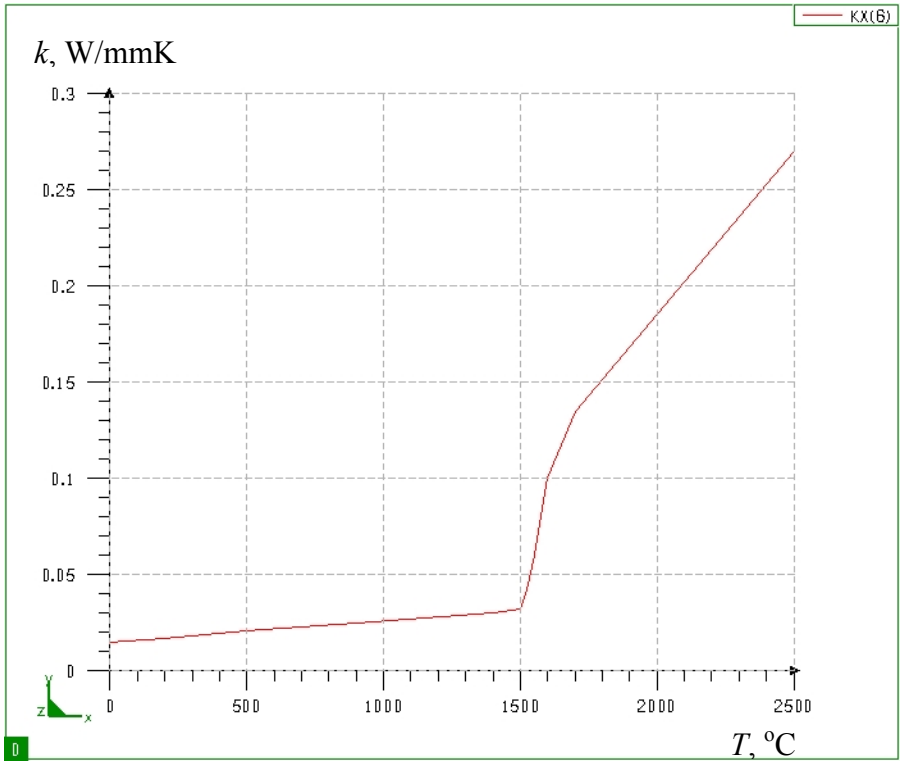


*Figure 4.3 Thermal conductivity of austenite as a function of temperature*

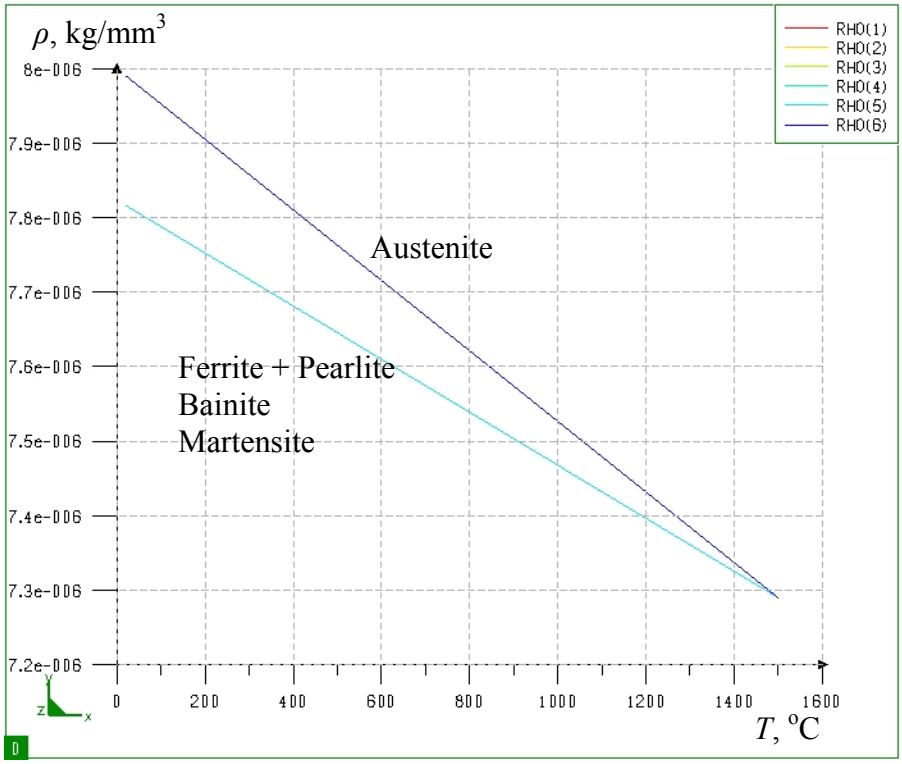


*Figure 4.4 The mass density as a function of temperature.*

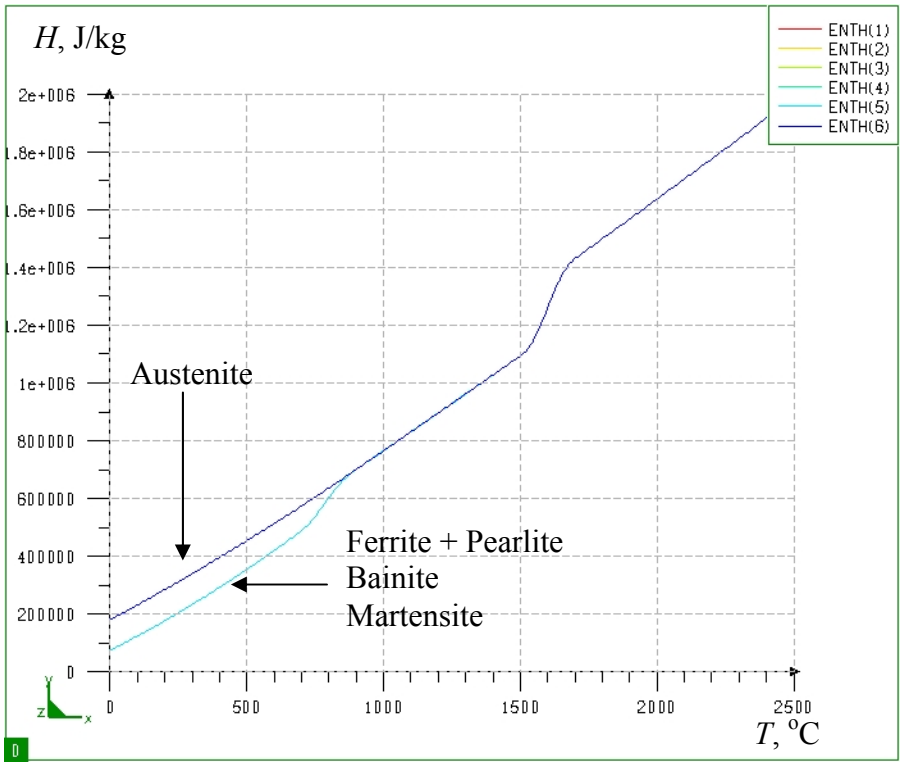


*Figure 4.5 The enthalpy as a function of temperature.*

### 4.5.2 Phase Transformations of Material

Transformation data are generally presented in two types of diagrams, isothermal TTT diagrams and continuous cooling (or heating) diagrams (CCT or TTA diagrams). For the calculations of hardening it may be argued that the data as obtained during continuous cooling

are more relevant comparing to isothermal TTT, since these represent the actual process more closely.

To describe the phase transformations for continuous cooling, the CCT and for continuous heating, the TTA diagrams are used as shown in *Figure 4.6* and *Figure 4.7*.

The methodology for the calibration of these diagrams, which is needed for extracting the data to be used in numerical calculations, consists of four steps:

- identification of phases and phase transformations,
- calibration of parameters for each transformation,
- transfer of the parameters into a standard data file,
- check of the calibrated diagram.

The phases taken into account for C45 steel are defined by the following numbers:

- phase no. 1: initial microstructure (ferrite + pearlite),
- phase no. 2: bainite,
- phase no. 3: martensite,
- phase no. 6: austenite.

In SYSWELD indices 4 and 5 are usually used for different phases that are not used in this case.

The initial microstructure is assumed to be an equilibrium type mixture of ferrite and pearlite and defined to the system as a single phase.

The phase transformations considered during modelling are

- During heating
  - Initial microstructure to austenite ( 1 → 6),
  - Bainite to austenite ( 2 → 6),
  - Martensite to austenite ( 3 → 6).
- During cooling
  - Austenite to initial microstructure ( 6 → 1),
  - Austenite to bainite ( 6 → 2),
  - Austenite to martensite ( 6 → 3).

As mentioned earlier, functions $p_{eq}$, $\tau$ , $F$ and $F'$ are therefore required for characterization of phase transformations using the Leblond's law. These model parameters are determined by close aligning to the CCT diagram in case of cooling and TTA diagram in case of heating. When inputting the transformations into the system, each phase transformation is treated separately by one set of parameters. For each cooling curve the cooling rate is determined in the temperature range of $800\ ^oC$ to $500\ ^oC$ as the methodology of the measured CCT diagrams, to fit the computed CCT diagram best to the measured CCT diagram. For each phase transformation the start and end time, temperature of the transformation and percentage of existing phases along each cooling curve are extracted.

The parameters' identification consequently involves executing successive tests with the numerical model for different parameters, then selecting those providing results comparable with those of the experimental diagrams.

For the austenitisation procedure the appropriate $p_{eq}$, and $\tau$ parameters are used, as shown in *Figure 4.8* and *Figure 4.9* for the Leblond's law assuming $F(\dot{T}) = F'(\dot{T}) = 1$.

When these parameters are used in *Eq. 4.11*, the accuracy can be checked by extraction of a diagram illustrating the phase proportion versus temperature for different heating rates, *Figure 4.10*.

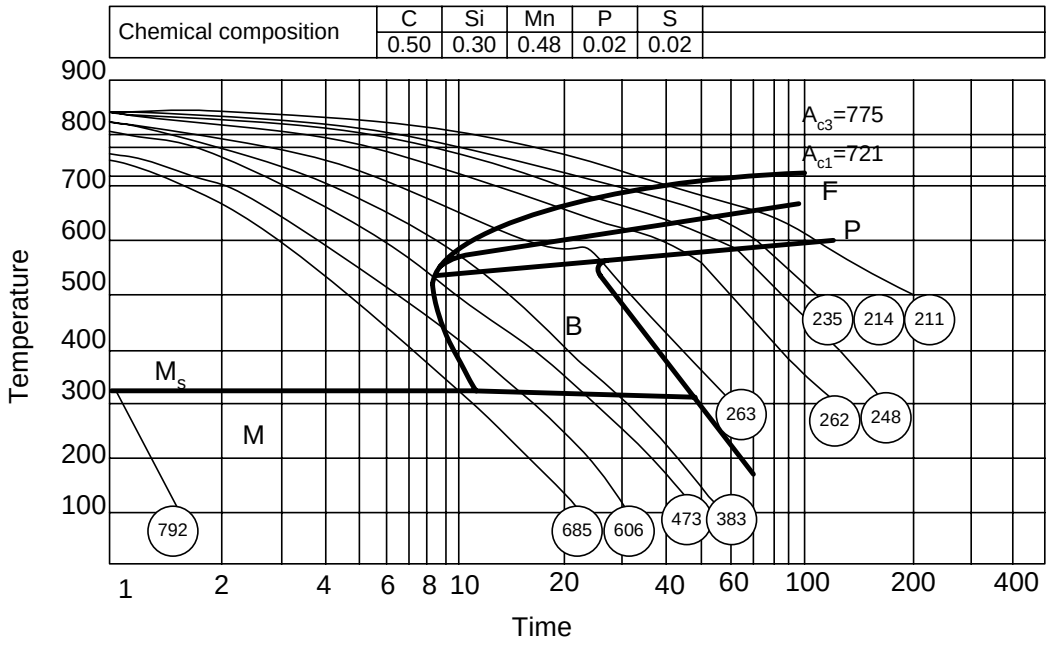


*Figure 4.6 Continuous Cooling Transformation (CCT) diagram of C45 steel* [47]

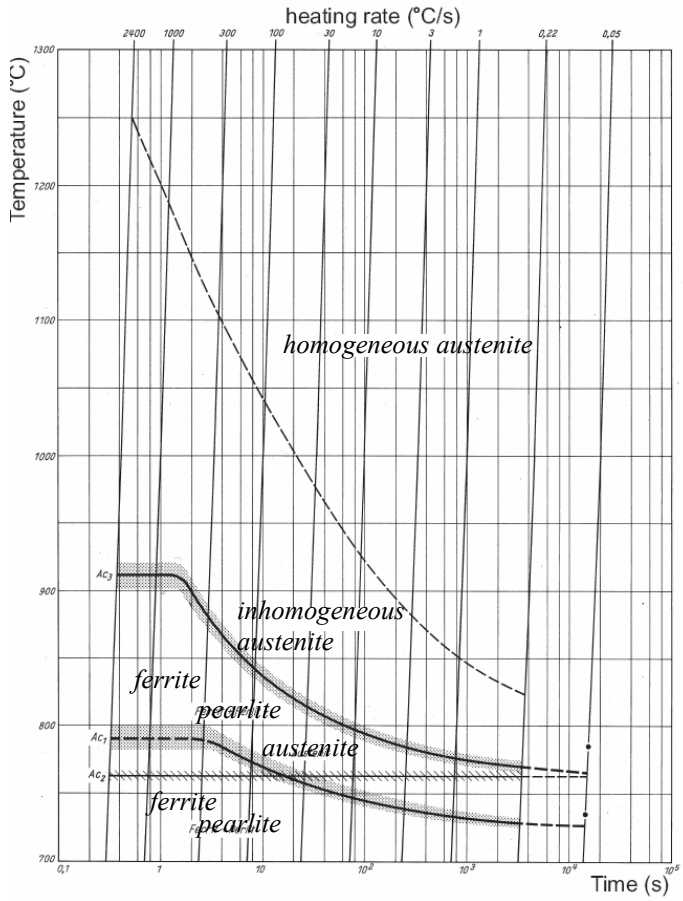


*Figure 4.7 Time Temperature Austenitisation (TTA) diagram of C45 steel* [48]

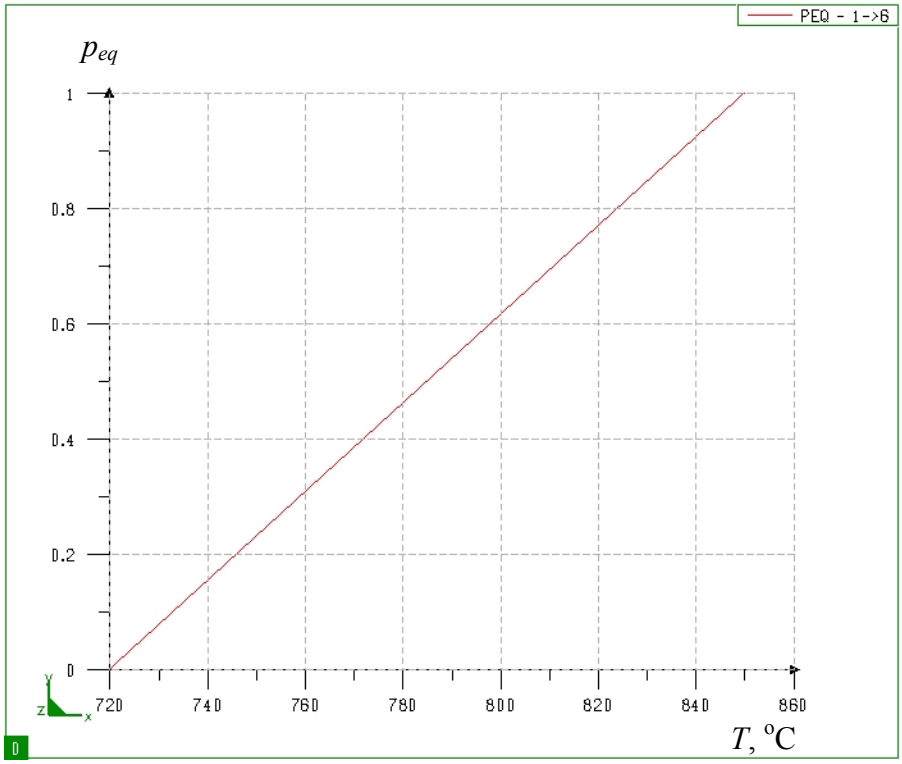


*Figure 4.8 Phase proportion at equilibrium as a function of temperature*

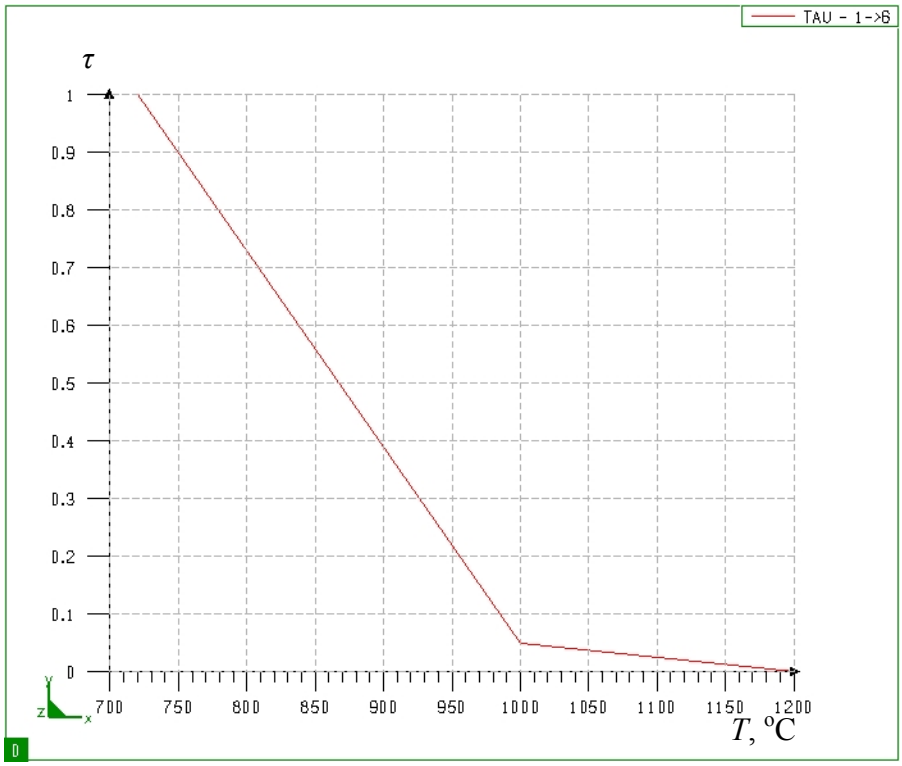


*Figure 4.9 Time delay as a function of temperature*

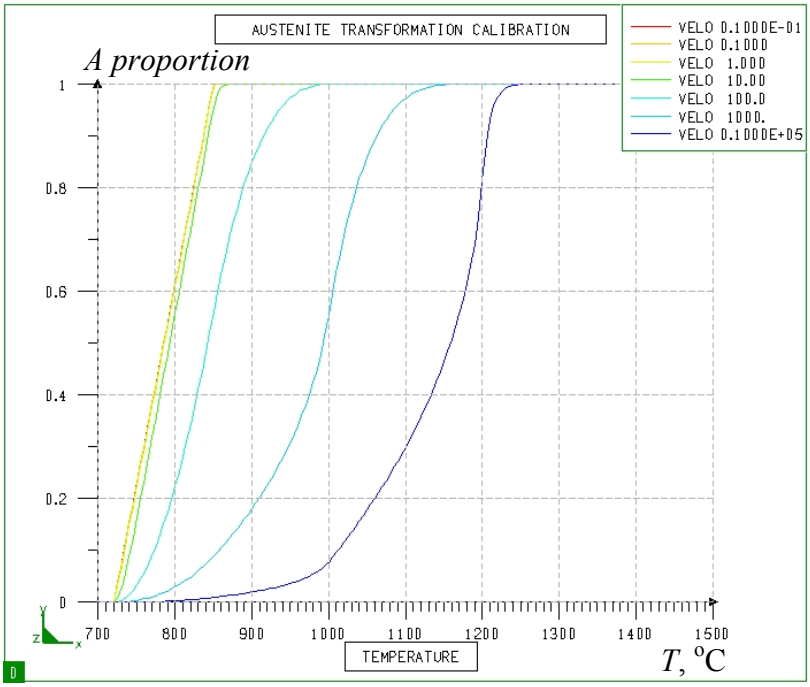


*Figure 4.10 Austenite phase proportion as a function of temperature and heating rate*

Ferrite + pearlite and bainite transformations are characterised by the parameters $p_{eq}$, $\tau$, $F$ and $F'$ assuming $F = F'$. Adjustments of these parameters can be controlled and fixed if needed using the so called calibration diagrams for each phase transformation. The calibration diagrams for the initial phase and bainite transformations are illustrated in *Figure 4.11* and *Figure 4.12* respectively.

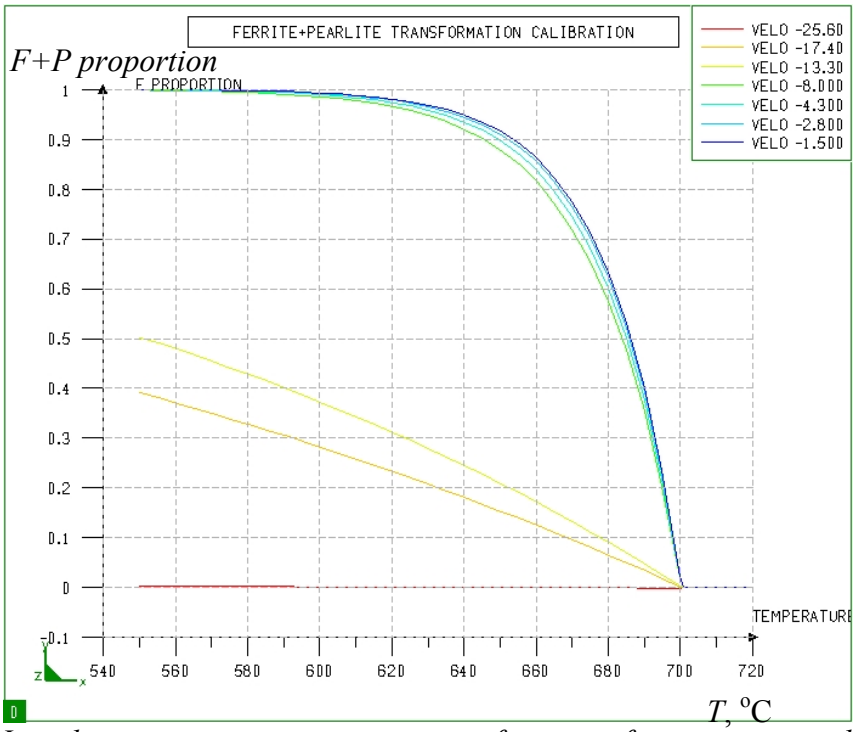


*Figure 4.11 Initial microstructure proportion as a function of temperature and cooling rate*

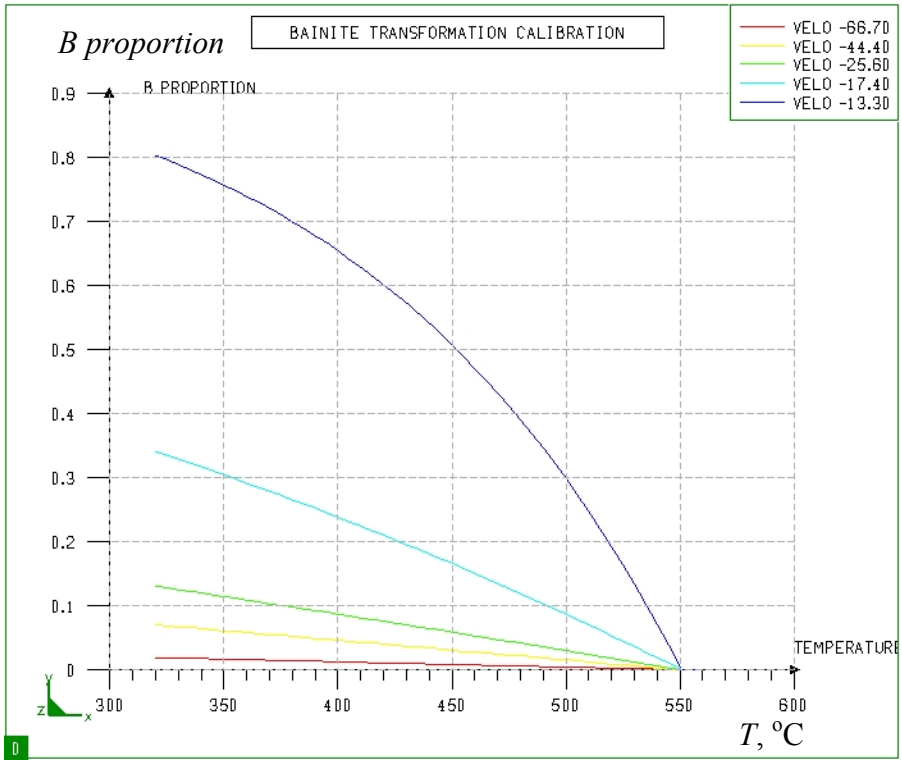


*Figure 4.12 Bainite phase proportion as a function of temperature and cooling rate*

The martensite transformation depends only on the temperature, and parameter *b* in Koistinen and Marburger equation (*Eq. 4.12*) should be defined properly. Parameter *b* differs for each steel and it should be calibrated considering the temperature, which can easily be extracted from the CCT diagram of the steel, and a second value that gives a martensite proportion at a discrete temperature. The retain percentage of austenite at room temperature were considered for this purpose. The rule of thumb was used for martensite finish temperature as $M_f = M_s - 215 \pm 15\ ^oC$, assuming that 99% martensite phase exists at $M_f$ temperature. The phase module can be used for defining parameter *b* knowing $M_s$ and $M_f$. The constant value $b = 0.017$ were calibrated for C45 steel as plotted in *Figure 4.13*.

All phase transformations defined are transferred and stored in a METALLURGY.DAT file ready for computation. To make sure that all parameters are selected properly, we make a final check with plotting the CCT diagram, extracted from the defined parameters (*Figure 4.14*).

The C45 steel phase transformation definition and calibration files and the final METALLURGY.DAT file are discussed in details in the Appendix 2.

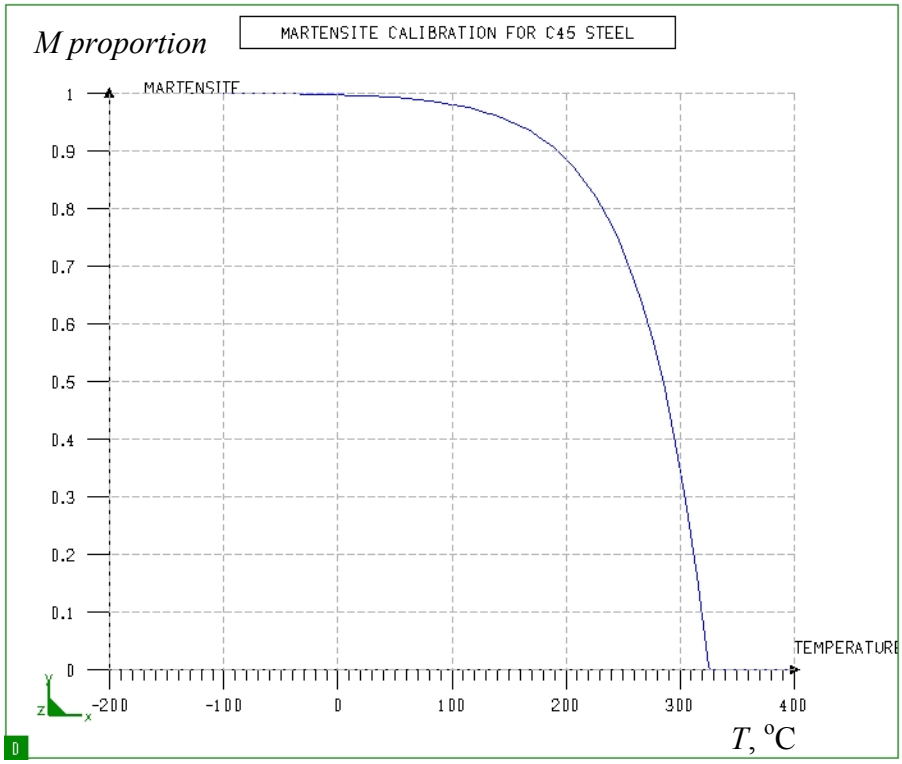


*Figure 4.13 Martensite phase proportion as a function of temperature*

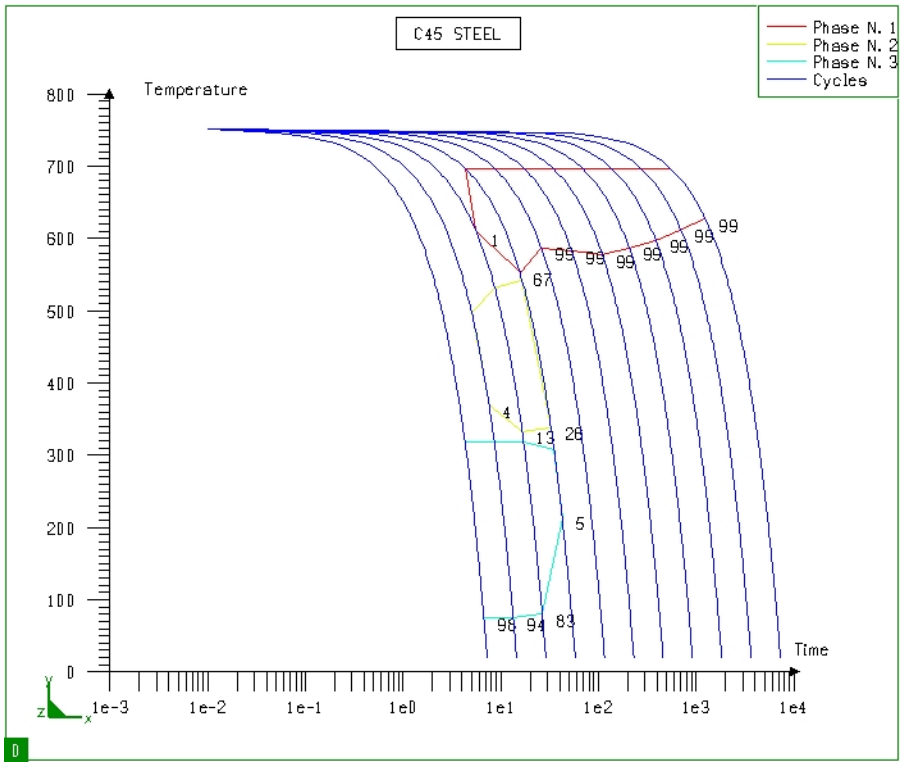


*Figure 4.14 Defined continues cooling curve CCT diagram of C45 steel in SYSWELD for validation*

## 4.6 Simulations of Standard Hardenability Tests

A well known method for determining hardenability is the so called Jominy test. A *100 mm* long bar is heated to austenitisation temperature and held there for the required time. Next it is quenched by applying a water jet directed to one of the end faces. The hardenability is determined by measuring the hardness along the length of the bar.

The main purpose of this calculation is to validate the data for the transformation kinetics. This is important not only for controlling the validity of the applied model and data files, but also for considering the particular steel in use instead of describing the material generally as steel grade. To this end the resulting martensite distribution is compared to the experimental results that illustrate a satisfactory agreement between them. This is shown in *Figure 4.15*.

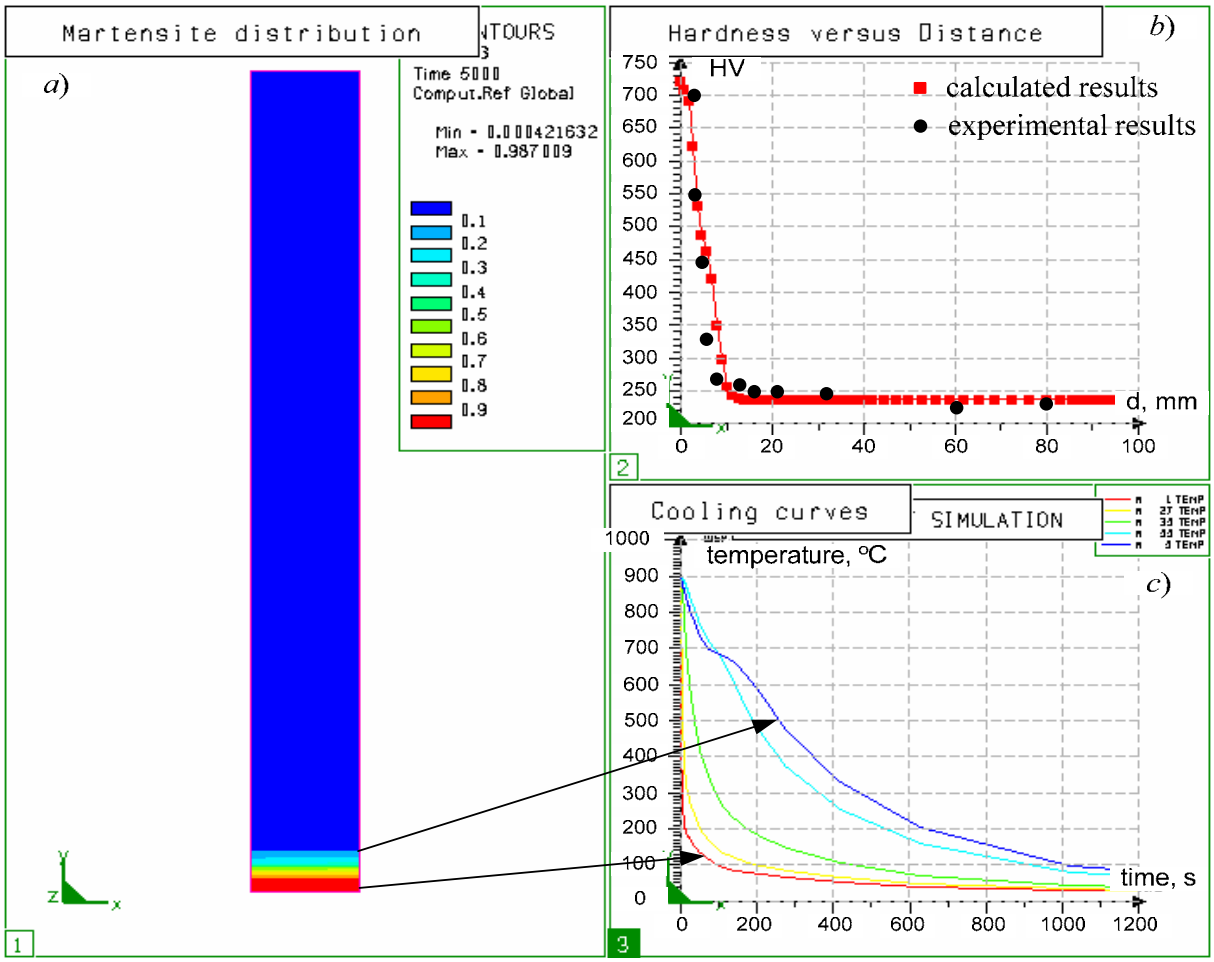


*Figure 4.15 Jominy test results a) martensite distribution b) hardness results comparison of FEM and experimental measurements c) FEM results of cooling curves*

## 4.7 Single Track LTH Modelling Using FEM

The following problem is the thermal and phase transformation analysis of single track laser beam interaction with a workpiece which is based on the development of a three dimensional model for the geometry shown in *Figure 4.16*.

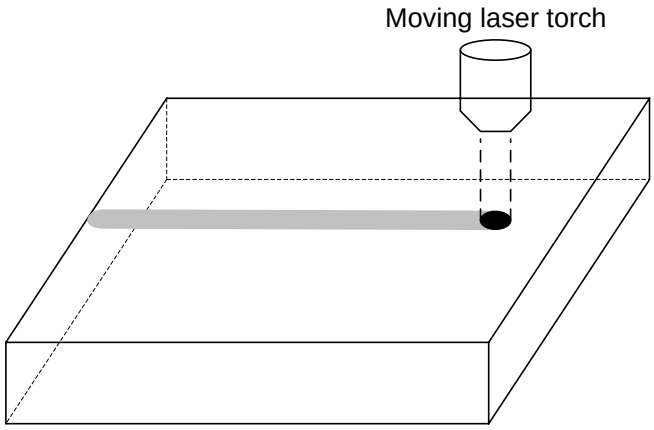


*Figure 4.16 Laser beam impinging on a workpiece of a finite size*

Generally, the procedure of a thermal analysis associated with metallurgical transformations is performed with geometry and mesh preparation using Graphical User Interface (GUI), defining the initial and boundary conditions and introducing the thermal and phase transformation properties of the material, as shown in *Figure 4.17*. Thermal properties and phase transformation as an input data for FEM calculations were discussed in section 4.2.

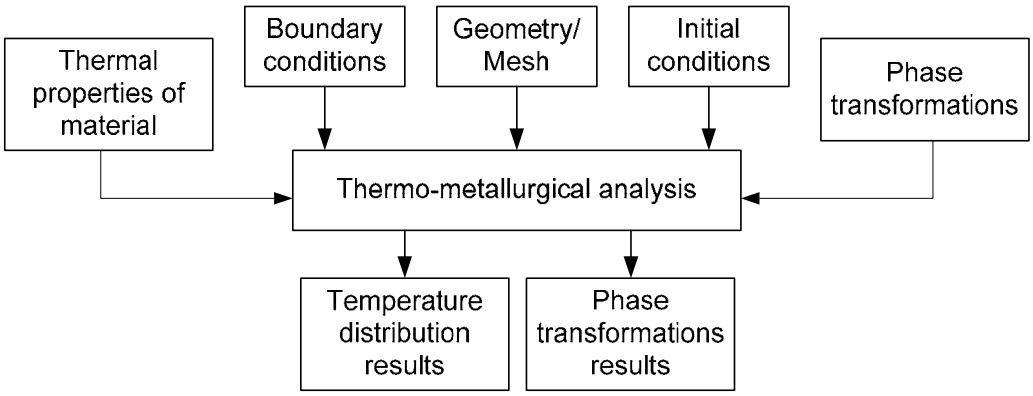


*Figure 4.17 Flowchart of LTH simulation procedure*

The finite element analyses are completed in stages in SYSWELD code, and therefore require separate input decks for each stage. The interaction of the different stages and files required for a complete laser transformation hardening simulation are shown in *Figure 4.18*. Coupled thermal and metallurgical calculations were used for different calculations (*Figure 4.19*).

In the following, the process of a single track laser transformation hardening and the geometry dimensions to be modelled in this chapter as shown in *Figure 4.20* will be demonstrated. The workpiece is subjected to a laser beam with a definite heat flux distribution which is travelling at a particular constant velocity.

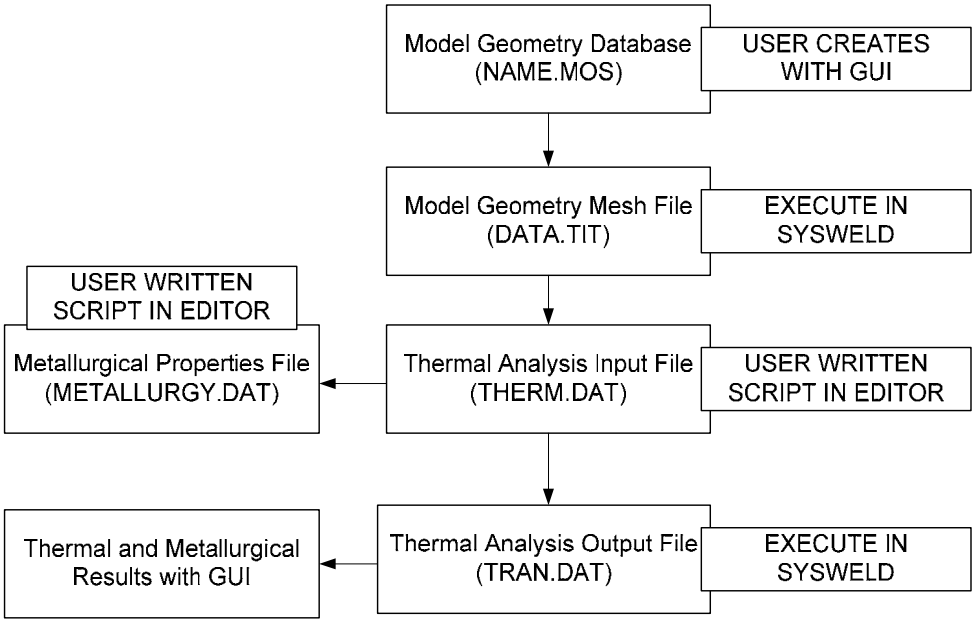


*Figure 4.18 Flowchart of SYSWELD analysis*

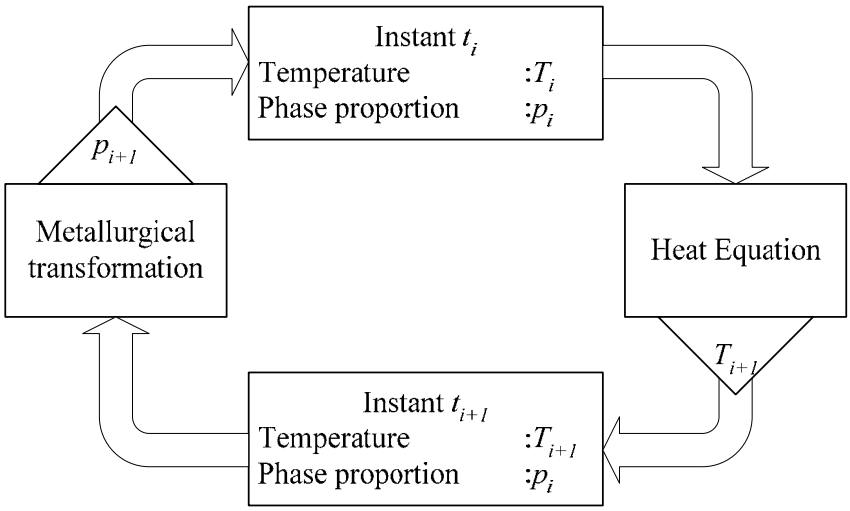


*Figure 4.19 Thermal and metallurgical coupling*

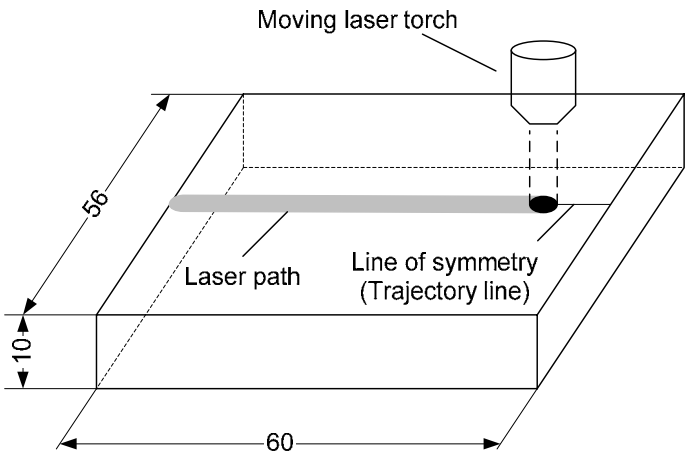


*Figure 4.20 Laser transformation hardening set up*

### 4.7.1 Finite Element Meshes for LTH

Since the loading is symmetric for a single track laser source travelling on a straight line, we call it "trajectory line", only half of the actual geometry is modelled (*Figure 4.21*) with a different boundary condition applied along the symmetry plane comparing to other planes. The finite element mesh model is shown in *Figure 4.22*.

Due to high peak temperatures, large spatial temperature gradients, and rapid temporal temperature fluctuations imposed by the laser heat source, it is necessary to have very small element sizes and consistent time steps using progressive mesh method. A fine mesh to capture the spatial gradients implies a small time step. That is to say, it is necessary to choose a time step which is small enough to resolve these large temperature variations for a given mesh.

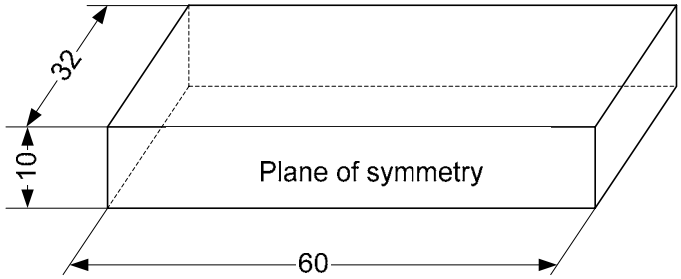


*Figure 4.21 Schematic of modelled geometry along the symmetry plane*

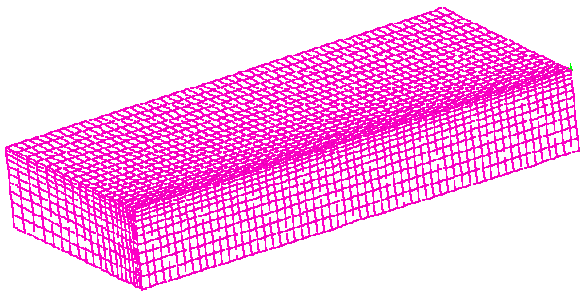

*Figure 4.22 Finite element mesh*

### 4.7.2 Initial and Boundary Conditions

Initial conditions are required only when dealing with transient heat transfer problems in which the temperature field in the material changes with time. The common initial condition in a material can be expressed as the temperature field is a specified function of only spatial coordinates [46]. The initial temperature field is given by

$T = T^0$ in the entire volume, $V$ *Eq. 4.16*

where $T^0$ is the prescribed initial temperature.

For the boundary conditions, the workpiece experiences a combination of three kinds of heat transfer processes during LTH: conduction, convection, and radiation. The convection and radiation occur only on the boundary of the workpiece.

The convective heat loss per unit area at the surface of the workpiece due to the external flow conditions can be expressed as

$$q_c = \beta(T - T_0), \qquad \textit{Eq. 4.17}$$

where $q_c$ is the convection heat flux, $\beta$ is the convective heat transfer coefficient, $T$ is the temperature of the workpiece, and $T_0$ is the ambient temperature.

When the rate of heat flow across a boundary is specified in terms of the emitted energy from the surface and the incident radiant thermal energy, the radiant energy emitted from the body per unit time and per unit area is $\delta\varepsilon T^4$, while the corresponding absorbed radiant energy from the outer sides is $\delta A T_0^4$. Therefore the net rate of heat flow per unit area as radiation energy from the body surface can be expressed as

$$q_r = \varepsilon\delta\left(T^4 - T_0^4\right), \qquad \textit{Eq. 4.18}$$

where $\delta$ is the Stefan-Boltzmann constant, $\varepsilon$ is the surface emissivity and $A$ stands for the surface absorptivity.

The heat source, which moves along a defined path (trajectory line), is modelled by input of a heat flux density directly assigned to each Gauss point of surface elements. The heat source is described as a function of time and space coordinates. Such a model enables an accurate definition of the heat input quantity according to the motion and thus the location of the heat source. In this study the heat source, which is introduced to the system by means of a simplified FORTRAN routine, is modelled as a Gaussian distribution.

All process parameters of laser transformation hardening are included in the definition of the Gaussian heat source, *Figure 4.23*, according to

$$q_G = q_0\, exp\left(-\frac{r_i^2}{r_0^2}\right). \qquad \textit{Eq. 4.19}$$

Here $q_G$ is the Gaussian heat flux density ($W/mm^2$), $q_0$ is the maximum heat flux density ($W/mm^2$) at the beam centre, $r_i$ is the segmental moving heat source radii varying from *0* to $r_0$, and $r_0$ is the Gaussian radius measured at $1/e$ of the maximum heat flux density.

The maximum heat flux density $q_0$ can be determined by integrating the segmental ring heat sources from $r_i = 0$ to $r_i = r_0$ as

$$P = \int_{r_i=0}^{r_i=r_0} q_0\, exp\left(-\frac{r_i^2}{r_0^2}\right) 2\pi r_i dr_i \qquad \textit{Eq. 4.20}$$

and therefore the maximum heat flux density can be regarded as

$$q_0 = \frac{P}{r_0^2\pi}, \qquad \textit{Eq. 4.21}$$

where $P$ stands for the power in $W$.

To consider the fraction of the incident energy which is absorbed by the surface, the power should be multiplied by the surface absorptivity $A$ as

$$q_0 = \frac{AP}{r_0^2\pi}. \qquad \textit{Eq. 4.22}$$

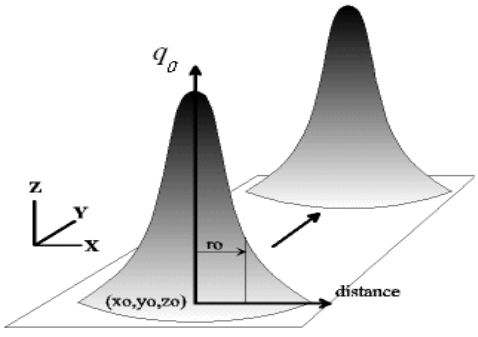


*Figure 4.23 Moving Gaussian heat source*

The maximum heat flux density and the Gaussian radius are the two constant parameters of the Gaussian heat source that can be seen in Appendix 3 SIN_HT.DAT file.

To give a better insight of the LTH process and its modelling, schematic diagram of the process is illustrated in *Figure 4.24*. Taking the temperature distribution into consideration around point *A* shown in the figure, the surface temperature along the laser travel direction rapidly increases within the laser spot area and suddenly decreases past the laser irradiation spot area. The shape of the surface temperature distribution across the laser travel direction is similar to that of a Gaussian function. The temperature is the highest at the central point *A*, while it decreases farther from point *A*. In terms of the depth, the temperature decreases very steeply due to large heat conduction into the bulk material. With this temperature distribution, only a small surface part reaches the austenitisation temperature to undergo martensitic transformation.

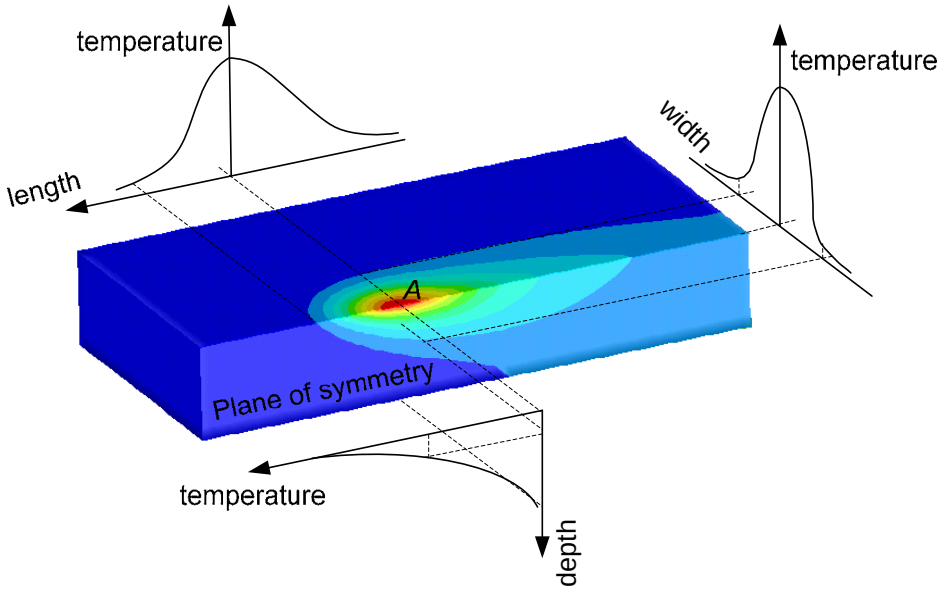


*Figure 4.24 Schematic diagram of a LTH process*

## 4.7.3 LTH Modelling Results

A prescribed Gaussian heat input with maximum heat flux density of $23\ W/mm^2$, $5\ mm$ radius and $10\ mm/s$ scanning rate is the applied load on the workpiece with dimensions shown in *Figure 4.21*. Heat loss as convection and radiation are defined to all sides of the workpiece except the symmetry plane.

The temperature profile and austenite phase distribution of the laser transformation hardening of the steel is as shown in *Figure 4.25*. Due to the time required to obtain a quasi steady state condition in the beginning of the process, temperature results show that at this stage material surface does not reach the required temperature to form austenite, considering the high heating rate (*Figure 4.25 a, d*). Approximately at the time interval of *1* to *5.4 s* the temperature is about $1390\ ^oC$, which is a sufficient value to start the austenitisation transformation. At the end of the process $t = 6\ s$, a maximum temperature of $1511\ ^oC$ was calculated which will result in melting of the material surface (*Figure 4.25 c*). This can be observed more clearly in *Figure 4.26* which shows the time-temperate curves of all nodes of

the trajectory line lying under the centre of the laser beam, while *Figure 4.27* illustrates the time-temperature curves of five selected nodes of the trajectory line.

These temperature differences result in less amount of martensite at the starting region and slight more martensite will be resulted at the end of the path, as shown in *Figure 4.28*. Insufficient heat input at the beginning of the process for austenite transformation is the reason of no or less martensite in this stage.

Similarly to the temperature results, phase transformation of every single node of the workpiece model can be investigated. These kinds of results give the opportunity to follow and have an insight to such a complex and fast process. Result of austenite and martensite proportion of a single node (5410) of the trajectory line on the surface is shown in *Figure 4.29*.

Further calculations have been done for the hardness distribution and the calculated results for surface and in depth of the workpiece can be seen in *Figure 4.30* and *Figure 4.31* respectively. The hardness results confirm that the modelling of the LTH process was successful, as the maximum hardness obtained and the shape of transition between the hardened zone and the base material is realistic. These results were compared to experimental results applied on the modelled steel grade using continuous $CO_2$ laser machine. The experimental procedures are explained in Appendix 1.

Concerning the modelling procedures, initial conditions, boundary conditions, heat source (SIN_HT.DAT), thermal calculation (SIN_HT_C.DAT) and the hardness calculation (Hardness.DAT) files are attached in Appendix 3.

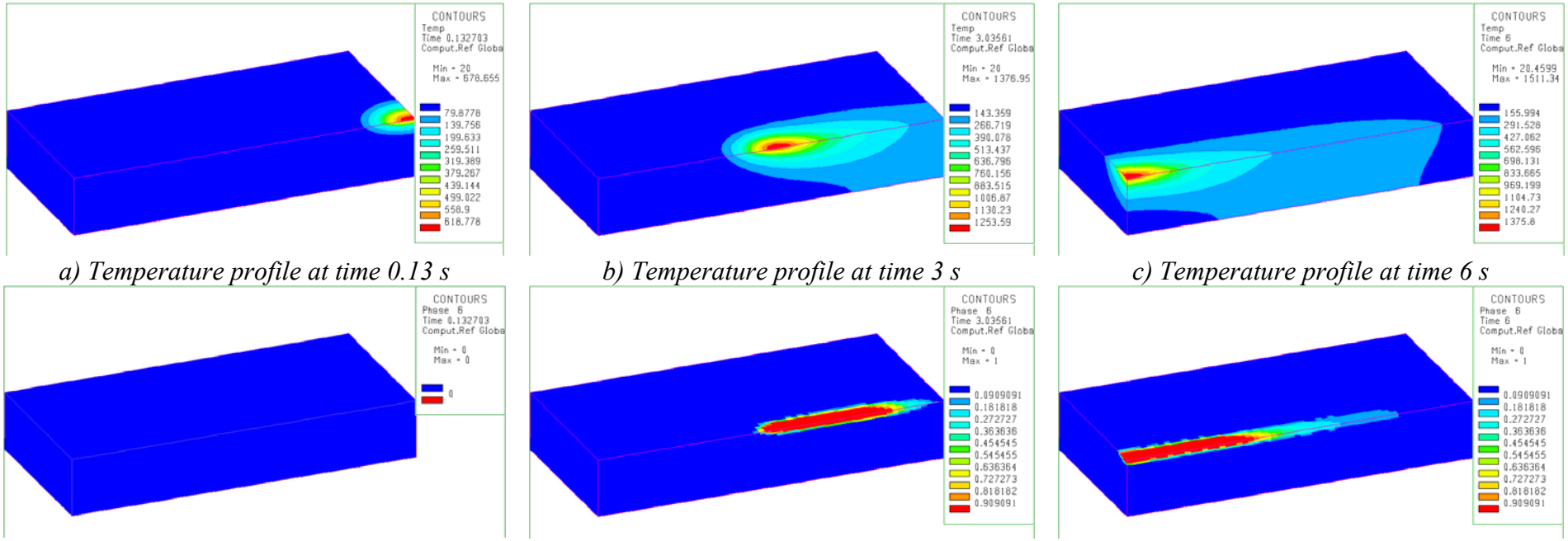


*a) Temperature profile at time 0.13 s* *b) Temperature profile at time 3 s* *c) Temperature profile at time 6 s*

*d) Austenite distribution at time 0.13 s* *e) Austenite distribution at time 3 s* *f) Austenite distribution at time 6 s*

*Figure 4.25 Temperature profiles and austenite phase distribution of LTH in different times*

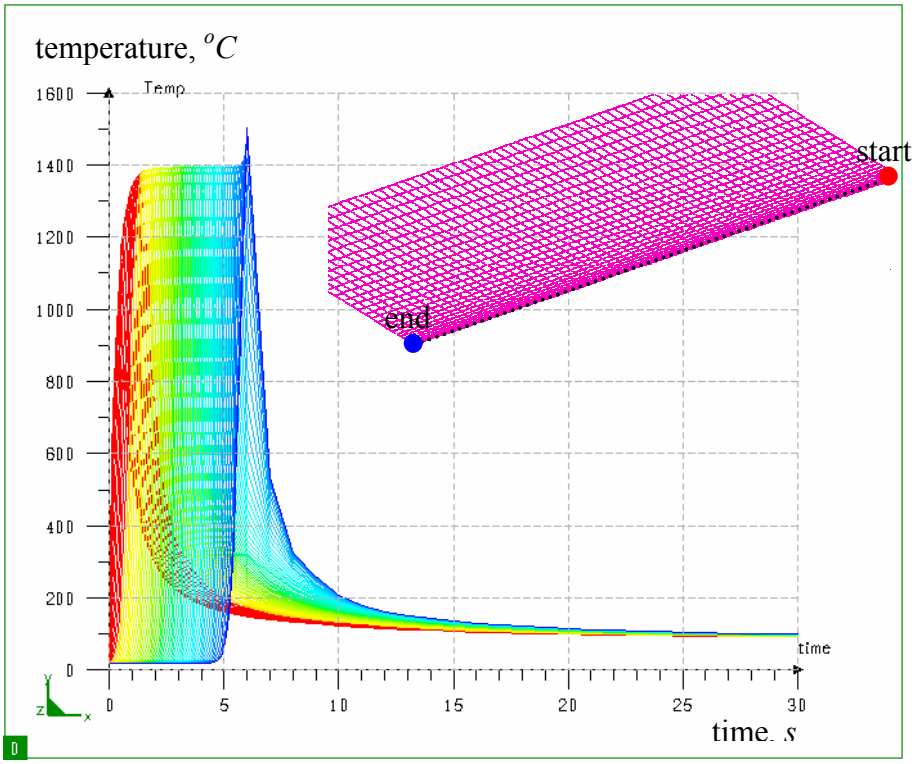


*Figure 4.26 Time-temperature curves of all nodes of the trajectory line*

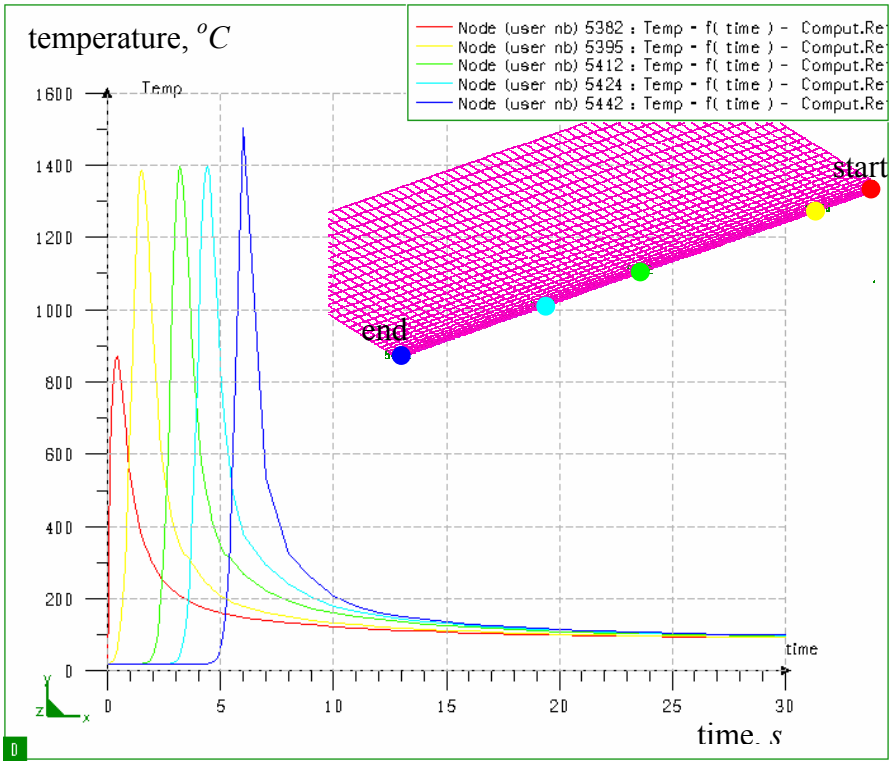


*Figure 4.27 Time-temperature curves of different nodes over the surface*

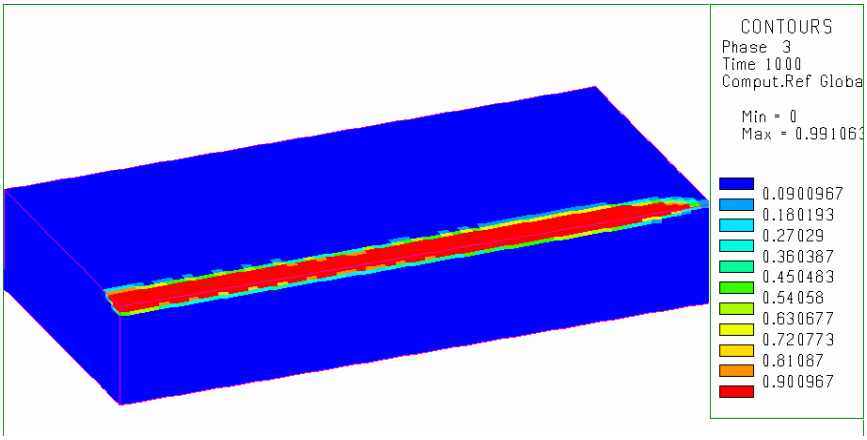


*Figure 4.28 Martensite distributions along the laser path*

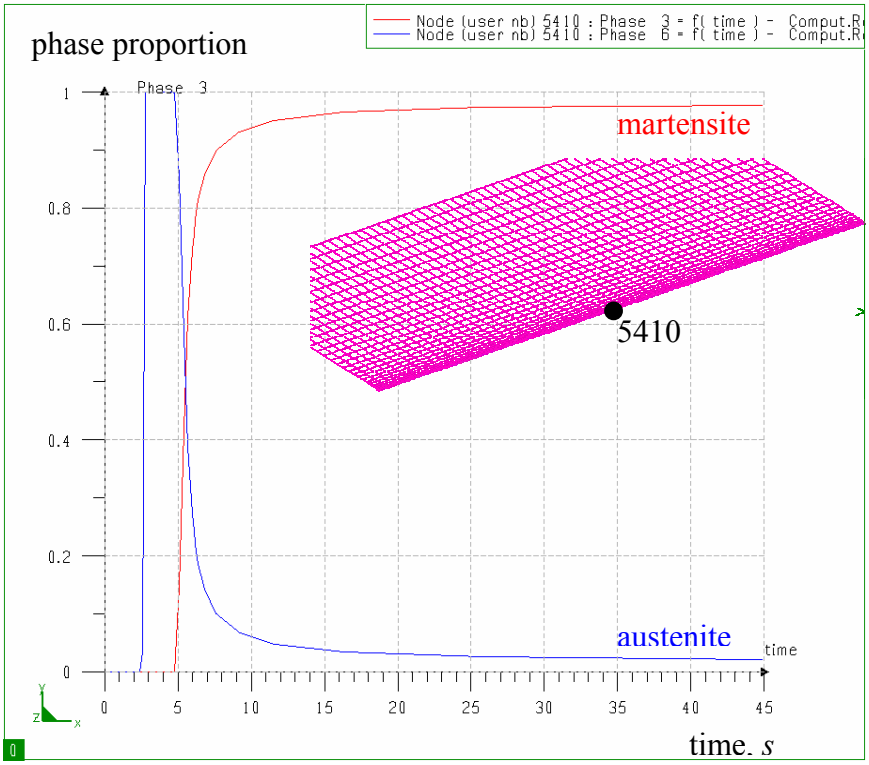


*Figure 4.29 Phase proportion versus time of a single node on the surface*

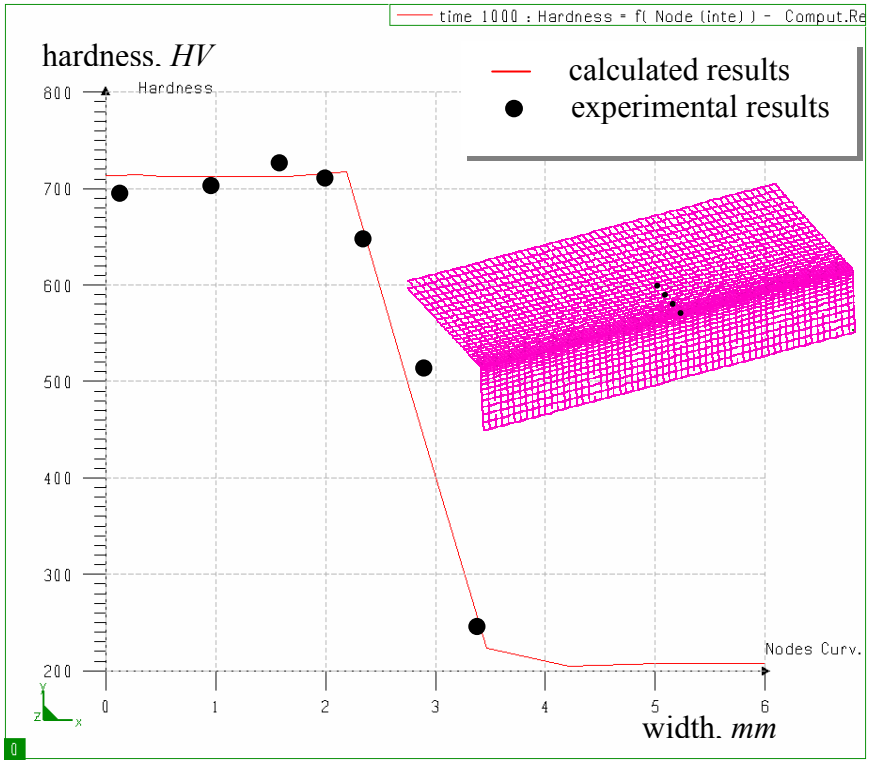


*Figure 4.30 Hardness profiles along the surface*

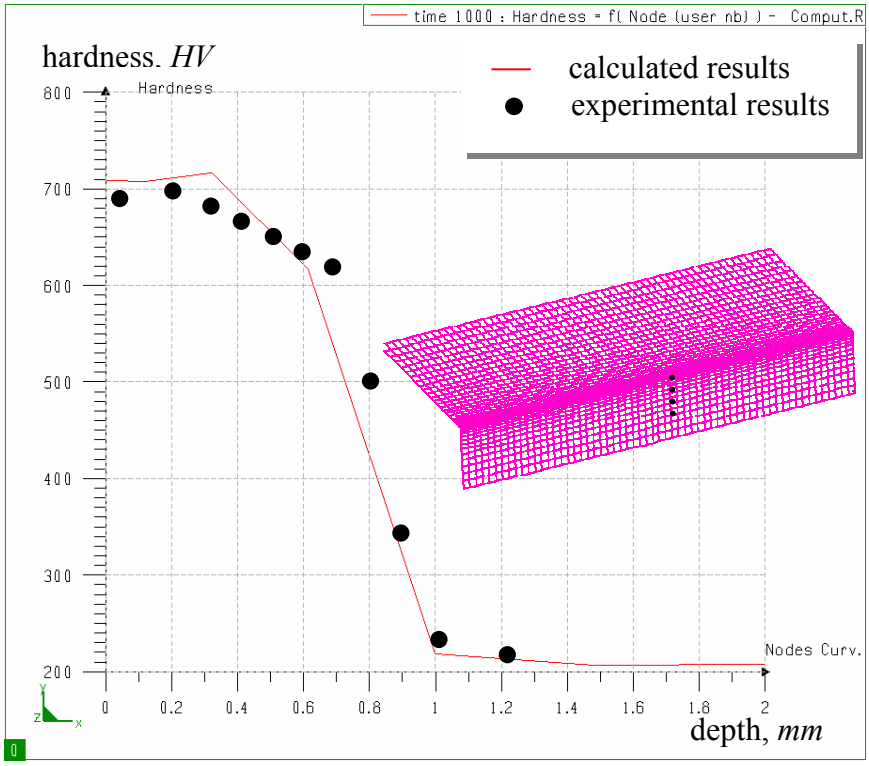


*Figure 4.31 Hardness profiles in depth*

## 4.8 LTH Operable Regions for Quasi Steady State Condition

For a better and wider application of LTH process in industries, it is necessary to establish appropriate relationship between the output and the input parameters. It is necessary to know the operating range of these parameters for LTH of steels for proper application in industries.

In the following, operating regions of quasi steady state conditions where the process is assumed to be steady along the travel direction of the laser beam will be introduced. The procedure is to find the process parameters for LTH namely, laser power ($P$), beam radius ($r_0$), and the scanning rate ($v$) within two constraints, namely, critical beam radius for no melting of the surface and critical beam radius for a hardening depth of *0.12 mm*. The simulation procedures are shown in *Figure 4.32*.

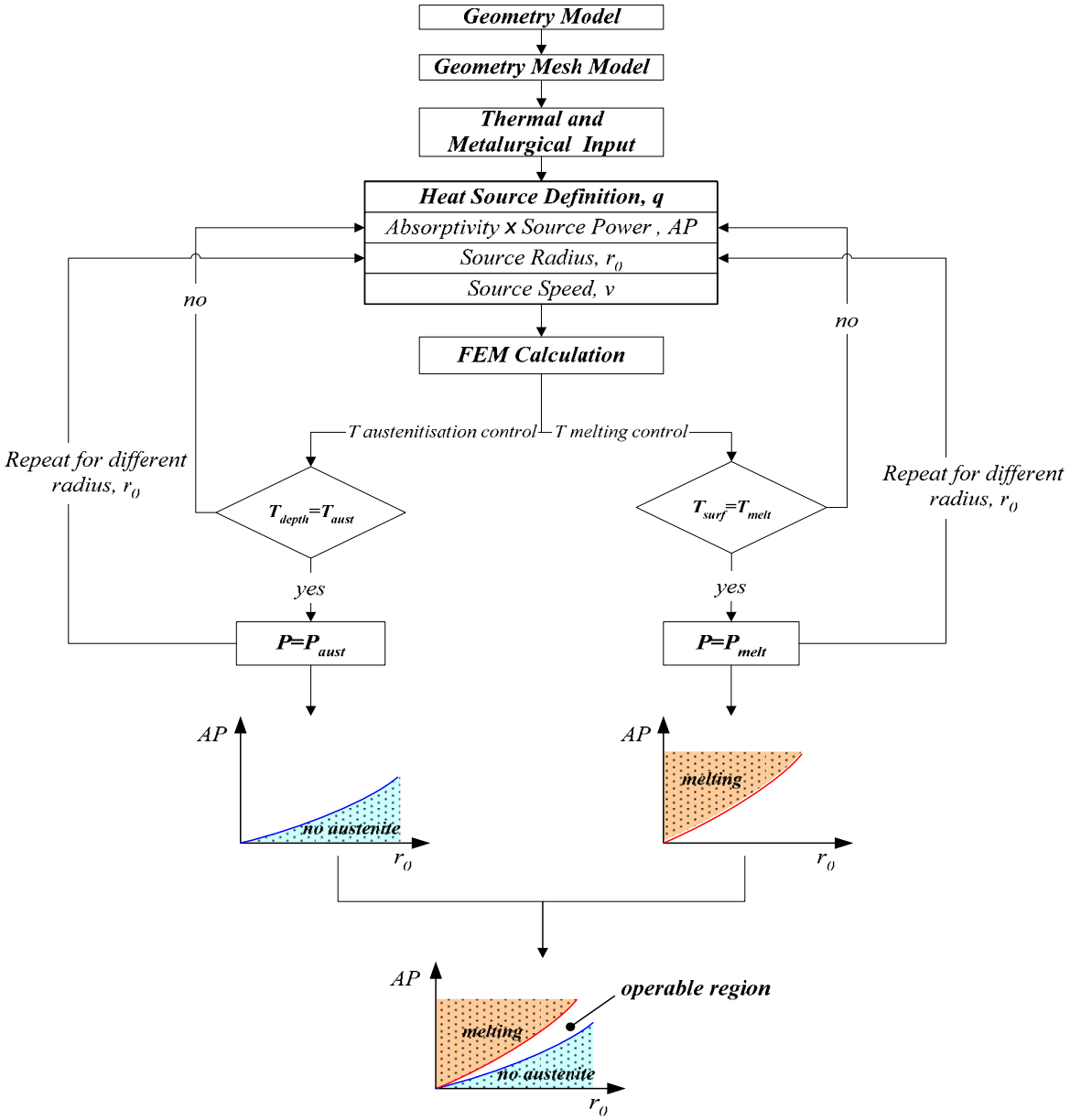


*Figure 4.32 Simulation procedures to find operable regions for single track steady state LTH conditions*

In this figure $q$ is the heat flux density of the Gaussian source, $A$ is the absorptivity, $r_0$ is the beam radius, $v$ is the laser scanning rate, $T_{depth}$ is the temperature at a defined depth, $T_{asut}$ is the austenitisation temperature, $T_{surf}$ is the surface temperature, $T_{melt}$ is the melting temperature, $P_{aust}$ is the power sufficient to reach the austenitisation temperature at a defined depth and $P_{melt}$ is the power which results in melting of the surface.

The finite element thermal calculations were applied for C45 steel using laser scanning rates of *10*, *20*, *30*, *40* and *50 mm/s* and laser beam radii, Gaussian radius ($r_0$), of *0.5*, *1*, *2*, *3*, *4* and *5 mm* to determine the safe operation region for LTH processes.

The phase transition temperature for C45 steel is taken as *930 $^oC$* and the melting temperature as *1450 $^oC$*. For no surface melting calculations, maximum temperature of the surface nodes were kept just below *1450 $^oC$* and for hardening depth, the minimum temperature of nodes below the surface by *0.12 mm* were kept above *930 $^oC$*.

The variation of the laser beam radius $r_0$, with laser beam power $P$, multiplied by the absorptivity $A$ of the material surface for different laser scanning rate $v$ are shown in *Figure 4.33*. These results indicate that the application of LTH process with a small laser spot, even for low power, can cause difficulties because the austenitisation and melting limit curves are intersecting or very close to each other. Low powers cannot be used because the power density will be too low to enable phase transition for the points in the workpiece at a depth of *0.12 mm* beneath the surface. Obviously further simulations can be done for wider laser spots.

Using the same FEM results, variation of the critical scanning rate for a hardening depth of *0.12 mm* and for no surface melting with laser power for different laser beam radii are shown in *Figure 4.34*.

These operating range diagrams give an indication of the degree of flexibility of laser transformation hardening process.

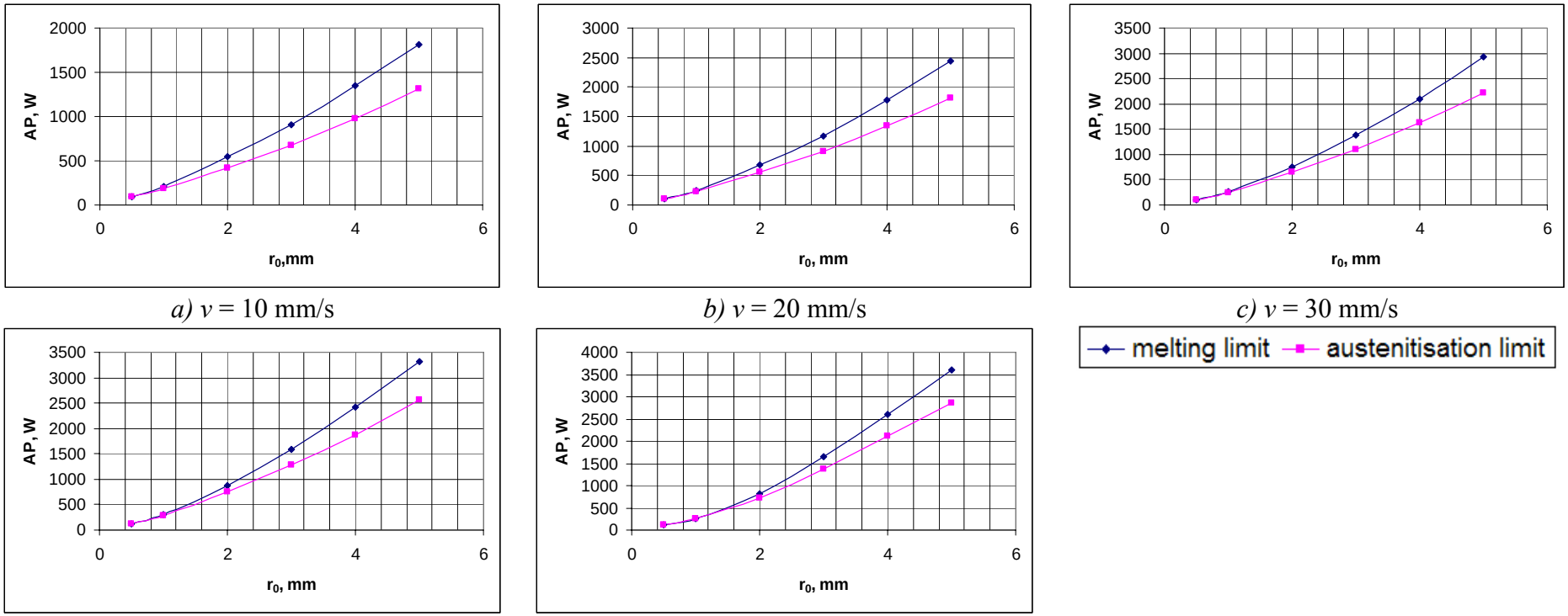


*a)* $v$ = 10 mm/s

*b)* $v$ = 20 mm/s

*c)* $v$ = 30 mm/s

*d)* $v$ = 40 mm/s

*e)* $v$ = 50 mm/s

*Figure 4.33 Operating regions by variation of laser beam radius with power for LTH of C45 steel with different scanning rates*

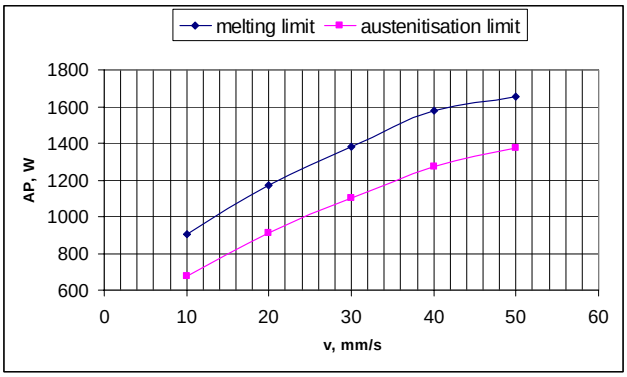


*a) $r_0$ = 3mm*

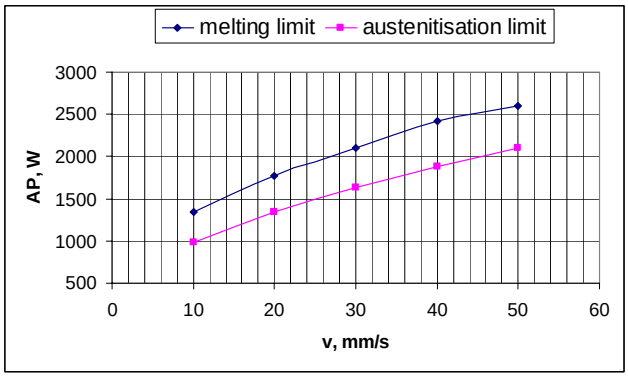


*b) $r_0$ = 4mm*

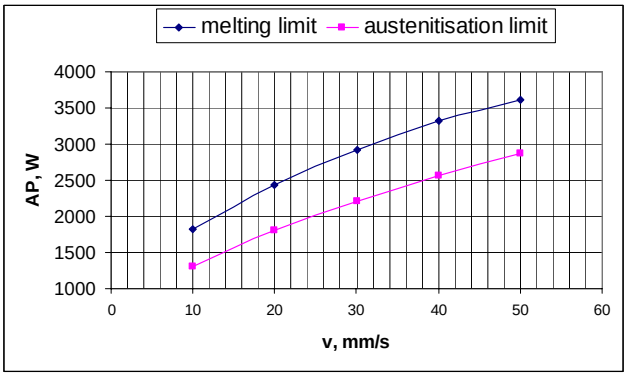


*c) $r_0$ = 5mm*

*Figure 4.34 Operating regions by variation of laser scanning rate with power for LTH of C45 steel with different beam radii*

# 5. TEMPERATURE CONTROL DURING LTH PROCESS

## 5.1 Introduction

In order to achieve successful laser transformation hardening and maintain the quality of the workpiece, it is of the utmost importance to reach the austenitisation temperature at the desired depth and avoid surface melting. The new contribution of this chapter is the development of the optimal temperature control strategy for laser transformation hardening using System Interface Language (SIL). SIL is the communication interface language between the user and SYSWELD code. Since in LTH usually the moving velocity (scanning rate) of laser beam is kept constant, the most important control parameter is the input laser energy. The input laser energy is modelled as a Gaussian distribution, described in the previous chapter. The method is to control the input laser energy to achieve a constant temperature interval, or even a constant temperature at any point of the workpiece. The simulation result is then a constant temperature interval for selected group of nodes and a text file with changing maximum heat flux density, $q_0$, as a function of time, $s$.

## 5.2 System Interface Language

The proposed language, SIL, is the SYSWELD FEM code system interface language. SIL enables users to carry on an interactive dialogue on the screen or perform a non interactive processing in which the user has the possibility of writing own commands called procedures or functions called user functions.

The structure for a SIL program is the function. Functions are structured by blocks, and grouped in procedures associated with files. Distinction is made between three structure levels. These are the procedure, function and instruction blocks (*Figure 5.1*). An instruction block can contain other instruction blocks. On the other hand, a function cannot contain the definition of another function.

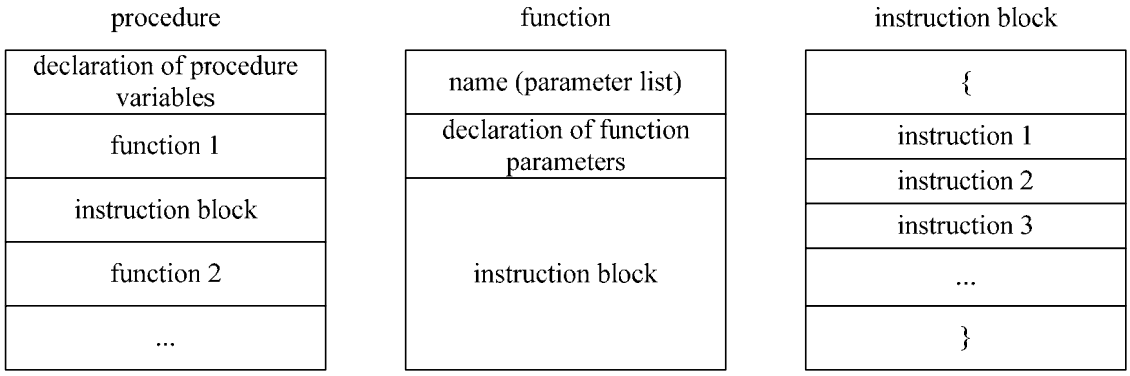


*Figure 5.1 Procedures, functions and instruction blocks*

A procedure is used to associate a name with an algorithm operation. It comprises a variable declaration field, and a set of functions. A function is used in common with a procedure to associate a name with an algorithm operation, although the characteristic of a function is that it delivers a value which can be used in an expression. A function comprises its declaration, containing a parameter list, a parameter declaration field and a single instruction block.

There are two types of functions:
- SIL standard functions,
- user functions.

Instruction block comprises symbol "{", and a sequence of instructions followed by the symbol "}".

To access SIL, three working modes are available:
- man-machine interface mode: the user enters instructions and commands in a specific graphic window,
- alphanumeric mode: execution of all instructions from analysis command interpreter,
- execution of instruction mode: execution of any single instruction from analysis command interpreter.

The other possibility is to define a file search path, using an environment variable. This variable can be used to define a list of directories in which SIL executes a systematic search for files, procedures or functions to be loaded [50].

## 5.3 Steps of Temperature Control Strategy

Geometry model and meshing which are followed by thermal and metallurgical phase transformation definition should be prepared. The heat source is modelled as a Gaussian heat distribution explained in section 4.7.2, that is a predefined maximum heat flux density and a constant laser spot (Gaussian radius, $r_0$) are the two parameters described analytically in the user written script, FORTRAN subroutine. To initiate the SIL program, an initial calculation

for time 0 should be done. A constant temperature ($T_{constant}$) with a $\Delta T$, which can be admitted as the temperature deviation, is defined in the program. This temperature restriction will be applied to any arbitrary group or groups of nodes that are already created in SYSWELD code. By these definitions the finite element analysis will start the first time step and calculate the temperatures of all nodes when starting the SIL program and the related files. In the next stage the program will search for the maximum temperature ($T_{max}$) calculated for the defined group(s) of nodes and will compare it to $T_{constant}$. If the maximum temperature is equal to $T_{constant}$ or is within $T_{constant} \pm \Delta T$ interval, the maximum heat flux density and corresponding time will be printed to a text file and the calculation will carry on with the next time step until the final time step of the process is reached.

If $T_{max}$ is not equal to $T_{constant}$ or not within $T_{constant} \pm \Delta T$ interval, the two possibilities of $T_{max} > T_{constant}$ and $T_{max} < T_{constant}$ are considered. If $T_{max} > T_{constant}$ , the program will automatically change the value of the maximum heat flux density ( $q_0$ ) into a new maximum heat flux density ( $q_{0new}$ ), which will be used as an input of the next iteration, using the following formula,

$$q_{0new} = \left( \frac{T_{constant} - T_{max}}{T_{max}} + 1 \right) \cdot q_0 . \qquad \textit{Eq. 5.1}$$

For $T_{max} < T_{constant}$ , $q_{0new}$ is calculated as

$$q_{0new} = \left( \frac{T_{constant} - T_{max}}{T_{constant}} + 1 \right) \cdot q_0 . \qquad \textit{Eq. 5.2}$$

The flowchart of the temperature control strategy simulation is shown in *Figure 5.2*. To consider a constant temperature interval, the calculation is done in such a way not to exceed the upper and lower limits of the $T_{constant}$. By this method the temperature of any single point of a workpiece can be controlled regardless of the geometry, material and process parameters.

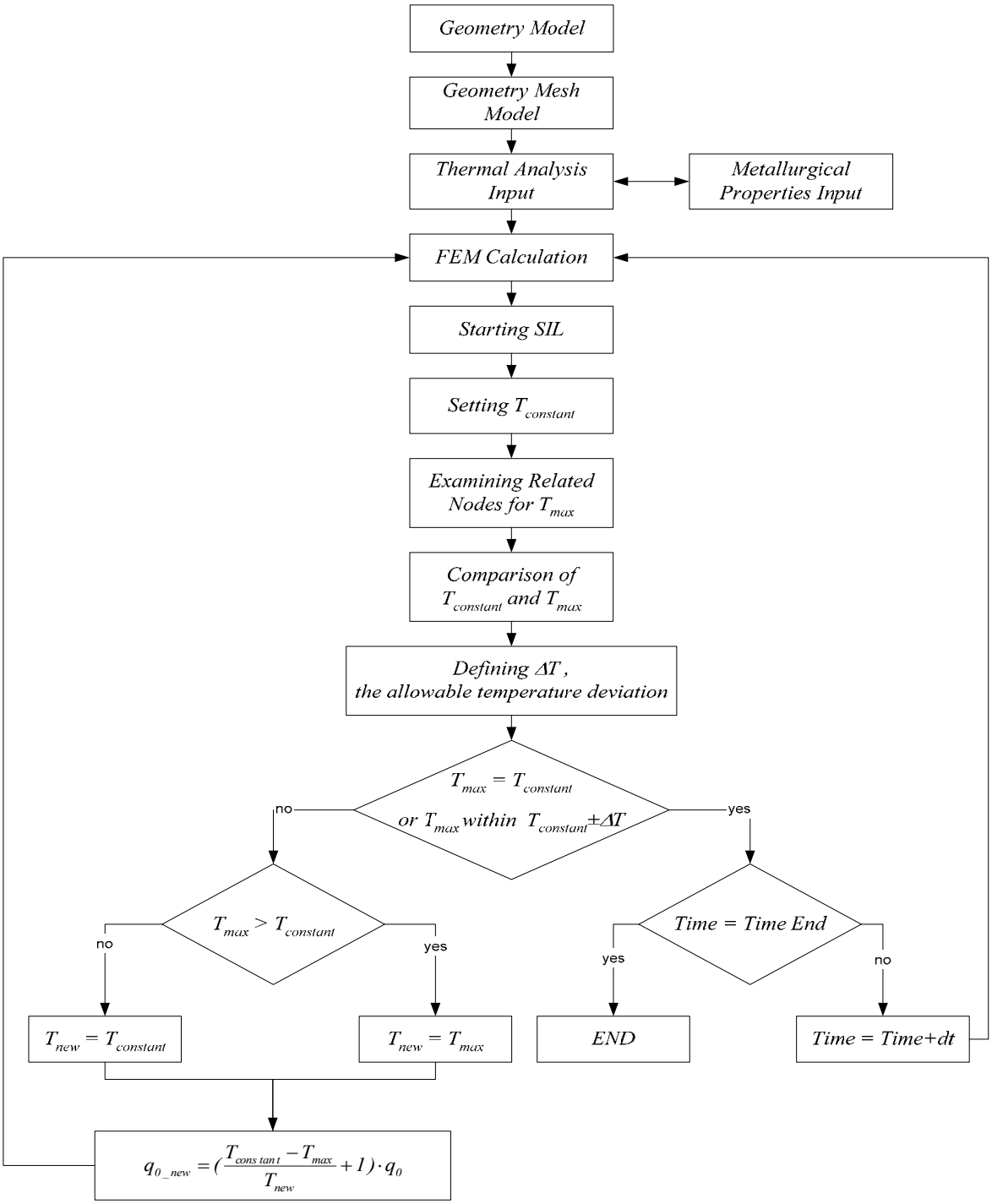


*Figure 5.2 Temperature control simulation strategy flowchart*

## 5.4 Application of Temperature Control Strategy

Obviously, controlling the temperature during a process can be an effective tool and is applicable in different thermal fields. Considering the laser transformation hardening it is of a great importance to overcome critical difficulties such as

- starting and ending moments of a process, in other words the transient states,
- being close to the edge of the workpiece and corner problems,

- complex geometry,
- necessity to overlap the hardening passes (influence of prior thermal effects).

### 5.4.1 Transient States and Edge Problems

In the following examples single track laser transformation hardening processes are modelled to overcome both the transient states and the edge problem together.

For the sake of comparisons, modelling of a single pass laser transformation hardening was made on a workpiece with the same geometry dimensions, material and process parameters used in the previous chapter. The difference here is that we have applied the developed temperature control SIL program module to keep the temperature of the surface in $T = 1395 \pm 10\ ^{o}C$ interval by variation of the laser input power. This temperature interval was taken as the melting limit of the surface or the maximum temperature to be allowed in the calculations. In other words, laser source with Gaussian distribution and radius of, $r_0 = 5$ mm, is applied on the workpiece surface. In this case the maximum heat flux density is to be calculated in iteration manner to attain the predefined temperature interval.

Considering the *10 mm/s* scanning rate and the length of the workpiece, the time in which the laser is impinging on the surface is *6 s*. The time increment set for calculation of laser impinging time, $t = 0 - 6s$, is *0.1 s*. To simulate the cooling period of the process when the laser source exits the workpiece, thermal load is removed and the final result of the previous calculation is taken as the initial condition of the new calculation without running the SIL program. The time increment for the cooling is *1 s*.

Temperature distribution results of single pass LTH simulation results without controlling the temperature, when the heat flux density is constant, are illustrated in *Figure 5.3*. Temperature distribution results of LTH with controlling the maximum temperature interval ($T = 1395 \pm 10\ ^{o}C$), by changing the heat flux density, using the new input subroutine are shown in *Figure 5.4*. The temperature along the trajectory line is kept within the defined interval while in *Figure 5.3* the maximum temperature at $t = 0.2s$ was $802\ ^{o}C$ and at $t = 6s$ was $1505\ ^{o}C$. This proves the validation of the temperature control model for a single pass LTH process.

Temperature deviation occurring during the process, results in an inhomogeneous martensite distribution (*Figure 5.5a*). The increase of maximum heat flux density, $q_0$, at the beginning of the process will increase the surface temperature to satisfy the austenitic transformation that is obviously followed by martensitic transformation. In this case a desired amount of martensite is the result as shown in *Figure 5.5b*.

To examine the phase transformations, nodes denoted by letter *A* and *A'*, for constant $q_0$ and temperature controlled calculations respectively, on the trajectory line at a distance of *1 mm* from the edge of the workpiece were chosen to demonstrate the phase transformations and their proportions in *Figure 5.5c* and *Figure 5.5d*. Austenite and martensite proportions were satisfactory during the whole process when the temperature was controlled. This cannot be stated for the case where $q_0$ is constant along the trajectory. The accumulation of heat at the end of the workpiece can lead to surface melting and the low temperature at the start of the process results in no austenite formation and consequently no martensite is formed in this section.

To have such constant temperature interval the maximum heat flux density should be changed as illustrated in *Figure 5.6*. This is the result of the simulation printed in a text file as mentioned earlier using SIL. Maximum heat flux density and the Gaussian radius are the characteristic parameters of the Gaussian source. Laser power, which is the area under the

Gaussian curve, can be calculated by *Eq. 4.19*. Therefore the results can be illustrated as a function of laser power which is a controllable process parameter for laser machines as in *Figure 5.7*.

Calculations of different laser spot sizes were made to examine the effect of the spot size on the process. If the Gaussian radius $r_0$ changes while all other parameters remain unchanged, diagrams with laser power versus time to keep the surface temperature just below the melting limit are shown in *Figure 5.8* for different scanning rates. The melting limit temperature was assumed to be $T = 1395 \pm 10\ ^oC$ as mentioned earlier.

Since the penetration depth of LTH process is small, the heated zone is rapidly quenched by self cooling, leading to martensitic transformations. Due to the high cooling rate of LTH we may assume that the austenite will be completely transformed into martensite. In other words, to decide the hardened part of the workpiece, it is sufficient to trace the austenitisation temperature.

To assure austenitisation at a desired depth, a group of nodes was created at the depth of *0.12 mm*, positioned under the centre of the laser source, and the temperature of these nodes was kept just above the austenitisation limit, which was assumed to be $930^oC$. Curves indicating power as a function of time for austenitisation limits of different laser spots and scanning rates can be observed in *Figure 5.9*.

As the laser beam spot becomes smaller it gives more local intensity heating but smaller depth of hardening. This means that a surface heated by a laser beam with small diameter reaches austenitisation temperature, even with a low laser power but the depth of hardened zone in this case is small. The depth of hardened layer can be predicted by the hardness where the high hardness attributes to the existence of martensite. Hardness results in *Figure 5.10* prove the dependency of the hardened depth on the spot size.

Laser scanning rate is one of the parameters which have a great influence on the LTH process. As the scanning rate of the laser beam increases, the required power to heat the surface of the material to a desired temperature should also increase. The introduced controlled temperature strategy gives the needed power as a function of time for every single time step of the calculations. Effect of scanning rates on the LTH for a laser spots of *4* and *5 mm*, by applying surface melting limit and austenitisation limit at depth of *0.12 mm* , are shown in *Figure 5.11*. While the surface temperature is kept below melting limit the depth of the hardened zone decreases by increasing the scanning rate. Austenitisation limit curves can be used to assure austenitisation at a desired depth by changing the laser power as a function of time to achieve the required temperature for austenite formation.

Obviously various operable regions can be extracted from the melting and austenitisation limits as shown in *Figure 5.12*.

The SIL initiation file (T0.DAT), SIL for meting and austenitisation limits (tc.cmd), the initial condition, boundary conditions, heat source definition program (T1.PAR), the cooling process (T_COOL.DAT) and hardness calculation (HARDNESS_ALL.DAT) files in Appendix 3 are the necessary files to run a single track LTH using the temperature control strategy.

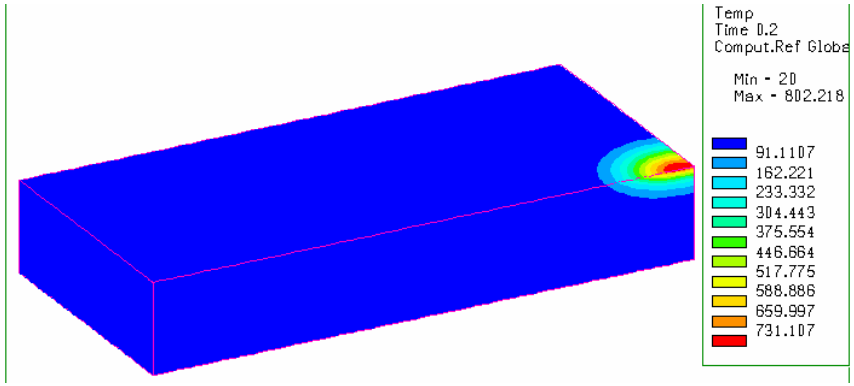


*a) Temperature profile at time 0.2s*

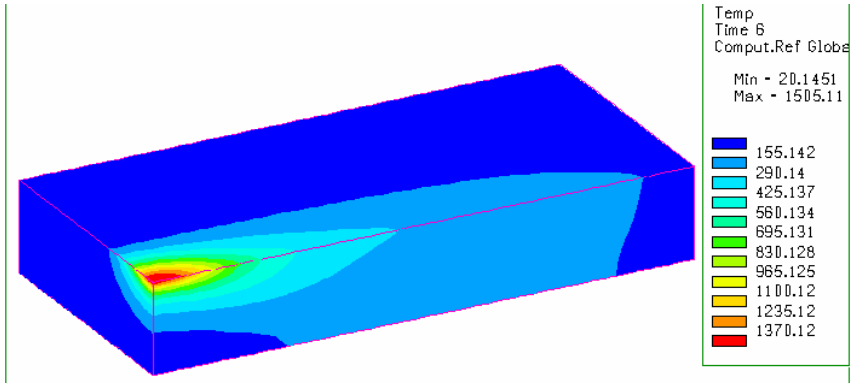


*b) Temperature profile at time 6s*

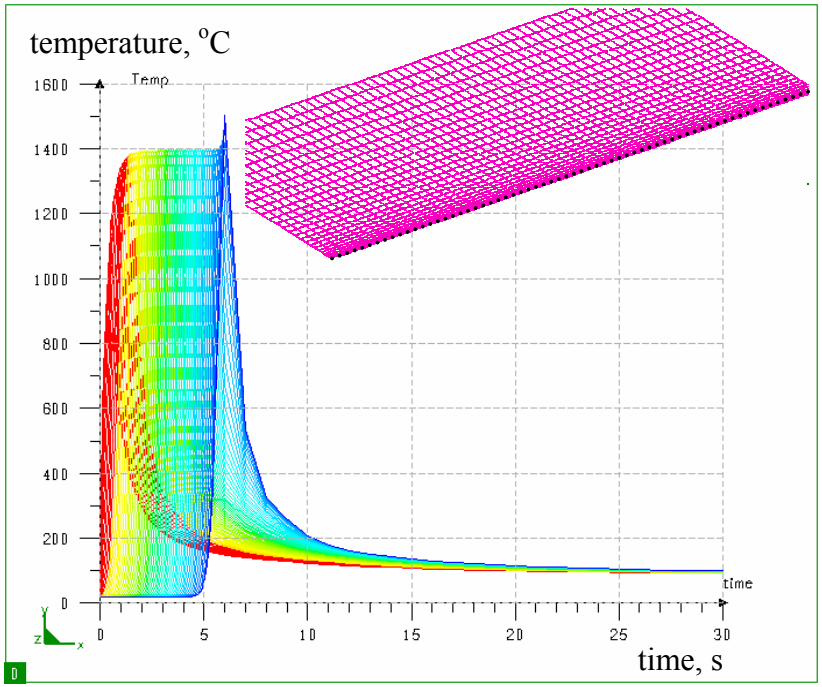


*c) Time-temperature curves of all nodes of the trajectory line*

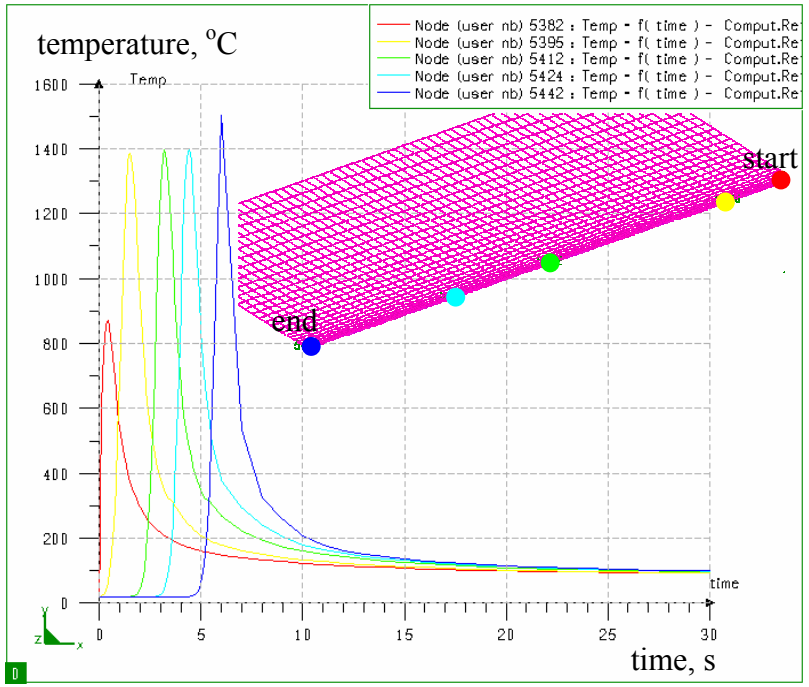


*d) Time-temperature curves of different nodes over the surface*

*Figure 5.3 Temperature profiles of single pass LTH of C45 steel with constant $q_0$*

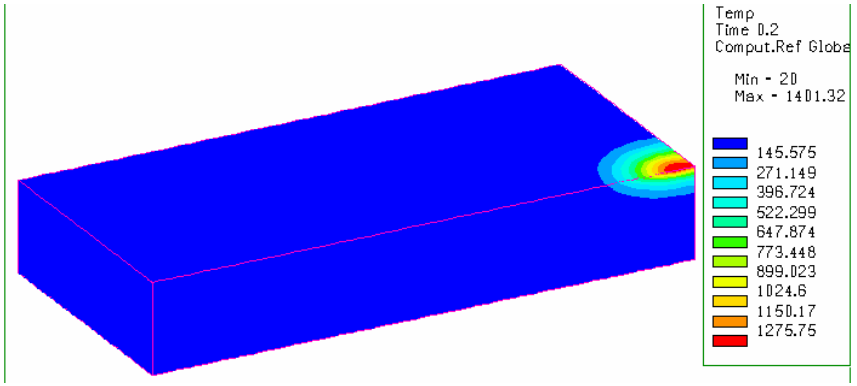


*a) Temperature profile at time 0.1s*

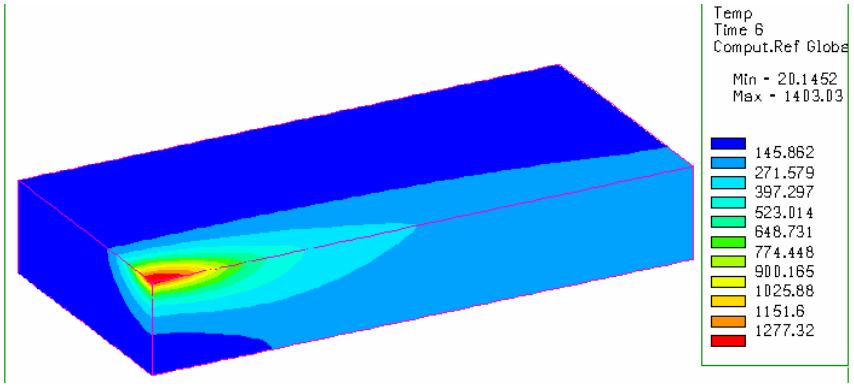


*b) Temperature profile at time 6s*

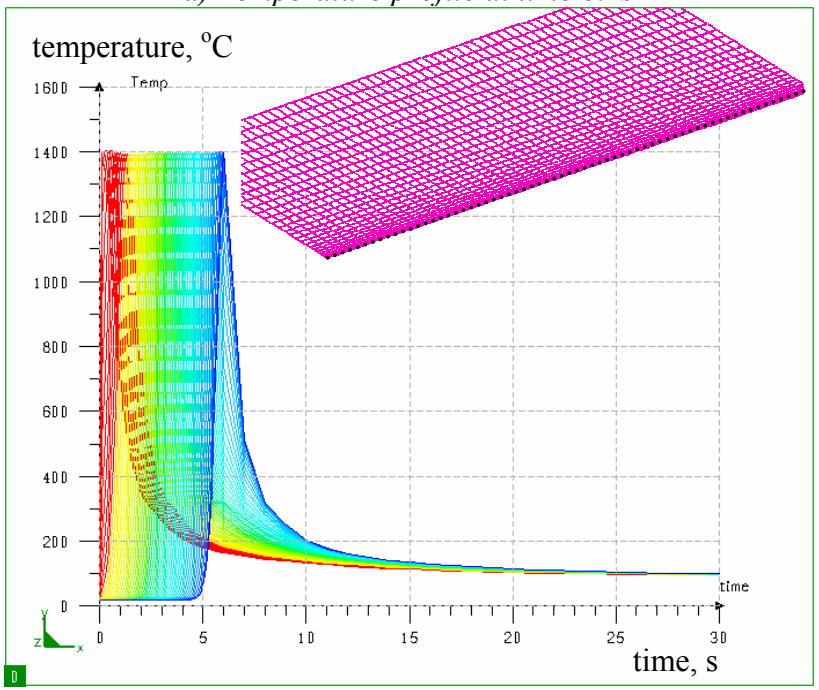


*c) Time-temperature curves of all nodes of the trajectory line*

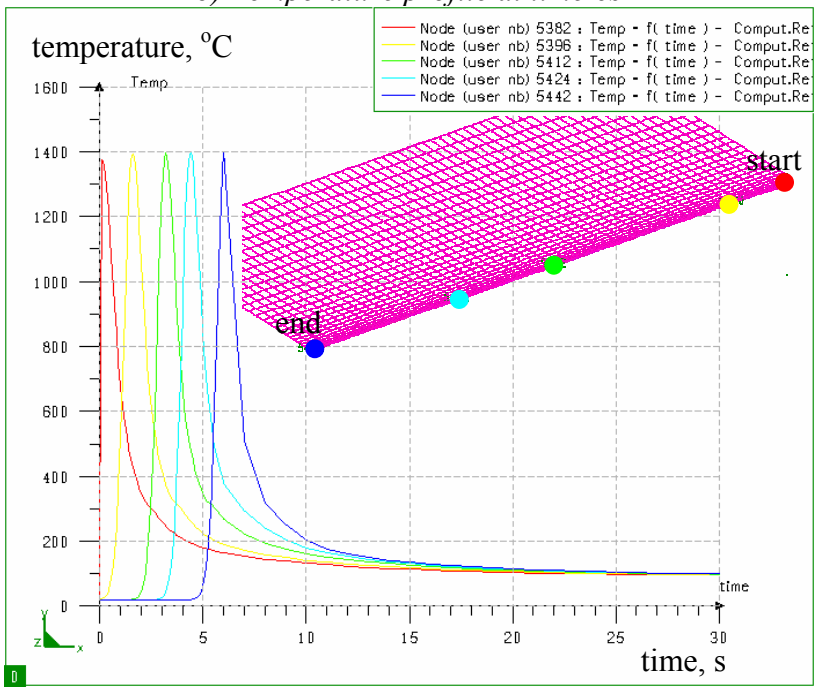


*d) Time-temperature curves of different nodes over the surface*

*Figure 5.4 Temperature profiles of single pass LTH of C45 steel controlled $q_0$*

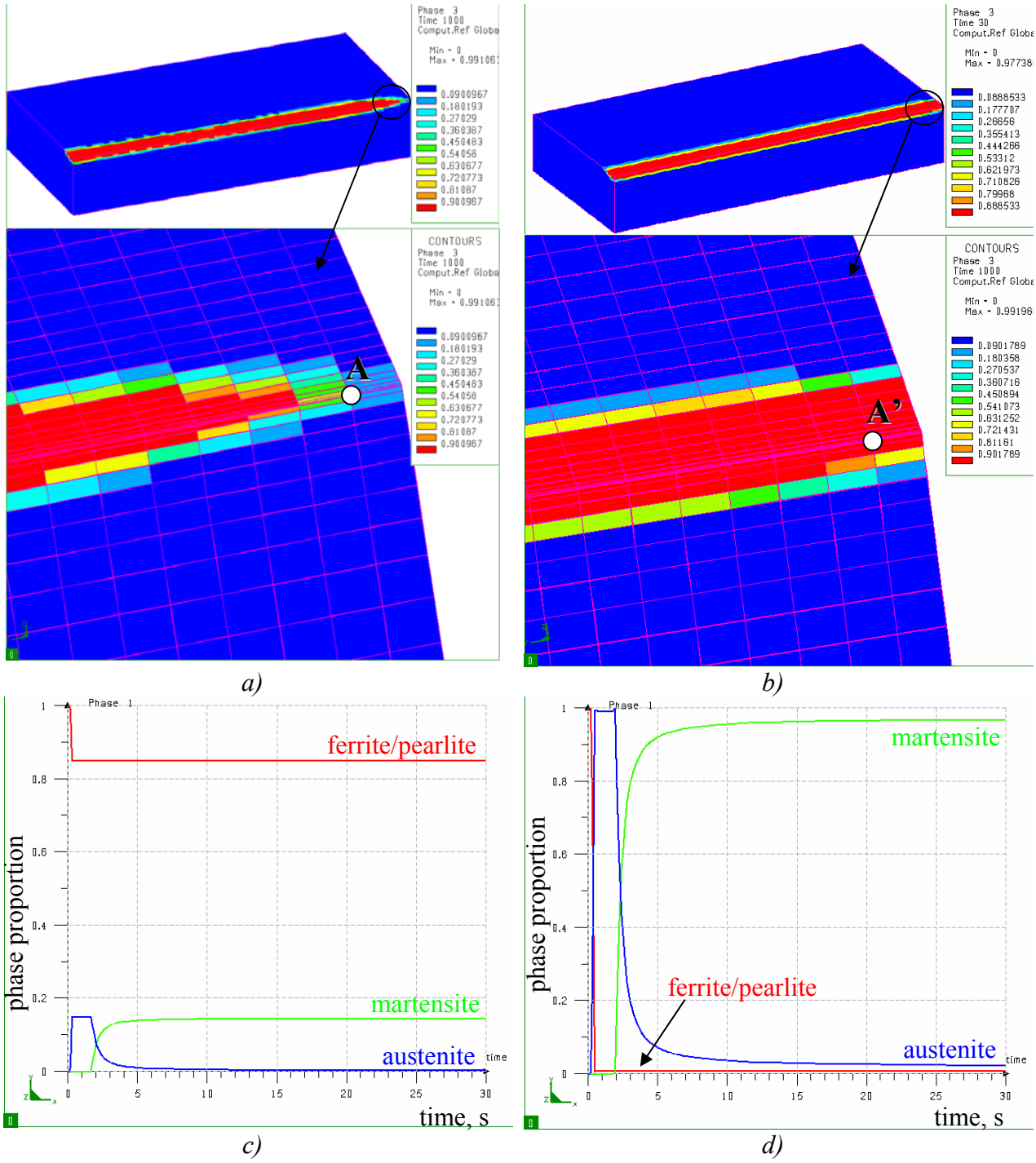


*Figure 5.5 Phase proportions; a) and c) martensite distribution and phase proportions of node A respectively for constant $q_0$, b) and d) martensite distribution and phase proportions of node A' respectively for controlled temperature*

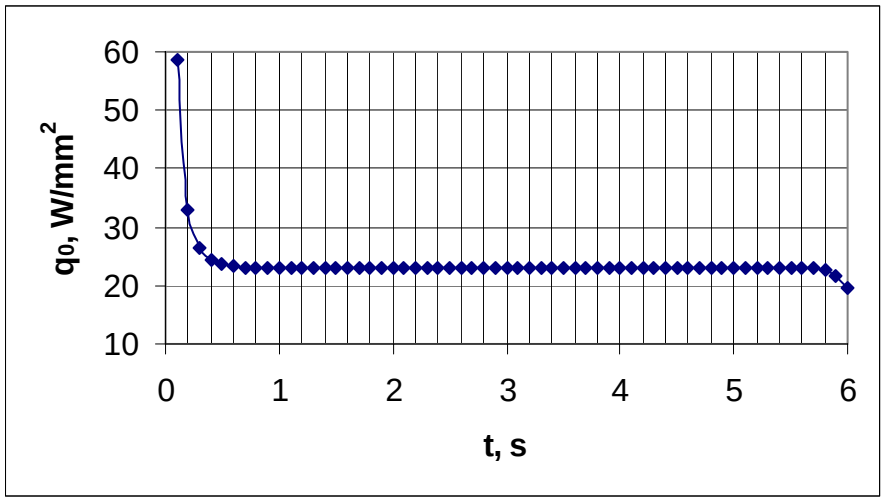


*Figure 5.6 Calculated maximum heat flux density as a function of time by SIL*

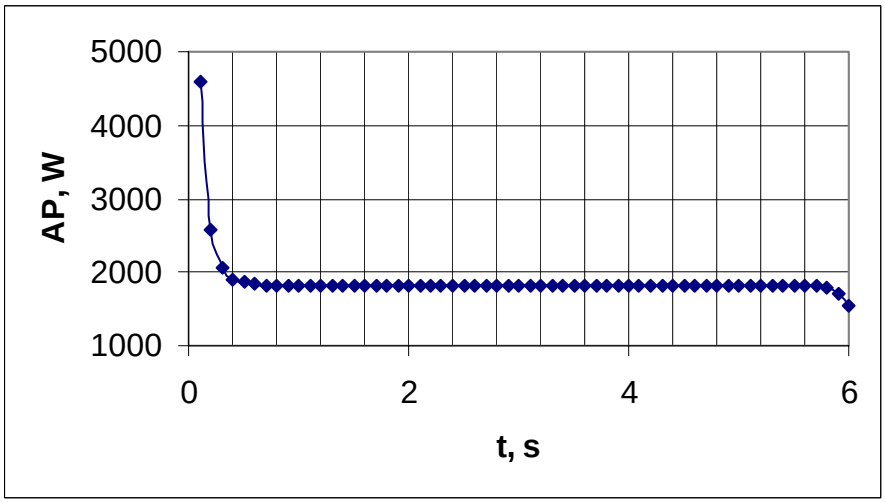


*Figure 5.7 Calculated power multiplied by the absorptivity as a function of time by SIL*

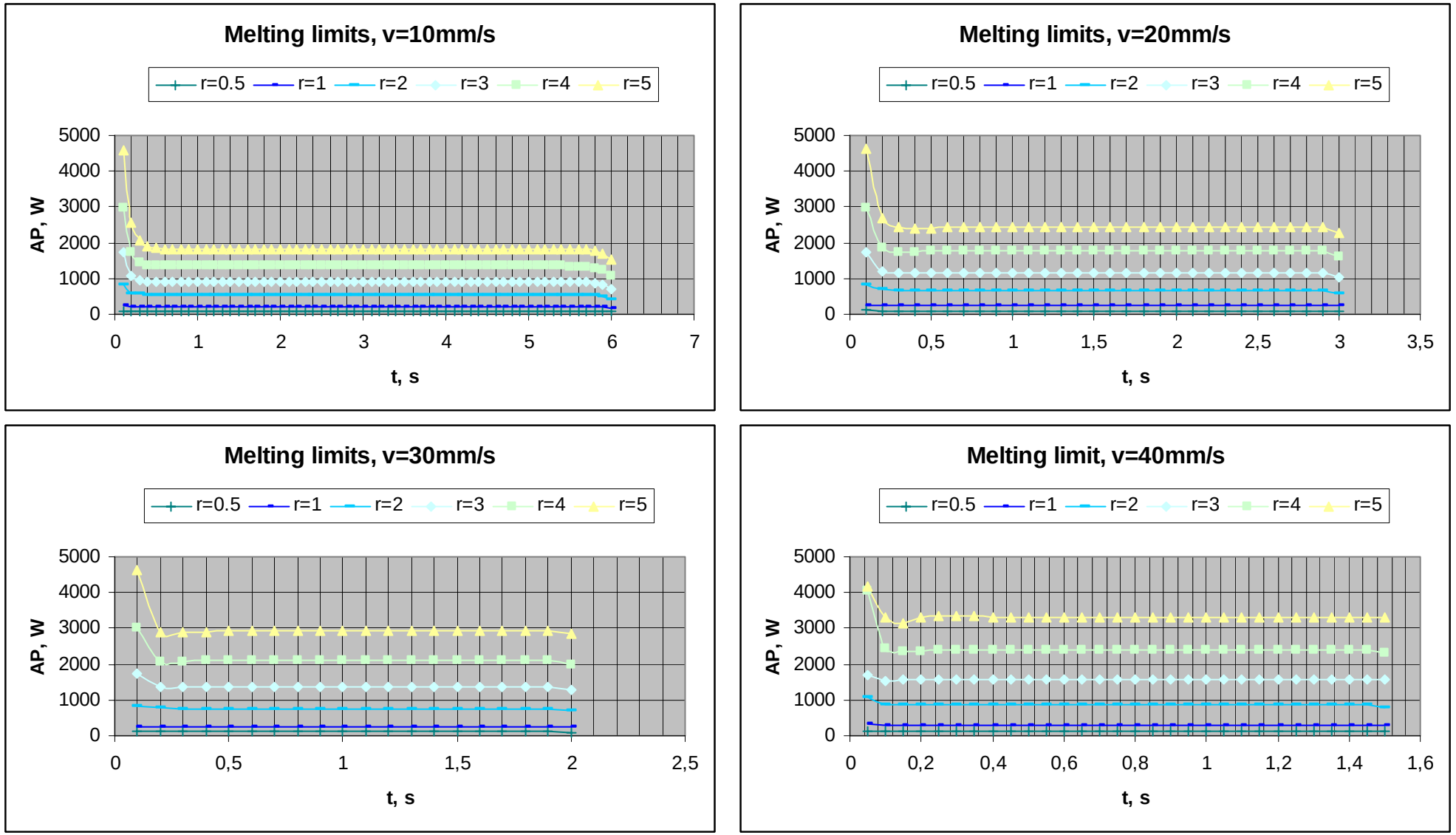


*Figure 5.8 Melting limit curves of single track LTH with variation of spot radius for different scanning rates*

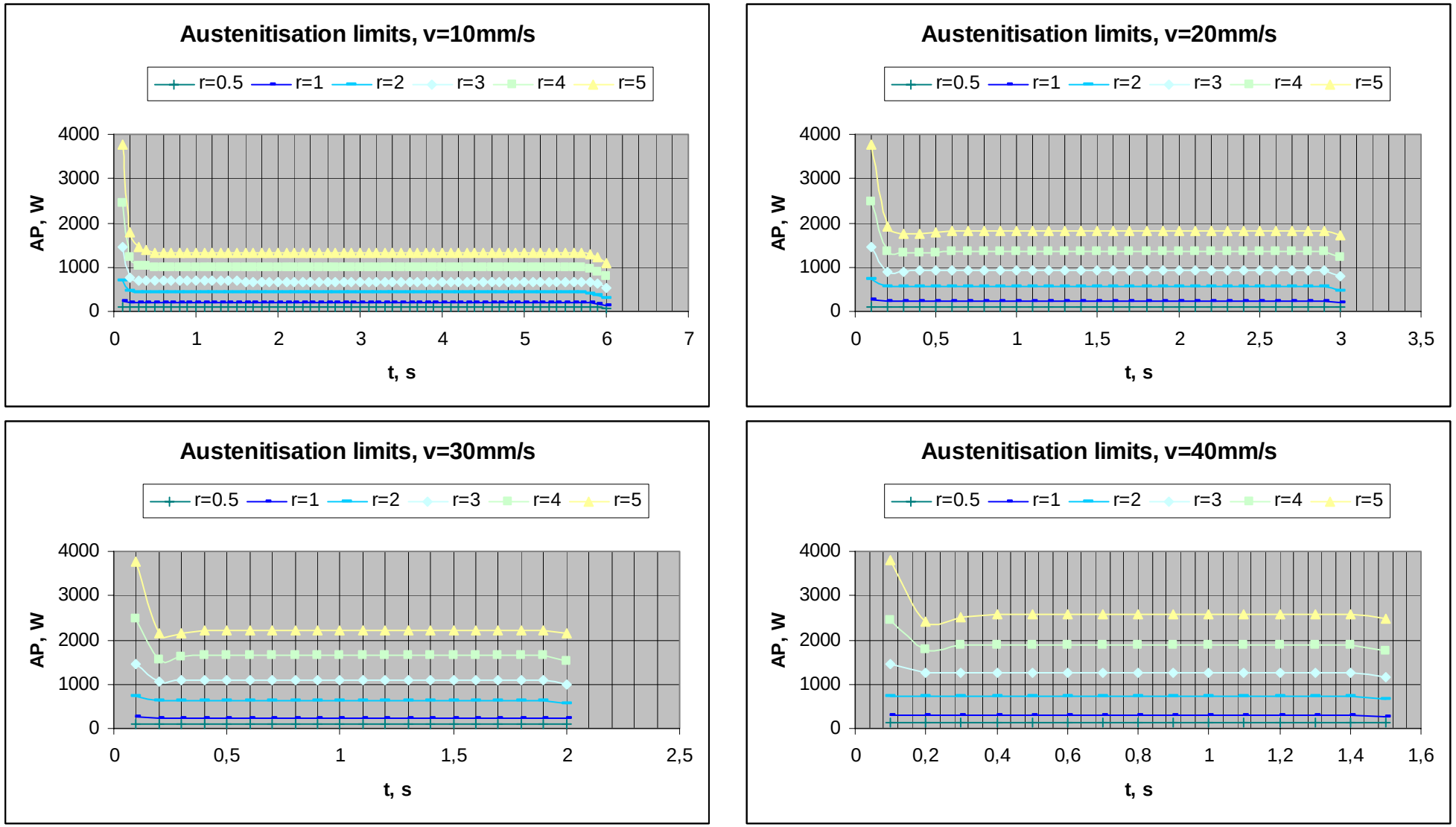


*Figure 5.9 Austenitisation limit curves of single track LTH with variation of spot radius for different scanning rates*

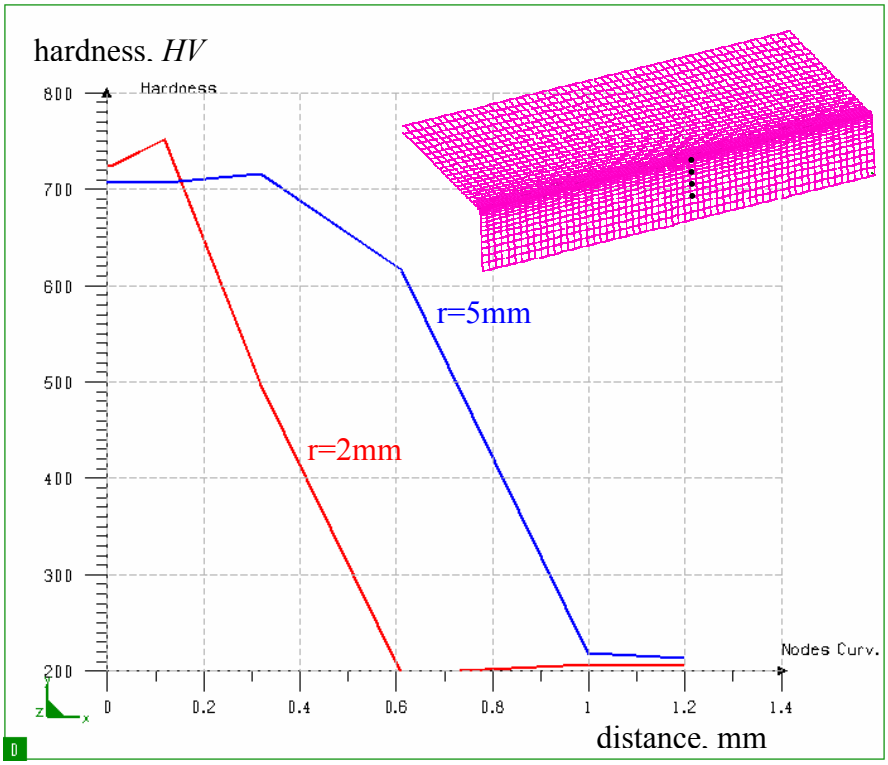


*Figure 5.10 Hardness profiles in depth for laser spot sizes*

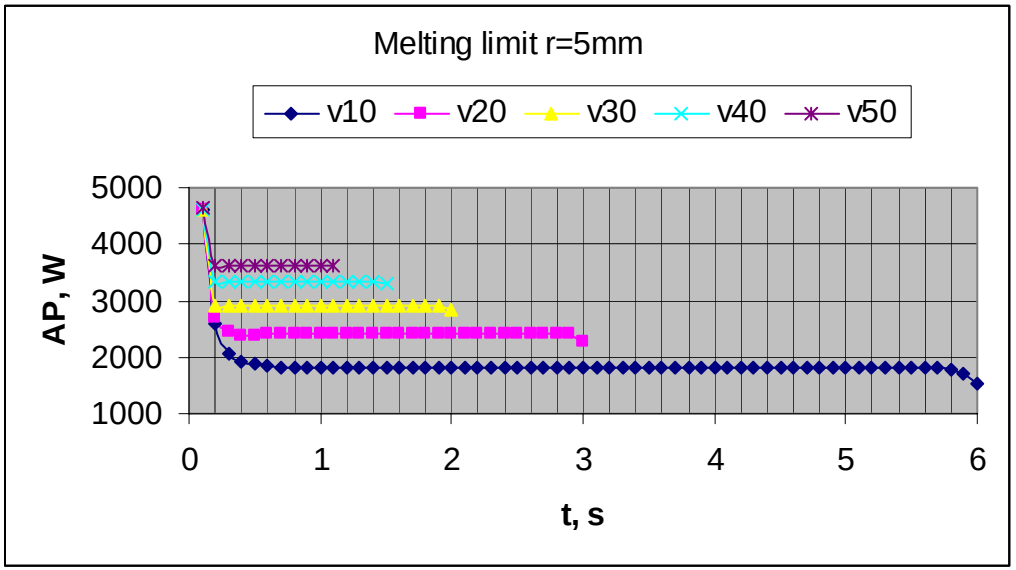


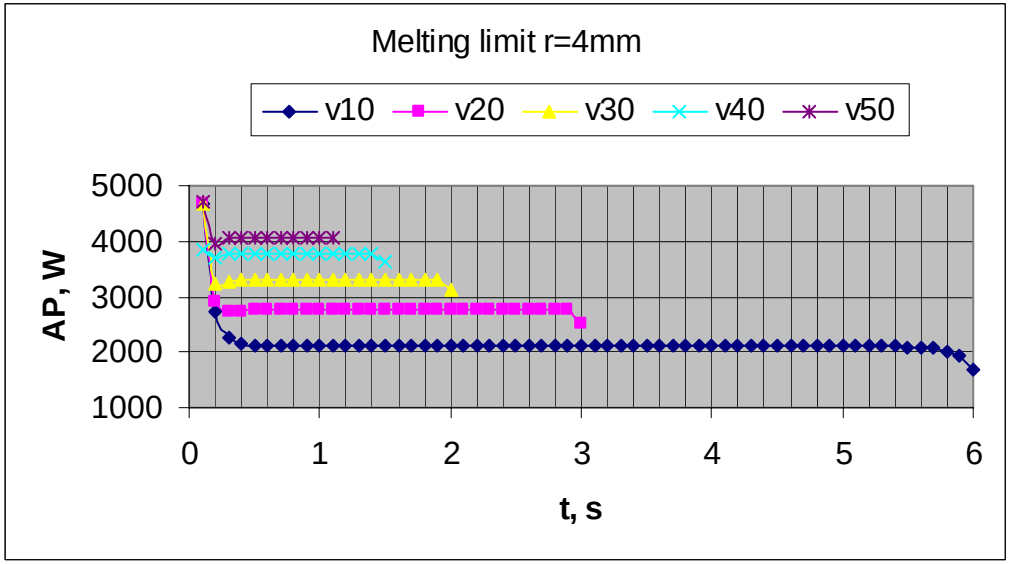


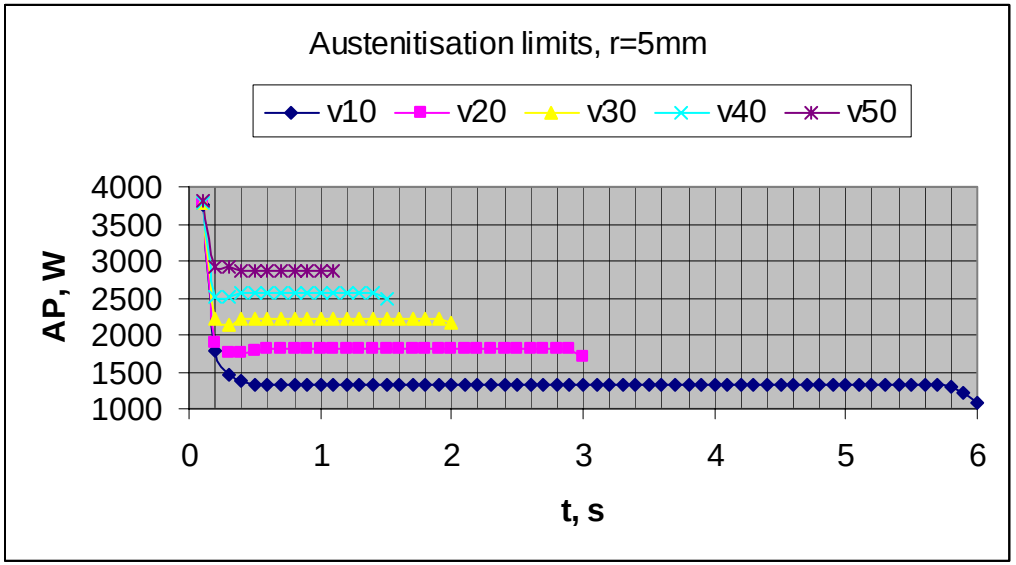


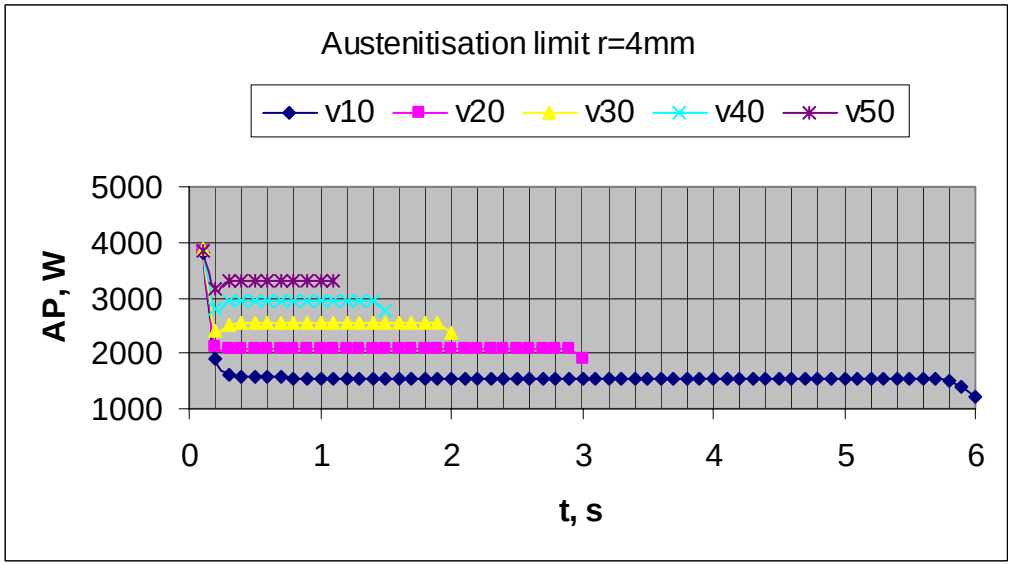


*Figure 5.11 Melting and austenitisation limit curves of single track LTH with variation of scanning rate for 4 and 5 mm spot radius*

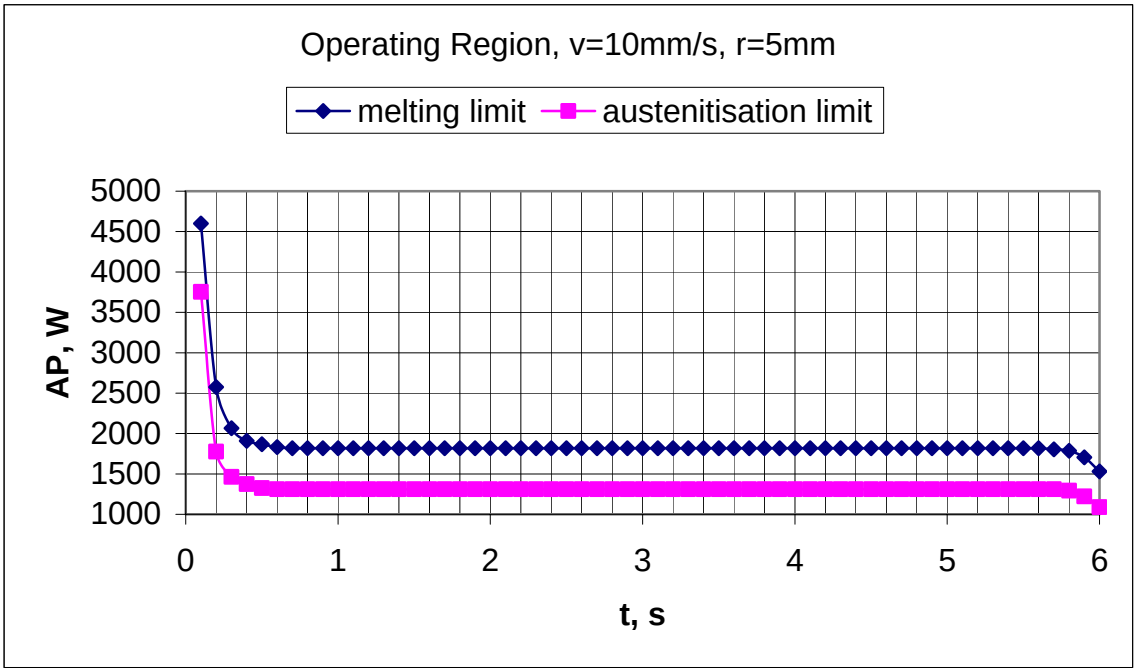


*Figure 5.12 Operating region of single track LTH for v=10mm/s and r=5mm*

### 5.4.2 Complex Geometries

Complexity of the workpiece or changes in geometry dimensions are other difficulties that one can face in laser transformation hardening processes. Two examples of single track laser hardening will be shown in this section to demonstrate the dimension change problems and the validity of the introduced temperature control strategy, to overcome these problems. Material definitions, initial condition, heat source and other boundary conditions are the same as previous models.

#### *Geometry With Inclined Surface*

The first geometry dimension with inclined surface can be seen in *Figure 5.13*. The laser source, applied normal to the surface of the workpiece, starts from the thicker edge, point A, and ends at the thinner edge, point B. The first simulation is carried out with constant process parameters, taken from LTH operating regions used for the steady state condition. Laser spot radius of *5 mm* with scanning rate of *10 mm/s* and maximum heat flux density of *23 W/mm*$^2$ are the parameters used for this calculation. Temperature distribution results for different time steps and the time temperature curves of the trajectory line nodes are illustrated in *Figure 5.14*.

Since the thickness of the workpiece decreases along the laser source movement, surface temperature starts to exceed the critical temperature at $t \approx 3$ s and it sharply increases as the process becomes closer to the end. Evidently, this is due to lack of bulk material to sink the heat that is the thermal conductivity behaviour of the workpiece changes at those locations.

To avoid the high deviation of the temperature during the whole process, the developed temperature control strategy was used in the following simulation to keep the temperature of the surface in the $T = 1395 \pm 10\ ^{o}C$ interval. *Figure 5.15* shows the results of this simulation. In this case the temperature remains within the defined interval by changing the laser power as a function of time as demonstrated in *Figure 5.16*. Comparing this result to the simple

geometry, with uniform thickness, power decrease starts earlier with higher magnitude, *Figure 5.17*.

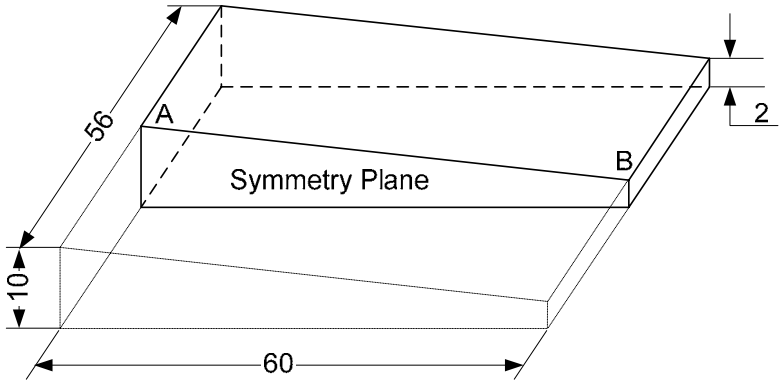


*Figure 5.13 Schematic illustration of geometry dimensions with an inclined surface*

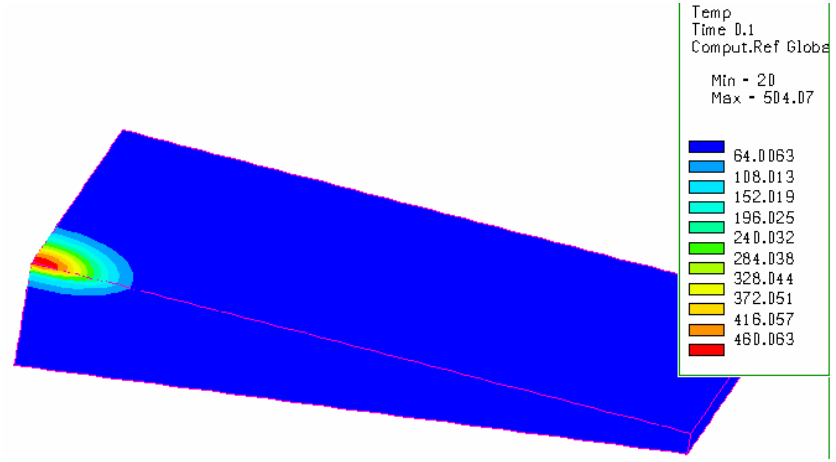


*a) Temperature profile at time 0.1s*

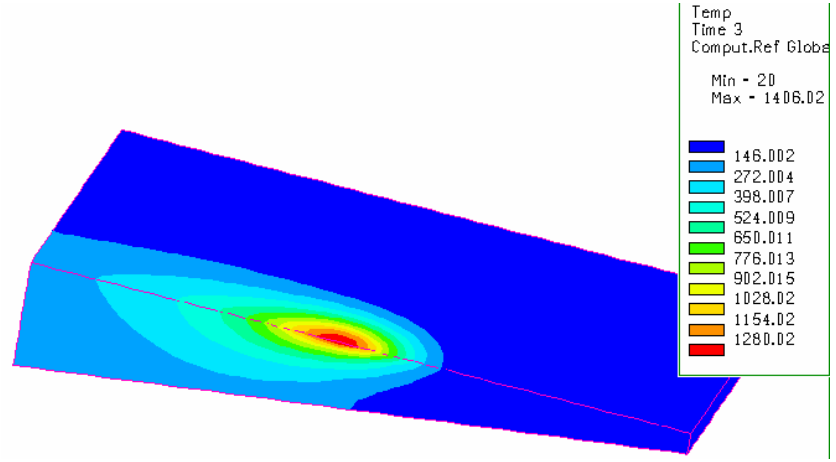


*b) Temperature profile at time 3s*

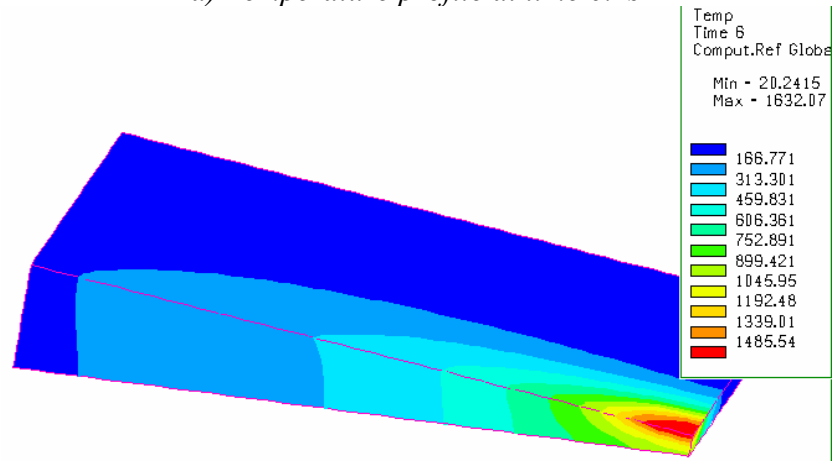


*c) Temperature profile at time 6s*

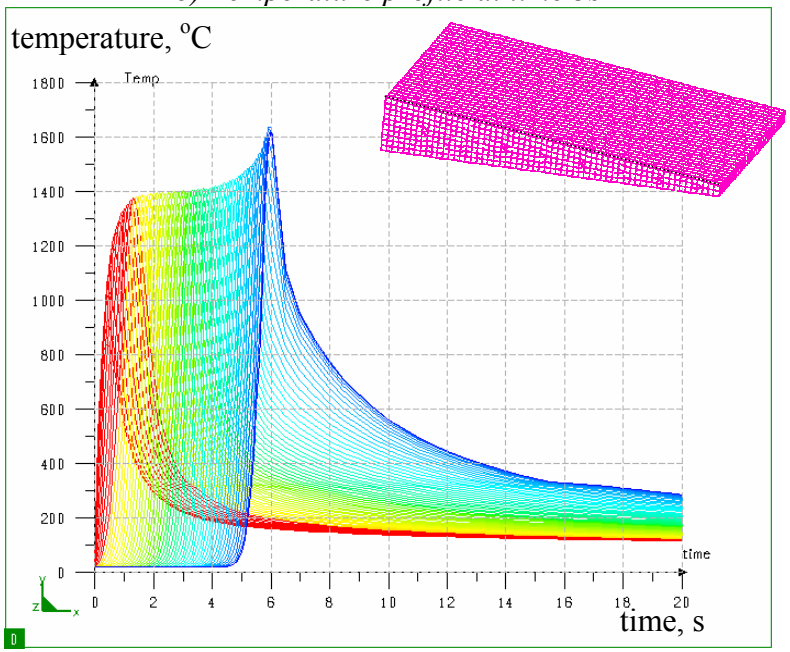


*d) Time temperature curves of all nodes of the trajectory line*

*Figure 5.14 Temperature profiles of single pass LTH of C45 steel with constant $q_0$*

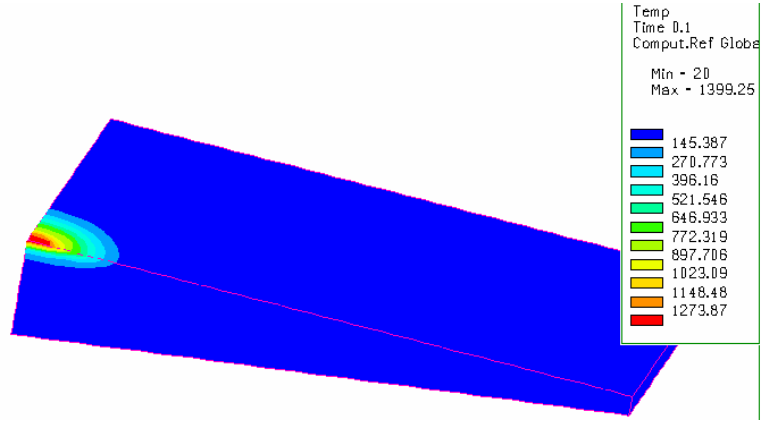


*a) Temperature profile at time 0.1s*

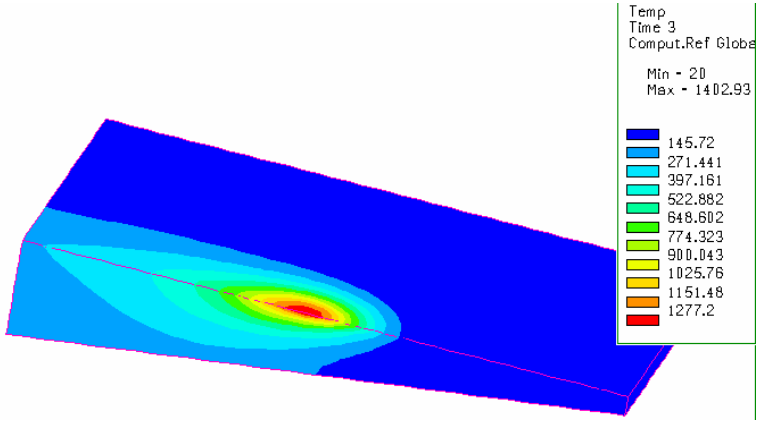


*b) Temperature profile at time 3s*

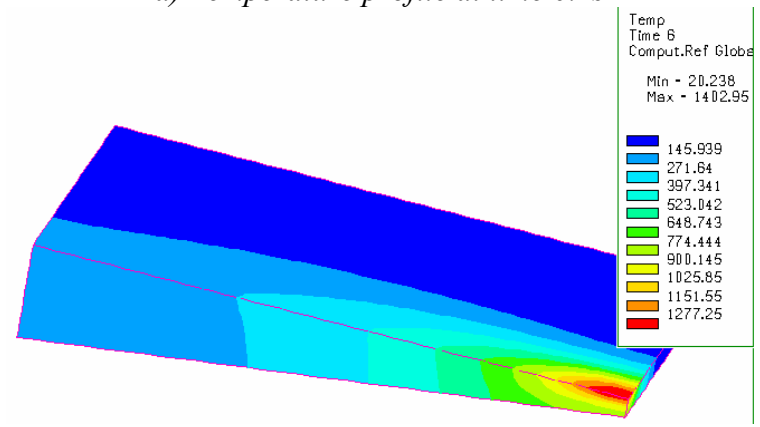


*c) Temperature profile at time 6s*

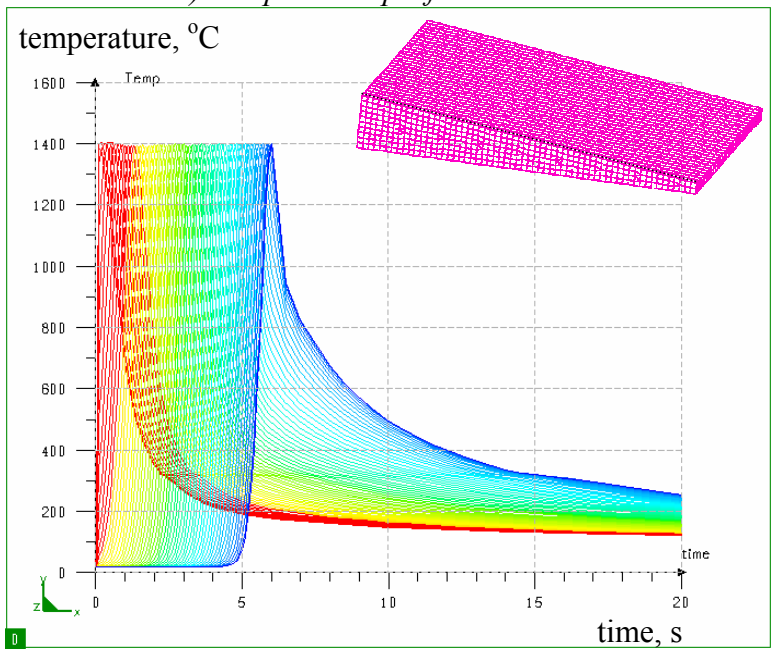


*d) Time temperature curves of all nodes of the trajectory line*

*Figure 5.15 Temperature profiles of single pass LTH of C45 steel applying constant temperature control strategy*

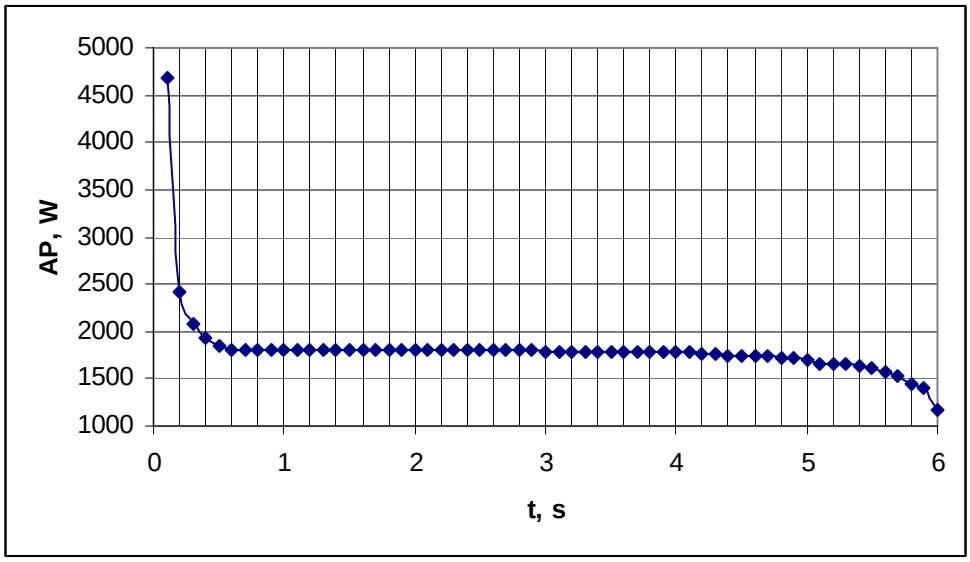


*Figure 5.16 Calculated power multiplied by the absorptivity as a function of time for the inclined surface*

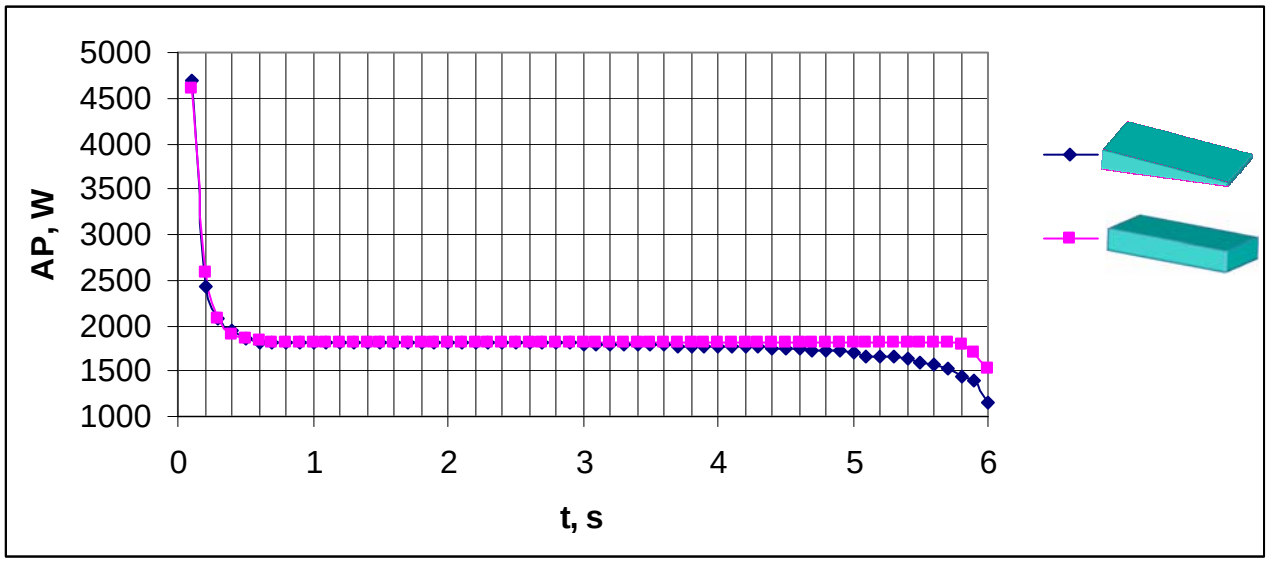


*Figure 5.17 Power multiplied by the absorptivity as a function of time for two different geometries*

***Geometry with Cavity***

To illustrate the general applicability of the methodology of temperature control strategy, investigation of a geometry with a cavity that causes discontinuity in the thickness of the workpiece is demonstrated in this section. The dimension of the workpiece to be modelled is shown in *Figure 5.18*.

Similarly to the previous example, the first simulation is carried out with constant process parameters. The laser spot radius of *5 mm* with a scanning rate of *10 mm/s* and maximum heat flux density of *23 W/mm*$^2$ are the parameters used for this investigation. Temperature distribution results are illustrated in *Figure 5.19*.

At the very beginning of the process the maximum temperature (*~503-890 $^oC$*) is not high enough for phase transformation, and then the surface will obtain a proper temperature value (*~1350-1390 $^oC$*) appropriate for austenite formation. This indicates that the process can be considered to be in quasi steady state condition. When laser source reaches the position where the thickness of the workpiece changes from *10 mm* to *2 mm*, due to a sudden decrease of the thickness, the surface temperature will increase and exceed the melting temperature (*~1619 $^oC$*). By continuing the process, surface temperature will decrease (*~1390 $^oC$*) on that part of the workpiece where the thickness increases. The edge problem, as explained earlier, results in temperature increase and therefore undesired melting. These temperature deviations can be followed in *Figure 5.19c-d.*

These results clearly demonstrate the difficulties of constant parameter applications. Surface hardening of such a complex geometry surface needs continuous change in process parameter(s).

In the second simulation the developed temperature control strategy was applied for the $T = 1395 \pm 10\ ^oC$ surface temperature interval. Results of this simulation are shown in *Figure 5.20*.

The deviation of the power in time to control the temperature within the defined interval is shown in *Figure 5.21* and compared to a workpiece with no cavity in *Figure 5.22*.

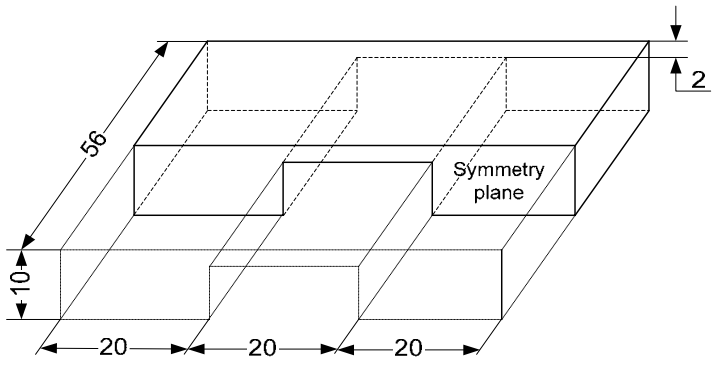


*Figure 5.18 Schematic illustration and dimension of the geometry with cavity*

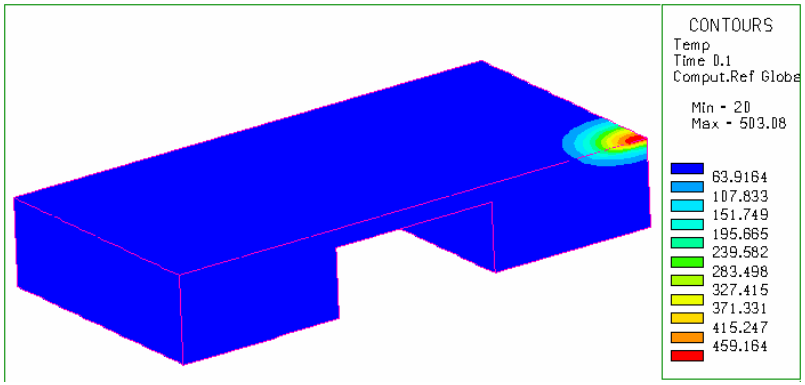


*a) Temperature profile at time 0.1s*

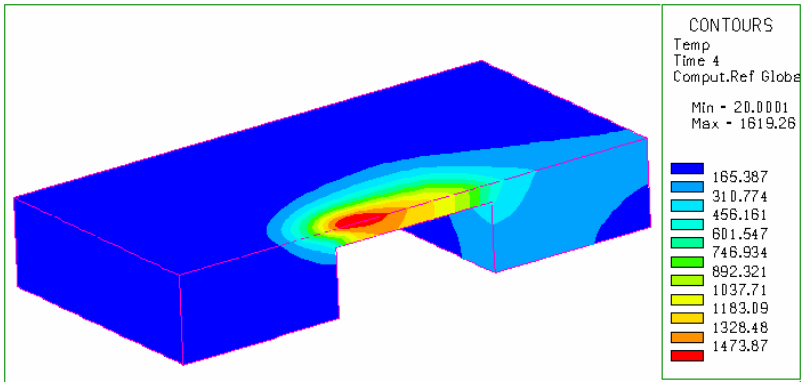


*b) Temperature profile at time 4s*

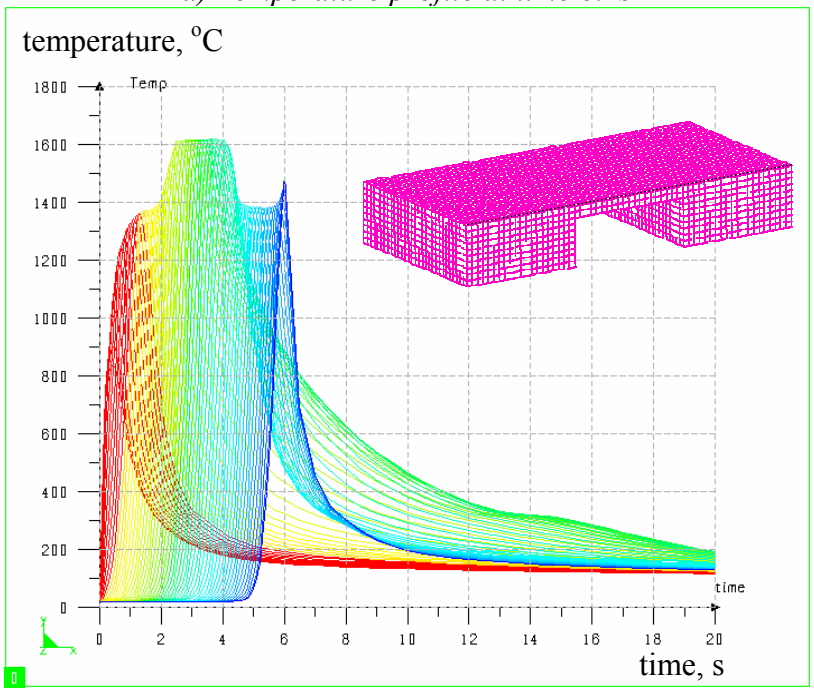


*c) Time-temperature curves of all nodes of the trajectory line*

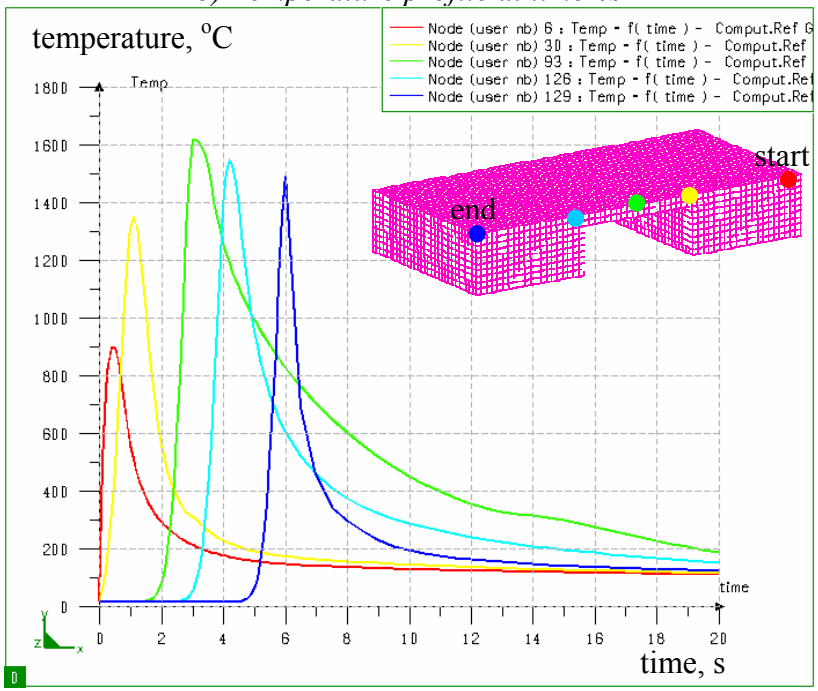


*d) Time-temperature curves of selected nodes on the trajectory line*

*Figure 5.19 Temperature profiles of single pass LTH of C45 steel with constant $q_0$*

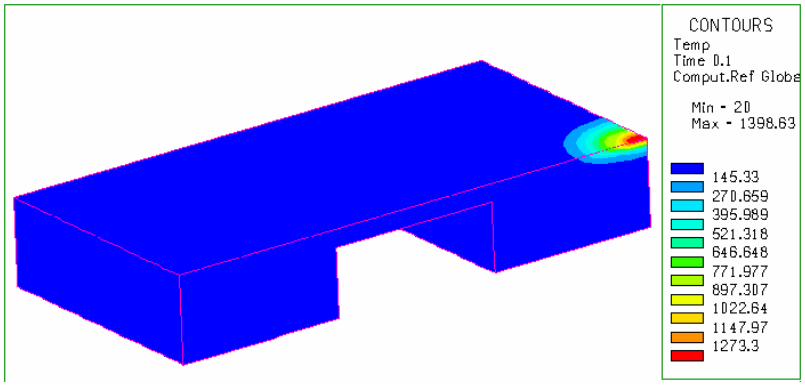


*a) Temperature profile at time 0.1s*

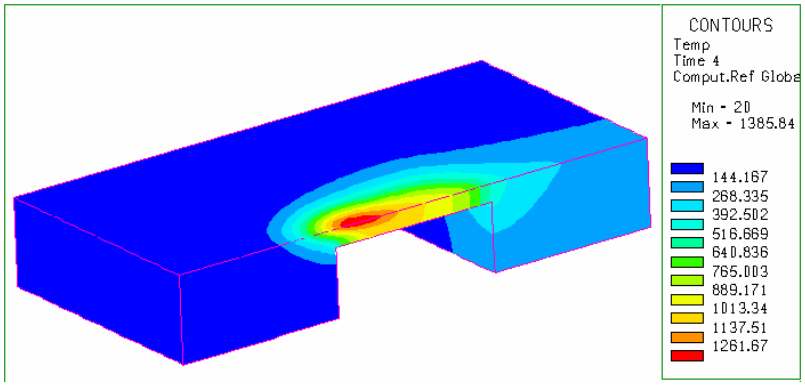


*b) Temperature profile at time 3s*

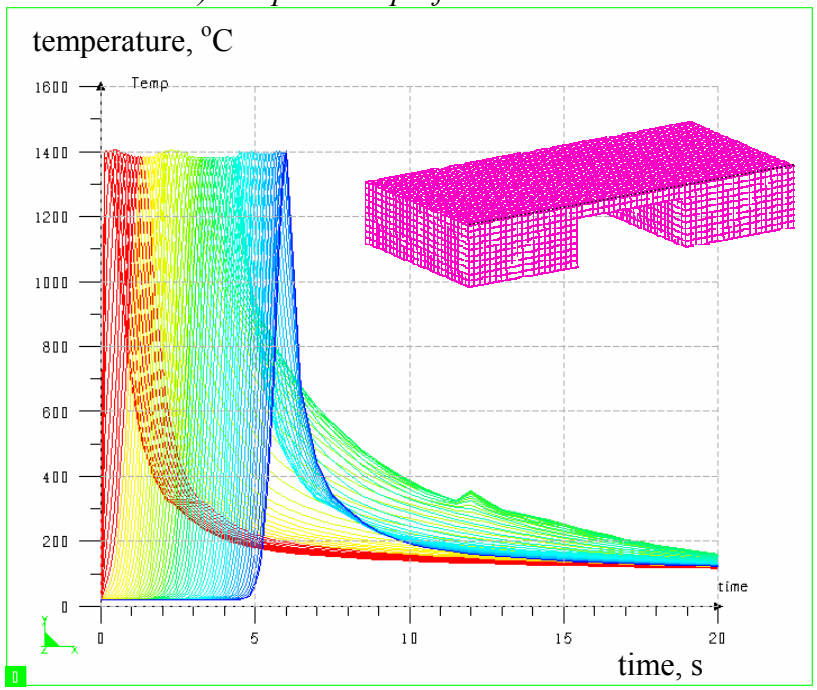


*c) Time-temperature curves of all nodes of the trajectory line*

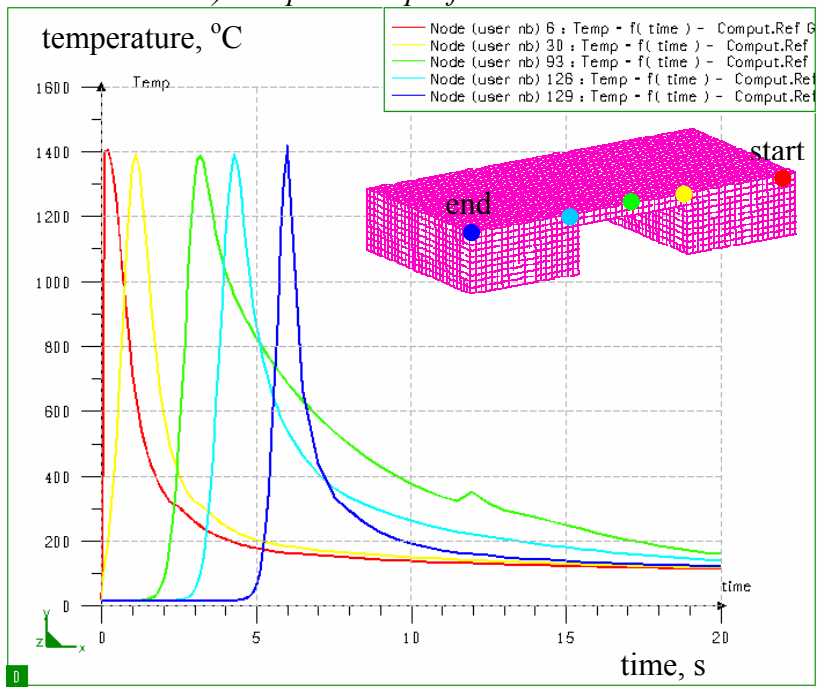


*d) Time-temperature curves of selected nodes on the trajectory line*

*Figure 5.20 Temperature profiles of single pass LTH of C45 steel applying constant temperature control strategy*

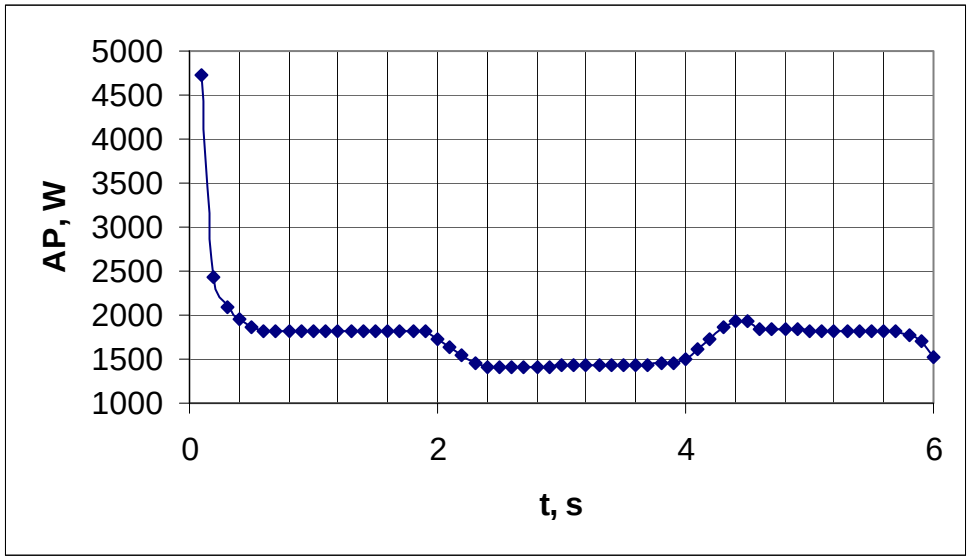


*Figure 5.21 Calculated power multiplied by the absorptivity as a function of time for a workpiece with cavity*

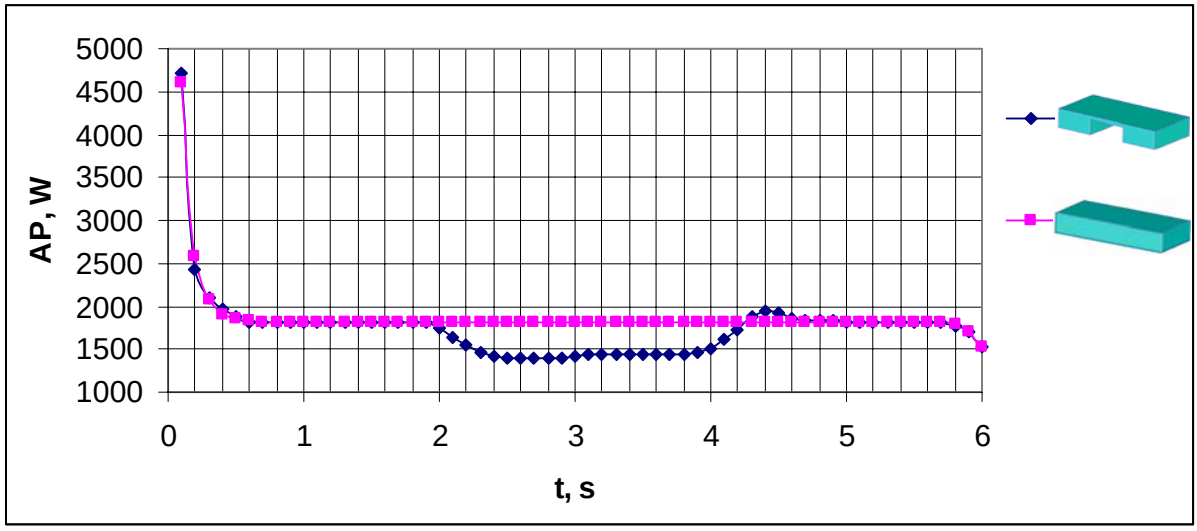


*Figure 5.22 Calculated power multiplied by the absorptivity as a function of time for two different geometries*

# 6. OVERLAPPING PHENOMENON OF LTH

## 6.1 Introduction

A problem associated with some laser transformation hardening applications is the necessity to overlap the hardening passes. This may occur at the closure of a path around a cylindrical part or in the overlap zone between parallel paths on a large flat surface being processed sequentially.

Depending on the laser machine power, the use of wider laser beam (larger size of beam spot) with uniform heat intensity distribution is preferable. Higher power lasers enable larger heating patterns to be produced. Rather expensive beam manipulator systems are a solution for maintaining wider and nearly uniform heat intensity distribution. These systems have also limitations for their beam size and even in this case multiple laser tracks should be applied.

To study the influence of overlapping, two laser tracks placed with a defined distance to one another in sequence are investigated. The general trend of the overlapping phenomenon can be described according to seven zones, *Figure 6.1*, as:

zone (1): completely martensitic zone as a result of the first laser track,
zone (2): completely martensitic zone as a result of the second laser track,
zone (3): completely martensitic structure as a result of re-austenitisation during the second laser track and quenching,
zone (4): partially re-austenitised and quenched zone due to the second laser track,
zone (5): tempered martensite zone as a result of the thermal affect of the second track,
zone (6): very thin partially austenitised and quenched zone,
zone (7): base metal not affected by the laser treatment.

The first two martensitic structure zones are obviously the results of sufficient heating of the initial material to austenitisation temperature which is followed by fast cooling. If the

second laser pass is close enough to the first one, a section of the martensitic structure of the first track will be re-austenitised and due to fast cooling it will be transformed into martensite once again, zone 3. Adjacent to this zone a thin layer (zone 4) of the former martensite produced by the first track, will be partially re-austenitised and subsequently quenched. Because of the lateral heat flow, a section of the martensitic structure of the first track will be tempered. This will result in unwanted softening of this area and decrease in the hardness of the laser treated layer that will cause inhomogeneity of hardness. The lowest affected area is a thin layer that is partially quenched, zone 6, which is followed by the unaffected area or the base material, zone 7.

Among the described zones, the tempered area is the most undesired result of the multi pass laser transformation hardening. Leaving a space between the tracks to avoid metallurgical overlapping, results in a zone with no phase transformation, and therefore soft base material in the boundary. If on the other hand the tracks are overlapping, tempering will occur which results in lower hardness value. Anyway the inhomogeneity of hardness in the surface layers can be predicted.

The lower the processing speed is, the more pronounced the effect becomes, due to relatively more heat which will have time to diffuse into the previously hardened area.

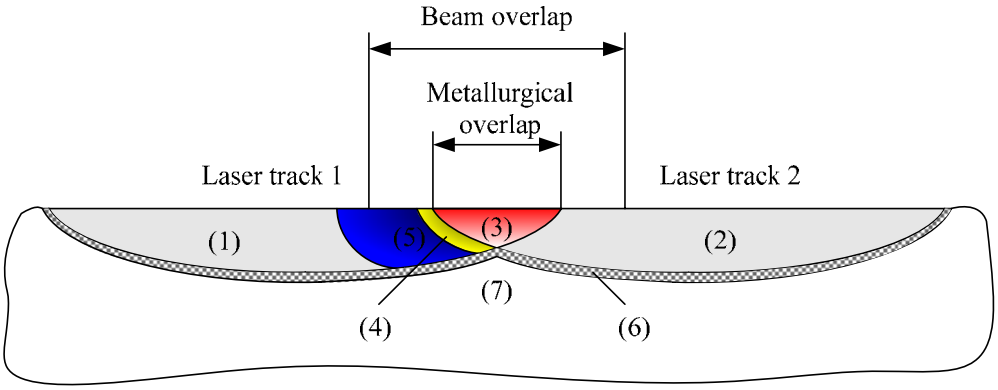


*Figure 6.1 Schematic illustration of two overlapped laser tracks*

Finite element modelling may offer predicting the level of inhomogeneity in hardness and may support measuring the optimal distance between adjacent tracks in order to minimise undesired hardness inhomogeneity.

## 6.2 Tempering of Martensite

Tempering is the heat treatment of hardened steels that has reduction of brittleness or increased toughness as its major objective. Any temperature up to the lower critical may be used for tempering., thus an extremely wide variation in properties and microstructure ranging from those of as-quenched martensite to spheroidized carbides in ferrite can be produced by tempering. As a result of systematic x-ray, dilatometric and microstructural observations, three distinct stages of tempering can be identified:

*Stage 1*: the formation of a transition carbide, ε-carbide, and the lowering of the carbon content of the matrix martensite to about 0.25% carbon.

*Stage 2*: the transformation of retained austenite to ferrite and cementite.

*Stage 3*: the replacement of the transition carbide and low carbon martensite by cementite and ferrite.

The temperature ranges for the three stages overlap, depending on the tempering times used. The formation of the alloy carbides responsible for secondary hardening is sometimes referred to as the fourth stage of tempering [51].

## 6.3 Numerical Modelling of Tempering

Similar to all diffusion type processes, tempering of steel is not only dependent on the temperature but also on the time factor which in some instances has a very great effect. From computational considerations, it is assumed that the kinetic equation describing the hardness is of the form

$$HV_t = f(p_g). \qquad \textit{Eq. 6.1}$$

$HV_t$ stands for the instantaneous hardness after tempering, $f$ is a suitably selected function and $p_g$ is the so-called generalised time-temperature parameter, which is applicable to the description of tempering processes [52].

Hollomon and Jaffe [53], among others have investigated this time-temperature factor which has led to the development of the expression for the tempering parameter, $p_{HJ}$ as

$$p_{HJ} = T(C_{HJ} + \log t) \qquad \textit{Eq. 6.2a}$$

or

$$p_{HJ} = T(C_{HJ} + \log t)10^{-3}, \qquad \textit{Eq. 6.2b}$$

where $T$ is the temperature (in degrees Kelvin), $t$ is the time in hours and $C_{HJ}$ is Hollomon and Jaffe composition dependent constant calculated by *Eq. 6.3* [54]

$$C_{HJ} = 21.53 - (5.8 \cdot C), \qquad \textit{Eq. 6.3}$$

where C is the carbon concentration of the steel.

The proper hardness of a given steel after tempering can be obtained by the variety of time and temperature combinations but the $p_{HJ}$ parameter for all combinations are the same. Experimental diagrams of hardness versus Hollomon and Jaffe parameters can be found in the literature. These curves can be described in different mathematical forms. I have adapted the following formula, *Eq. 6.4*, for C45 steel which fits the experimental data as shown in *Figure 6.2*

$$HV = 1.7\,p_{HJ}^2 - 92\,p_{HJ} + 1290\,. \qquad \textit{Eq. 6.4}$$

From *Eq. 6.2b* and *Eq. 6.4* curves of hardness as a function of time for different tempering temperatures are calculated and shown in *Figure 6.3*.

The proportion of a tempered structure as a function of time can be deduced from the previous curves. The method is simply to assume that for different time $t_i$ the tempered structure proportion $p_{tempered}$, can be described as a mixture of a certain proportion of the microstructure as "fully tempered" and the rest of it as "unaffected" phases.

The proportion $p_{tempered}$ is assessed as the ratio between hardness with $\Delta HV = HV_0 - HV_{100}$ and $\Delta HV_i = HV_i - HV_{100}$, so we obtain

$$p_{tempered} = \frac{\Delta HV - \Delta HV_i}{\Delta HV}, \qquad \textit{Eq. 6.5}$$

where $HV_0$ is the hardness of a quenched martensite, $HV_{100}$ is the final hardness of completely tempered structure and $HV_i$ is the actual hardness of the tempered structure at time $t_i$ as shown in *Figure 6.4*.

Finally, the needed curves $p_{tempered} = f(time)$ for different temperature are obtained to be the input data for modelling of tempering structures, *Figure 6.5*.

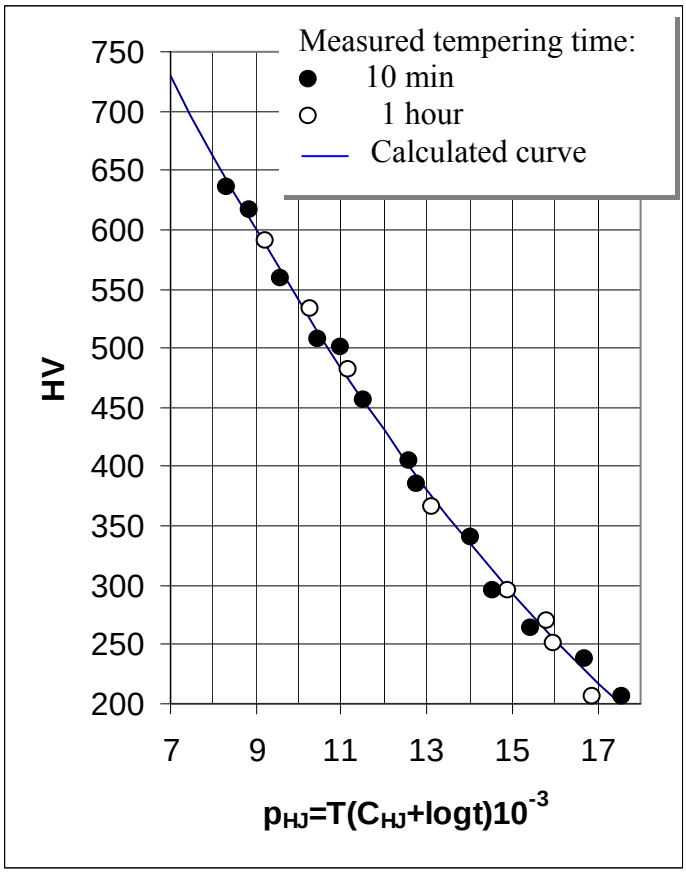


*Figure 6.2 Hardness of C45 steel after tempering as a function of $p_{HJ}$*

The proportion of the tempered structure or the "fiction phase" is adapted and calculated by a simplified form of the frequently used Johnson Mehl Avrami formula as *Eq. 6.6*,

$$p_{tempered} = p_{eq}\left(1 - exp(-\frac{t}{\tau})\right), \qquad \textit{Eq. 6.6}$$

where $p_{eq}$ is the tempered structure proportion obtained for an infinite time and $\tau$ is the time delay which is the incubation time needed for the start of diffusion process. By close aligning to the calculated curves, $p_{eq}$ and $\tau$ are calibrated and set as a phase in the "METALLURGY.DAT" file that contains all metallurgical transformations. Calibration results of $p_{eq}$ and $\tau$ are shown in *Figure 6.6* and *Figure 6.7* respectively.

For fully tempered structures it is reasonable to consider that the hardness is equivalent to those of spheroidite. During modelling the hardness of completely tempered martensite structure is considered to be similar to that of ferrite, only depends on the composition and calculated as follows:

$$HV_{tempered} = 62 + 223\,C + 15\,Si + 30\,Mn + 21\,Ni + 23\,CR + 19\,Mo + 260\,V\,. \qquad \textit{Eq. 6.7}$$

The hardness of the mixture maybe then computed in an incremental manner [43].

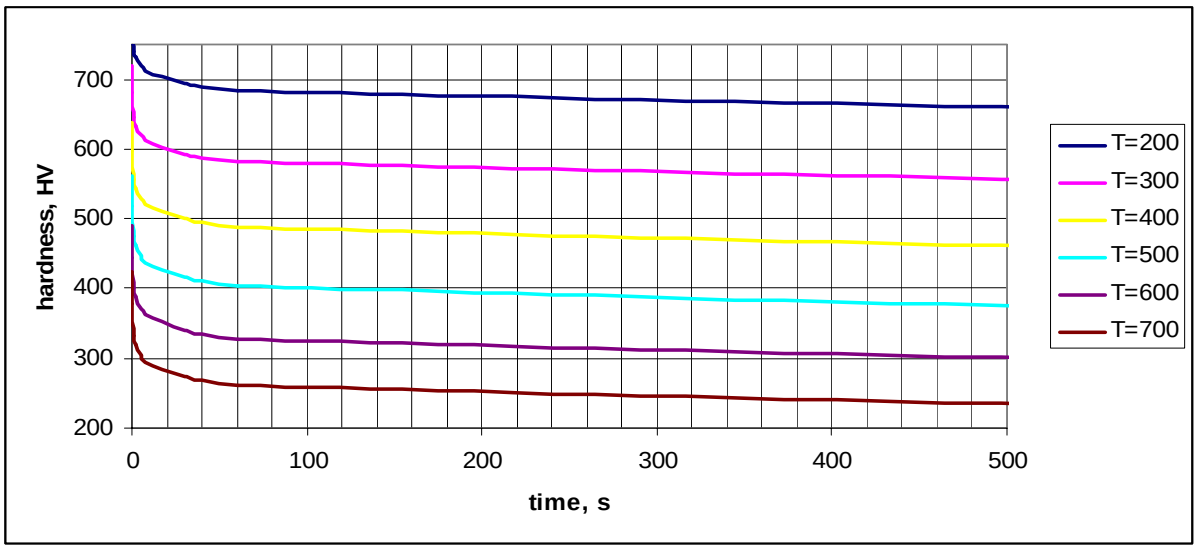


*Figure 6.3 Hardness changing of C45 steel after tempering as a function of $p_{HJ}$*

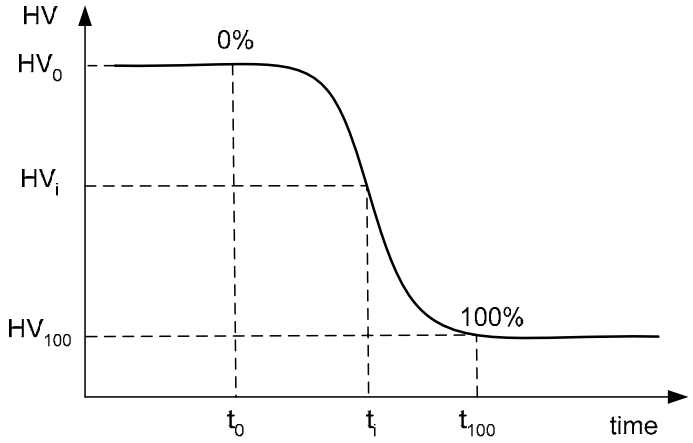


*Figure 6.4 Schematic illustration of hardness of a tempered structure as a function of time*

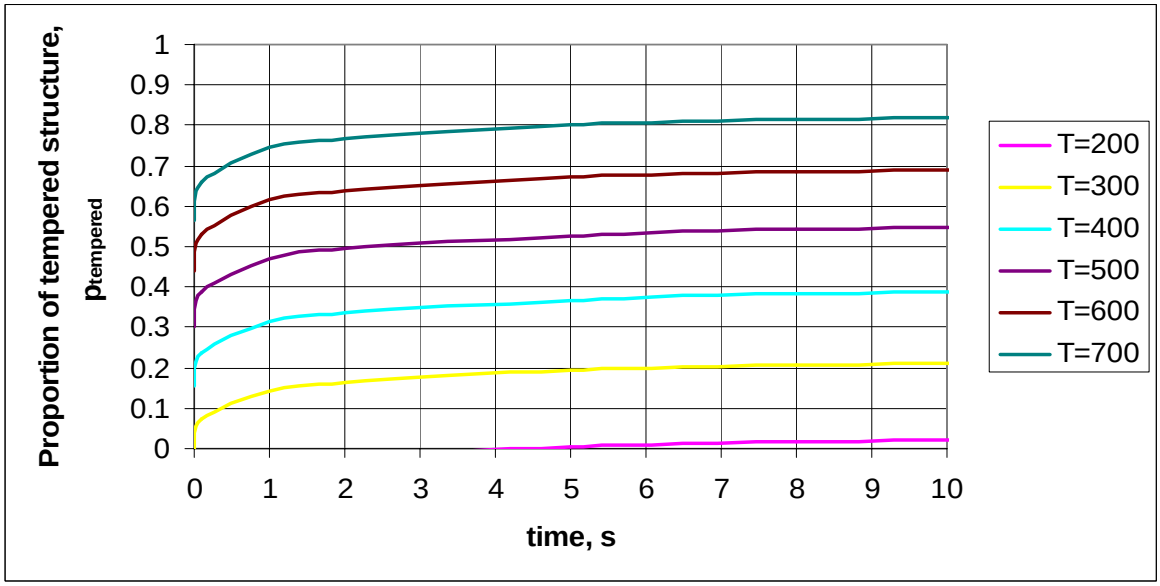


*Figure 6.5 Tempered structure proportion of C45 steel as a function of time for different tempering temperatures*

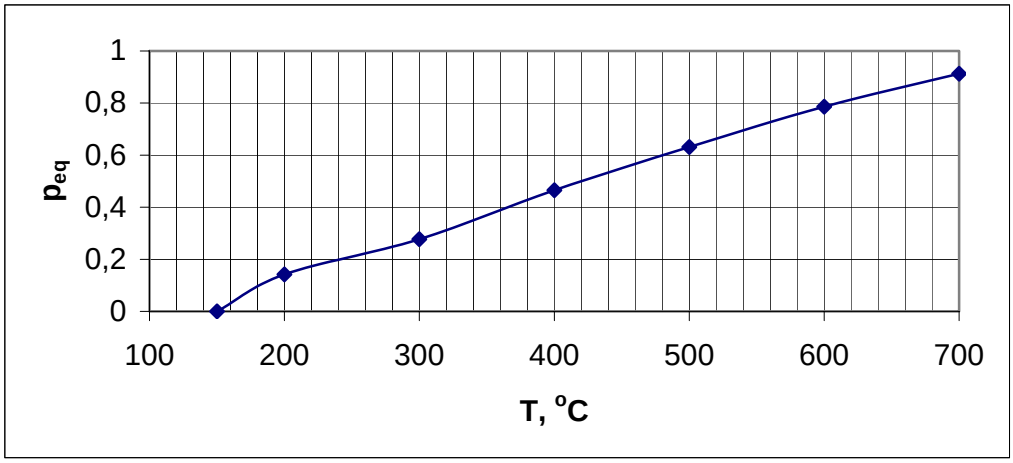


*Figure 6.6 Tempered structure proportion at equilibrium as a function of temperature*

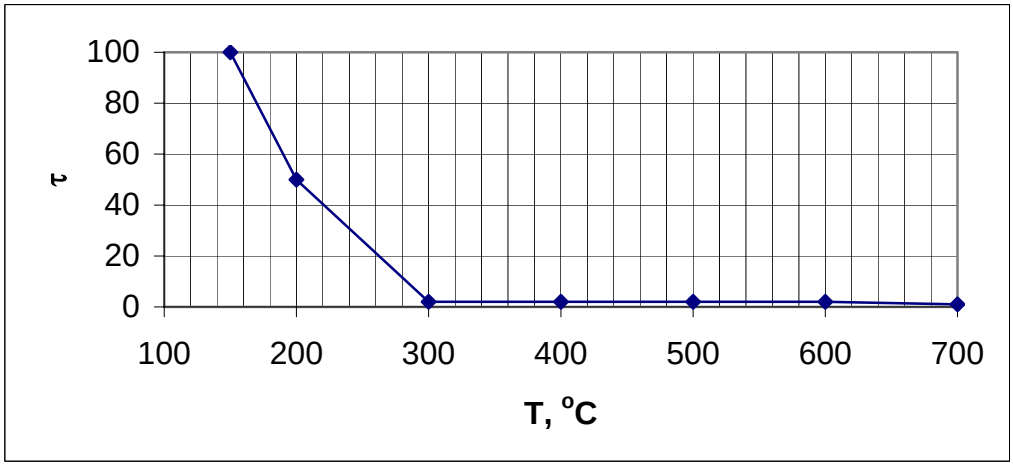


*Figure 6.7 Time delay as a function of temperature*

## 6.4 Finite Element Modelling of Multi pass LTH

Hardening of steels using multi pass LTH process can be considered as a complex engineering task. The closer the overlapping distance is, the higher the preheating temperature will be and the higher the reheating temperature of the already treated area of the first track will reach due to the second laser track. In situations where the two laser tracks are close to each other, temperature of the area to be treated by the second track may reach a high temperature value that can result in partial austenitisation. On the other hand, the second track, that causes reheating, may re-austenitise the martensite resulted from the first track.

To illustrate the mentioned possibilities and the complexity of the phenomena, an example of three consecutive laser tracks with 50% overlapping has been analysed. Temperature, austenite and martensite distribution of a single node lying under the centre line of the second laser track (*Figure 6.8*) is investigated in *Figure 6.9*. Partial austenitisation and re-austenitisation of martensite can be clearly seen in the figure.

Now the aim is to investigate the effect of tempering phenomenon during multi pass LTH of steel. Only two successive laser tracks on a C45 steel specimen were modelled in this case. Different simulations were applied for different distances between the first and the second tracks.

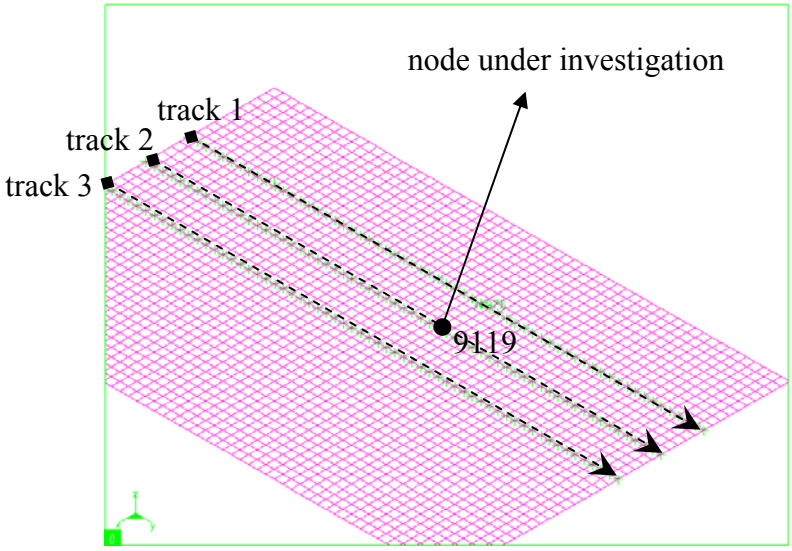


*Figures 6.8 Surface mesh of geometry hardened with three laser tracks*

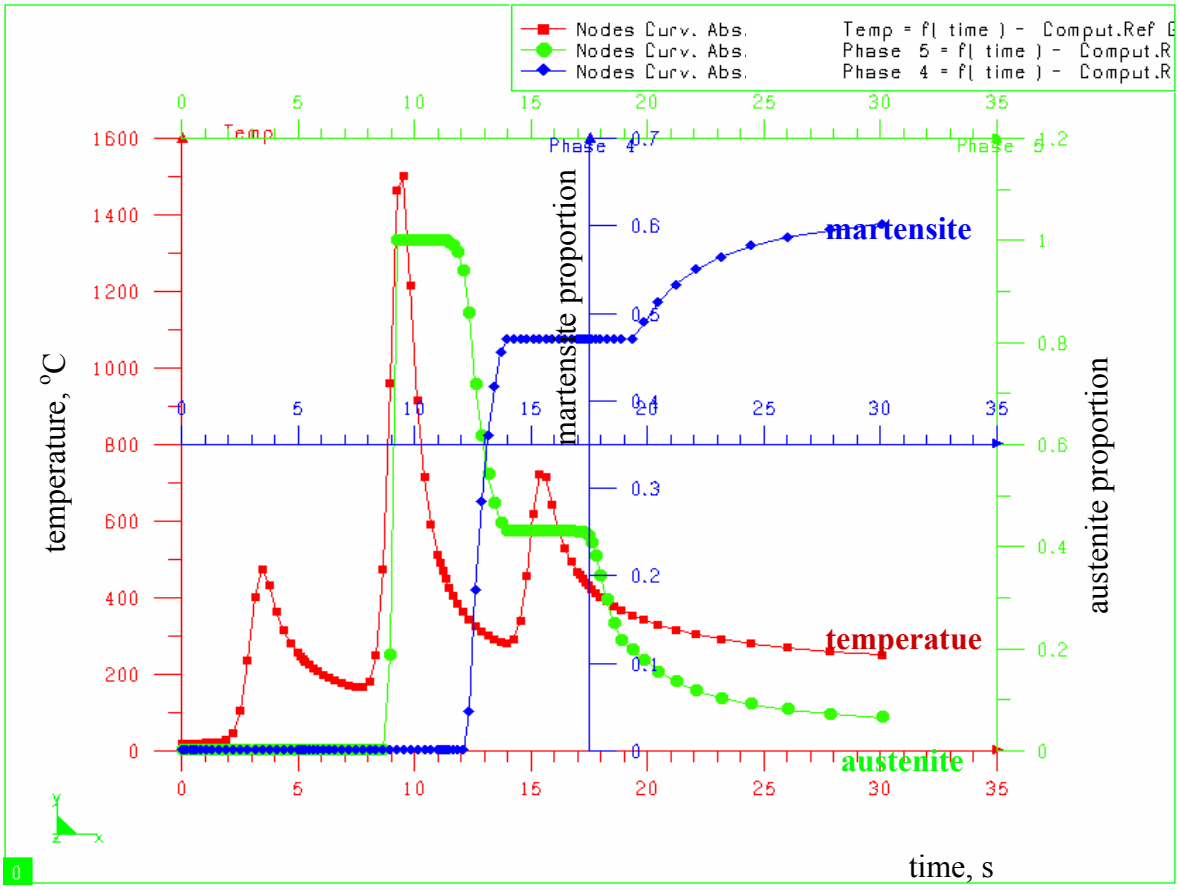


*Figures 6.9 Temperature distribution and phase proportions of a single nodes on the surface under the centre line of the second laser track*

Dimensions of the modelled workpiece are shown in *Figure 6.10*. The lines on the surface illustrate all centre lines of the laser passes and they are apart by *1 mm* from each other. The heat source diameter is *10 mm* during these simulations. The first two tracks are scanned at a distance of *10 mm* with no beam overlapping, and the distance of other pairs of tracks decrease by *1 mm* for each simulation. In the last model centre of the tracks are situated at a distance of *1 mm* from each other.

In normal circumstances, when the process parameters are constant, the first laser track preheats the workpiece and surface temperature will achieve a higher value after irradiation of the second laser track. The deviation of the temperature may result in an inhomogeneous microstructure and may also result in melting of the surface.

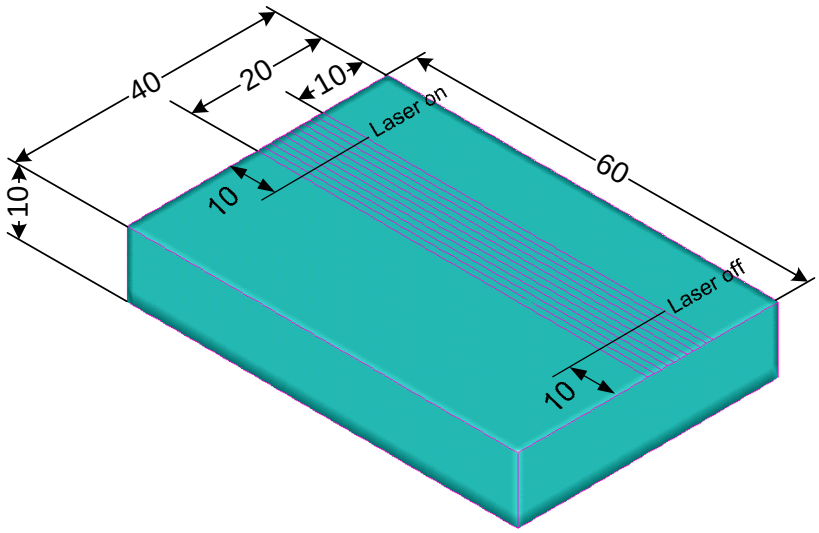


*Figure 6.10 Workpiece dimension and the centre lines of the tracks*

To avoid temperature deviation and its subsequences, the temperature control strategy was used. A Gaussian laser heat distribution with spot of $r_0 = 5$ *mm* and scanning rate of $v = 10$ *mm/s* is the modelled thermal load applied on the surface of the workpiece. It is assumed that the laser source will switch on and off at a distance of *10 mm* from the edges. The temperature of the surface was set to $T = 1395 \pm 10\ ^oC$ interval during the whole process.

Finite element modelling was concerned for the thermal, metallurgical and hardness calculations. An example of the temperature distributions of two successive laser tracks at a distance of 10 mm from each other are illustrated in *Figure 6.11*. Temperature distribution results of two selected nodes which are located on the centre of the first and the second tracks are shown in *Figure 6.12*. For all cases the temperature control strategy successfully keeps the maximum temperature of the surface below melting and overcome the preheating effects.

Hardness distribution results of the workpiece cross-section for different overlapping distances are illustrated in *Figures 6.13 - 6.16*. The curves with red lines illustrate the hardness distribution of the first track after *5000 s* without effect of the second track, while the curves with blue lines show the hardness distribution of the first and the second tracks taking the tempering of the first track into consideration.

Hardness decreasing caused by martensite inhomogeneity due to tempering of martensite can be followed and investigated. In case of adjacent beams with no overlapping, it results in an unaffected area between two hardened zones where the hardness drops to the initial

material hardness value. By decreasing the distance of the two tracks the hardness of the area between the two hardened zones will increase but the hardness of the first track will decrease due to the tempering phenomenon. *30*, *40* and *50%* overlapping can be regarded as the acceptable results of LTH with multi pass laser scanning.

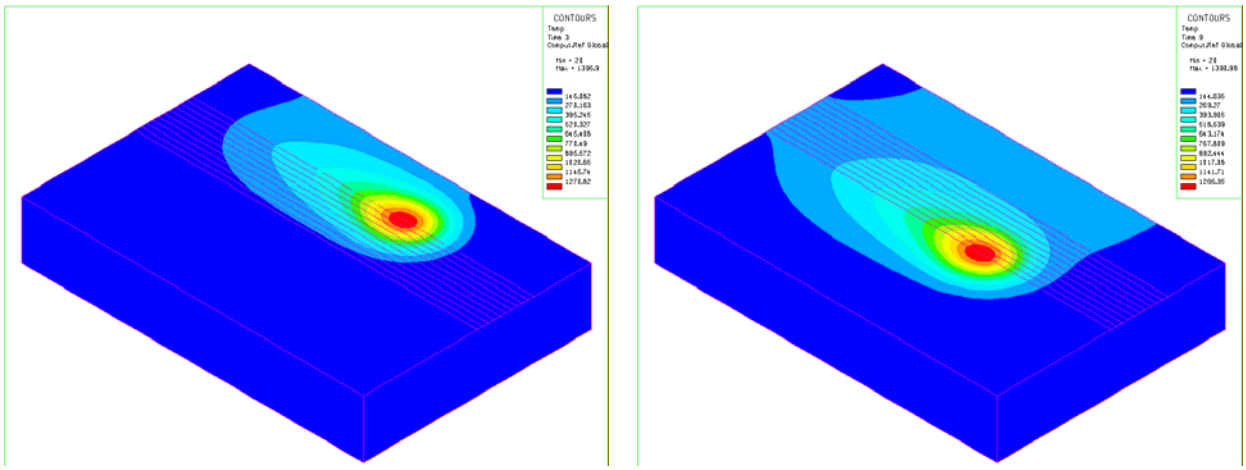

*a) Temperature results of the first track* *b) Temperature results of the second track*

*Figure 6.11 Temperature distribution of two consecutive laser track at a distance of 10 mm from each other (no overlapping)*

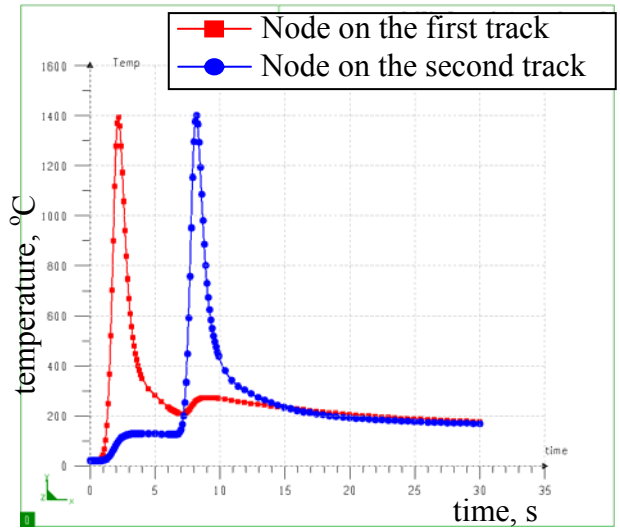


*a) 10 mm distance between the tracks*

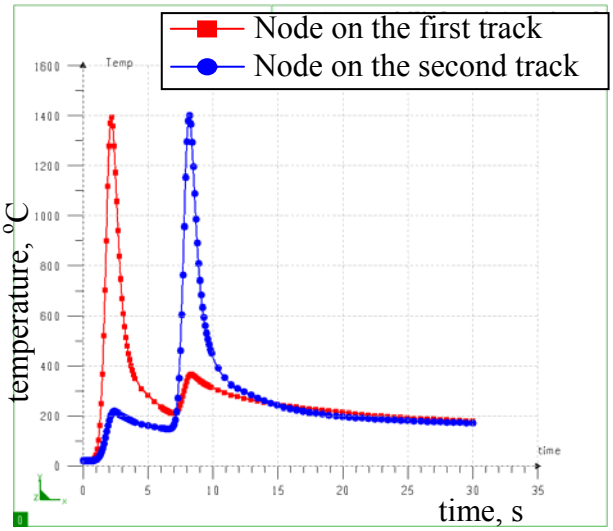


*b) 8 mm distance between the tracks*

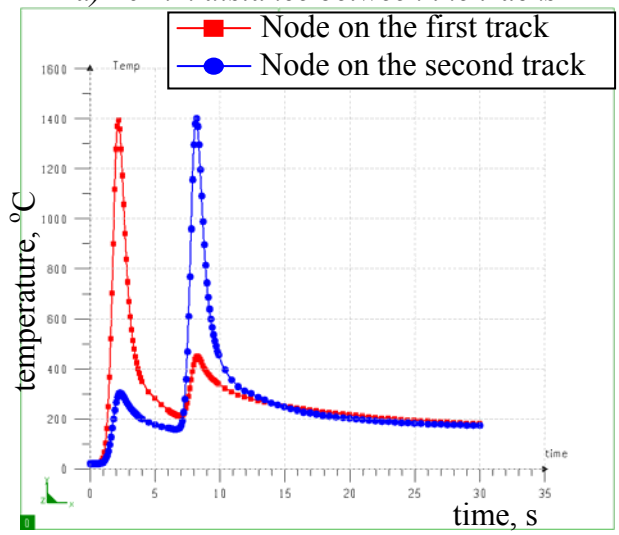


*c) 7 mm distance between the tracks*

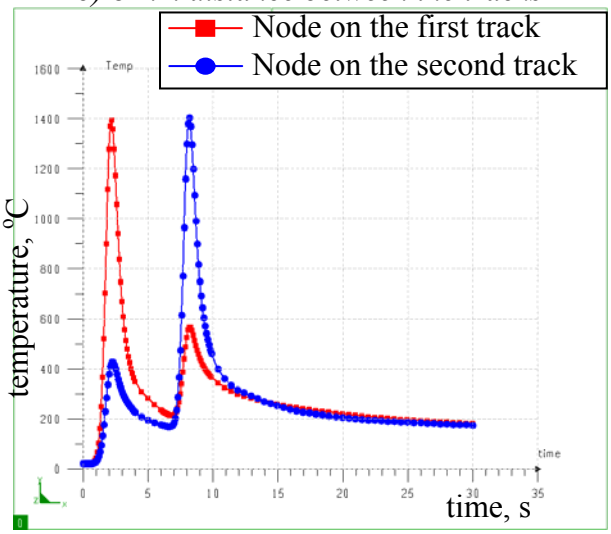


*d) 6 mm distance between the tracks*

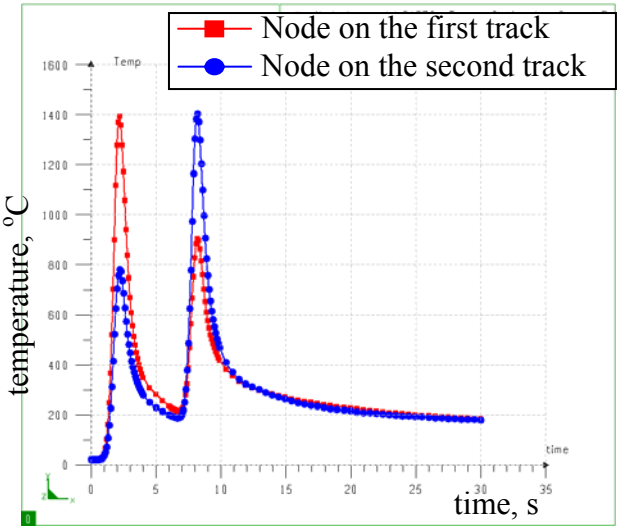


*e) 5 mm distance between the tracks*

*Figures 6.12 Time-temperature distribution of two nodes on the surface under the centre line of the first and the second tracks*

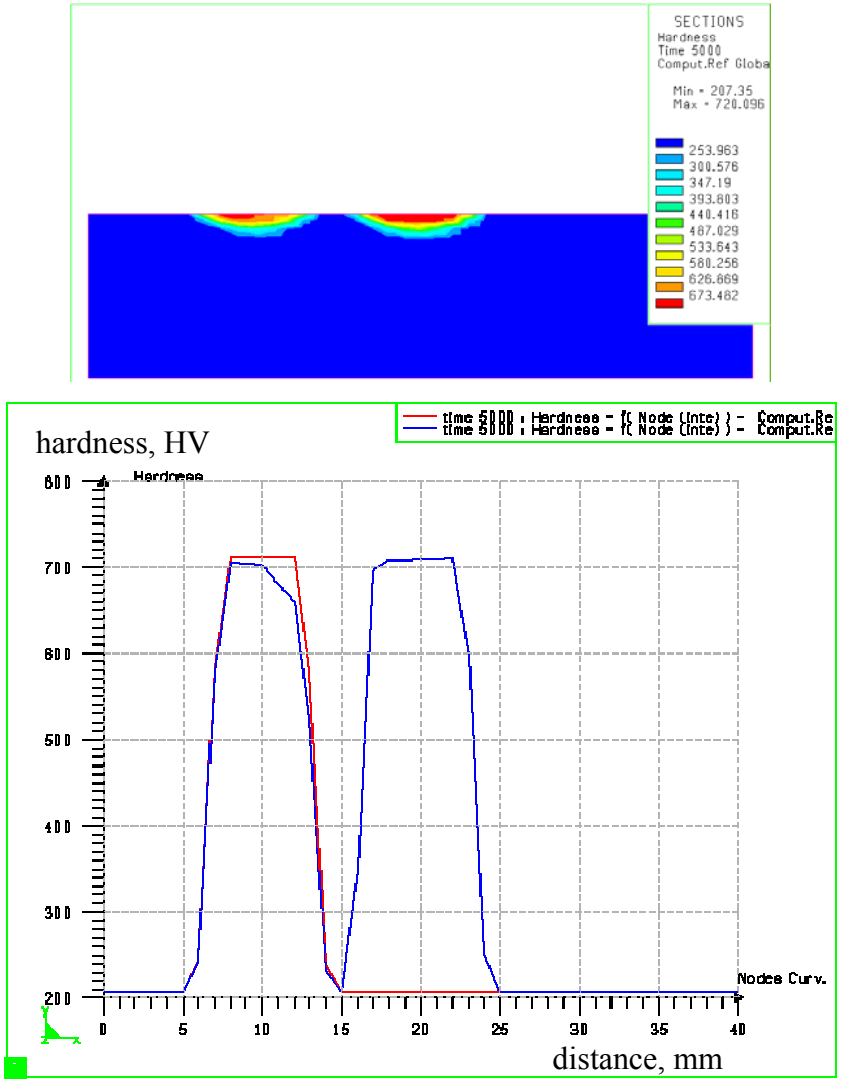


*a) 10 mm distance between the tracks*

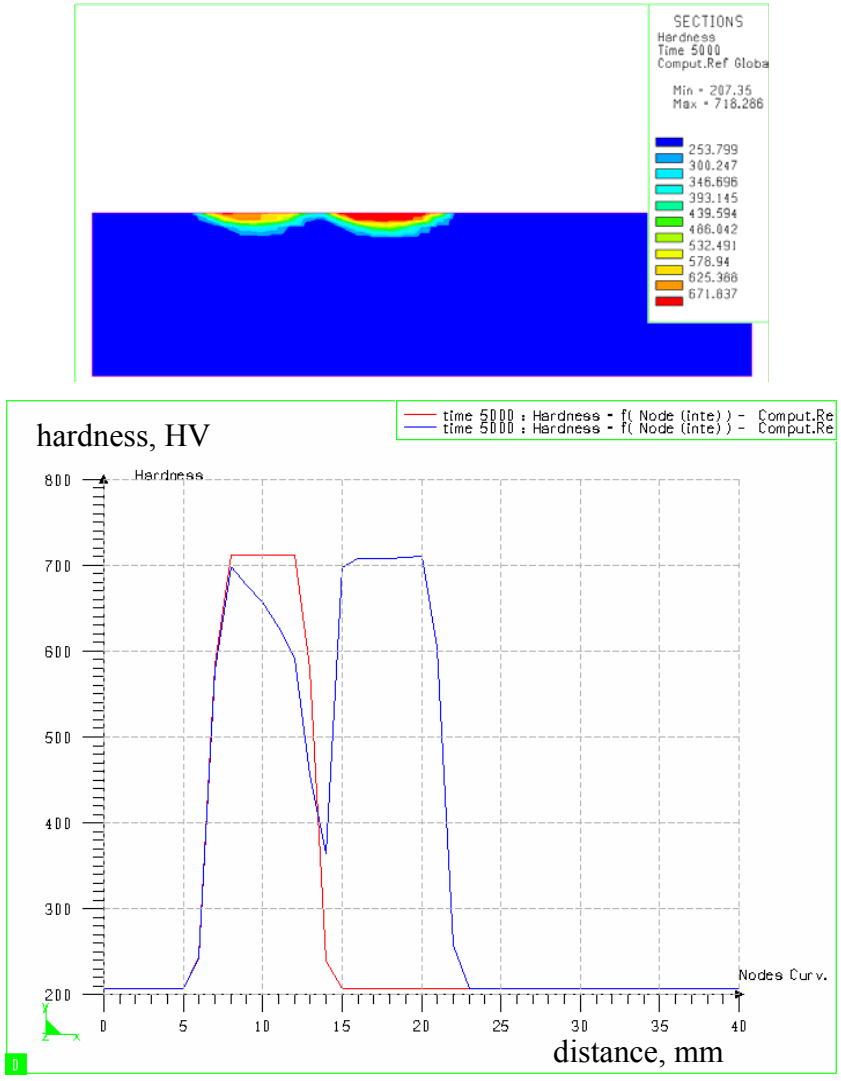


*b) 8 mm distance between the tracks*

*Figures 6.13 Hardness distribution along the cross-section of the workpieces*

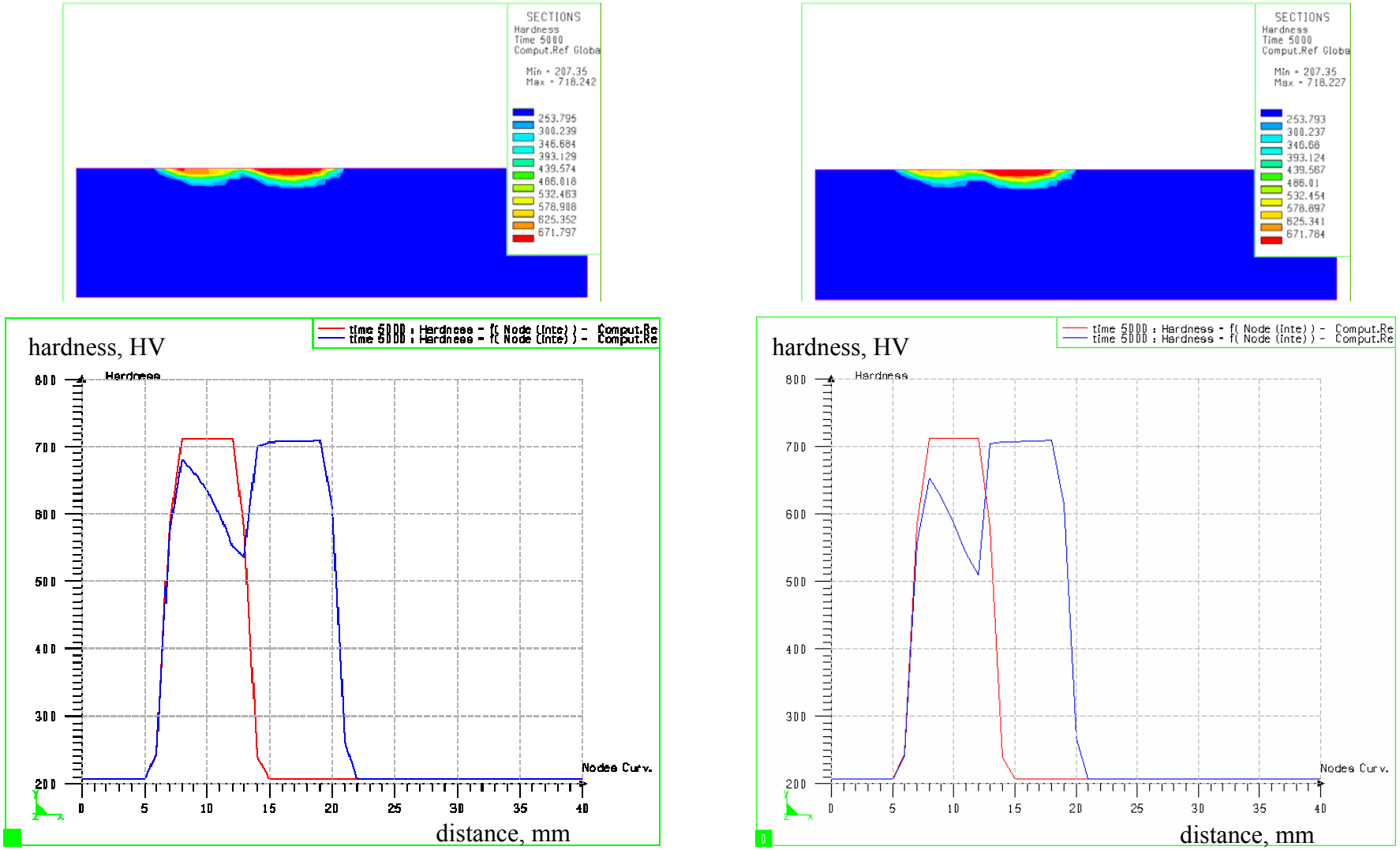


*a) 7 mm distance between the tracks* *b) 6 mm distance between the tracks*

*Figure 6.8 Hardness distribution along the cross-section of the workpieces*

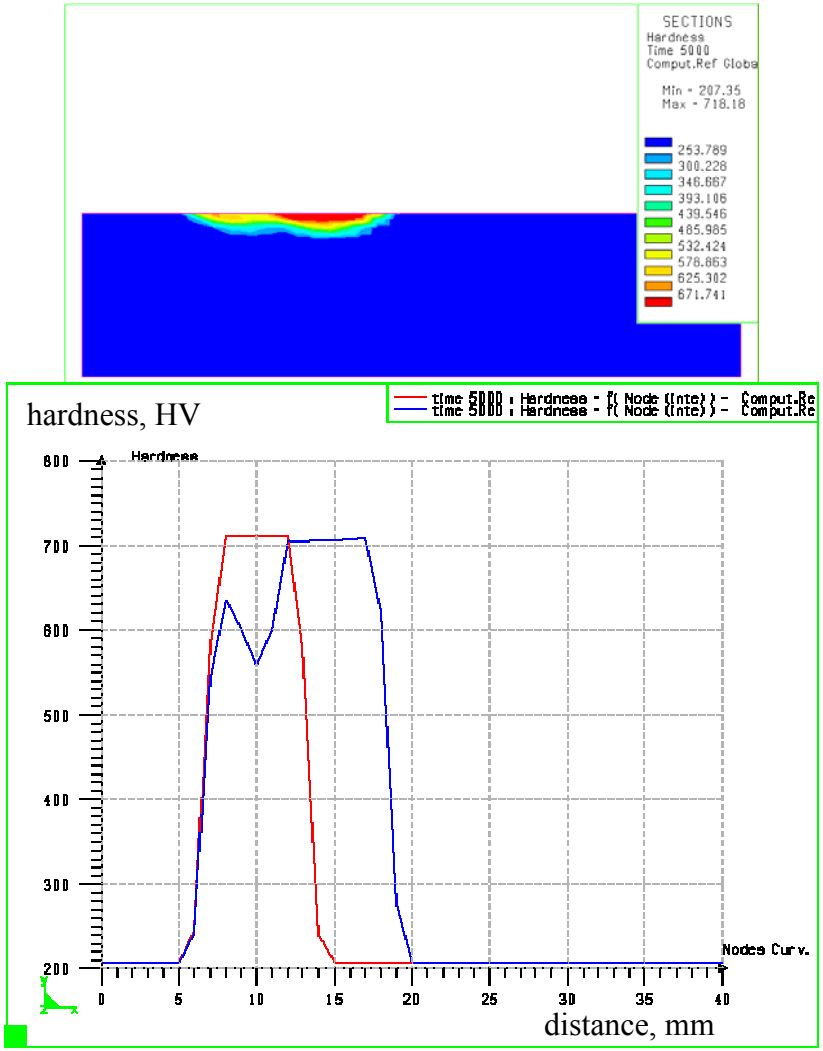


*a) 5 mm distance between the tracks*

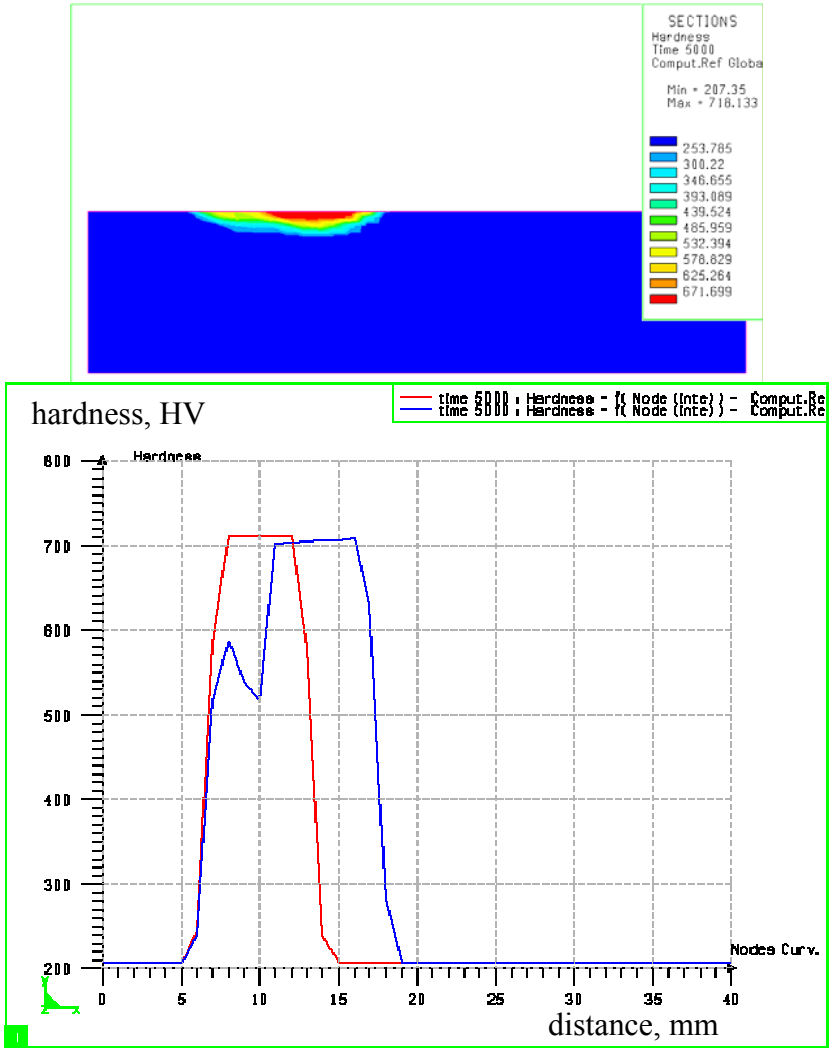


*b) 4 mm distance between the tracks*

*Figure 6.9 Hardness distribution along the cross-section of the workpieces*

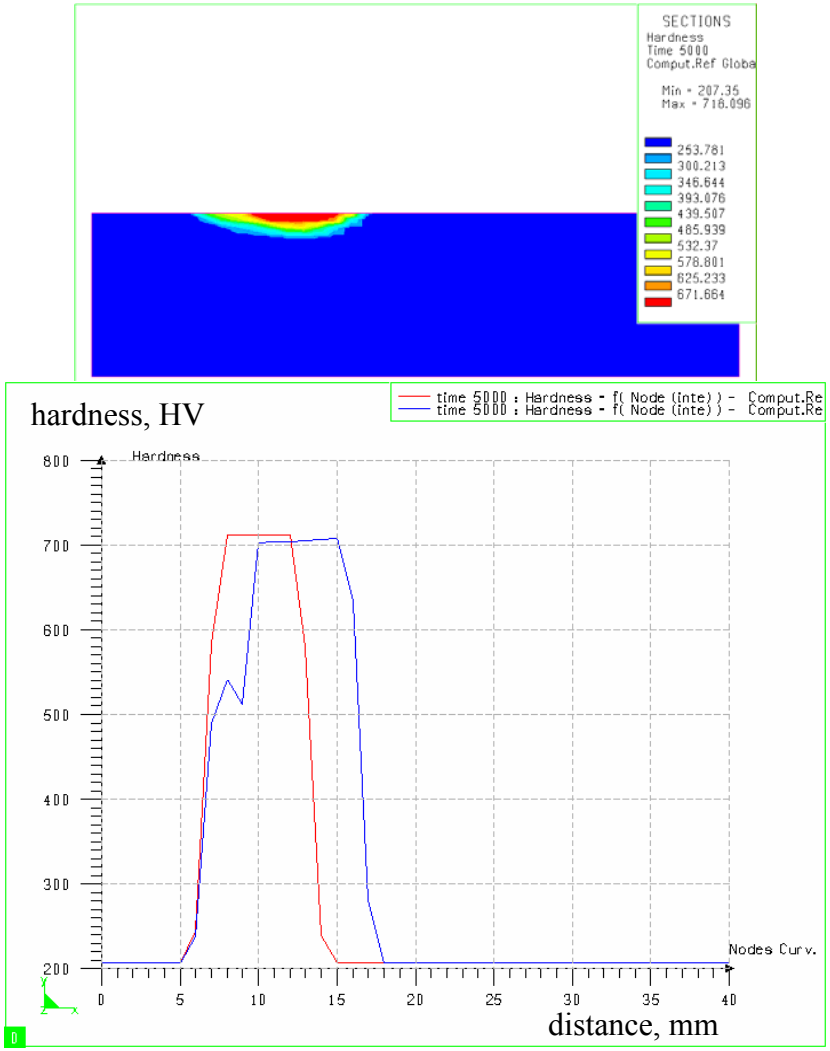


*a) 3 mm distance between the tracks*

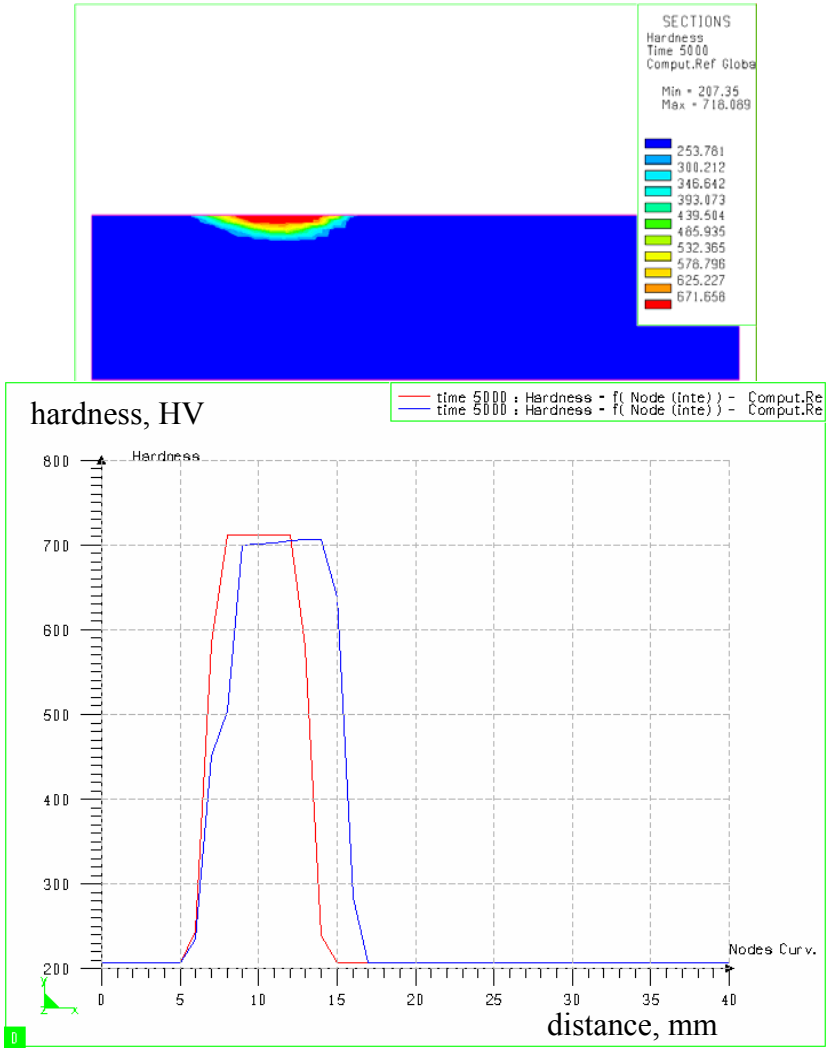


*b) 2 mm distance between the tracks*

*Figure 6.10 Hardness distribution along the cross-section of the workpieces*

# 7. CONCLUSIONS AND APPLICATIONS

The purpose of this research work was to enhance the insight in mechanisms that govern the laser transformation hardening process and to develop models using FEM code as numerical tools for assisting our engineering processes.

A literature survey had to be performed to get an idea of the state of the art. Mechanisms of laser transformation hardening and the applicability of the process were discussed in more details.

The first attempt was to model a single track LTH processes. Numerical, thermal, phase transformation and hardness analyses were performed using SYSWELD FEM code. After successful modelling of the process, series of simulations were done and the results were used to introduce operating regions for steady state LTH condition presenting the appropriate laser power as a function of beam radius, and laser power as a function of scanning rate to avoid melting on the surface and reaching austenitisation temperature at any desired depth.

The System Interface Language of the FEM code was used to develop a methodology named temperature control strategy for LTH process. The method is to control the input laser energy to achieve a constant temperature interval, or even a constant temperature at any point of the workpiece regardless of the process state and the complexity of the geometry. A Gaussian distribution was modelled as the heat input. During the process the maximum heat flux density of the source was changing in such a way to obey the set temperature interval that could be defined at any node of the finite element mesh. In other words the power which is the area under the Gaussian distribution was changing to keep the process within the set temperature interval.

This strategy was applied to overcome special difficulties in LTH processes. Examples of transient states, edge difficulties and complex geometries are among the problems that were solved using this strategy. The output results are maximum heat flux densities as a function of time that can be transformed into power as a function of time or displacement.

Even in these cases, non steady state conditions, the operating regions could be introduced to avoid surface melting and reaching the austenitisation temperature at any desired depth.

The temperature control strategy was also applied to reduce the difficulties of the LTH with overlapping. Surface melting can be avoided and the inhomogeneity of the microstructure can be predicted when using this method. Modelling of a tempered structure was adapted for overlapped tracks. Two tracks starting with no beam source overlapping until 90% overlapping were simulated to examine the phenomenon itself and the applicability of the model with tempered structure. Hardness results clearly demonstrate the tempering effect and they also show that this effect did not disappear when the metallurgical overlapping was present. Obviously the tempering effect can be minimised by the application of this modelling strategy.

### *Applications of the New Scientific Results*

The method for optimising process parameters with respect to various criteria that are presented in the first thesis is a powerful tool for finding safe operating regions in laser transformation hardening processes. Comparing empirical relationships and analytical solutions, the numerical calculations that take the variations of material properties into account, are more realistic. We can state that these results establish an appropriate relationship between the input data which are the technological parameters and the output data which are characteristics of the hardened layer are predictable, reliable and reproducible. These factors can help LTH processes to be more widely applicable in industry.

The temperature control strategy, while controlling the process temperature at any point of the workpiece, gives the proper heat flux density or the input power of the process. This strategy was implemented to avoid surface melting and assuring austenitisation at a specific depth that can be a solution for critical industrial problems concerning LTH.

Investigation of the tempering phenomena and its modelling in LTH process gives significant advantages to control the multi pass LTH usually applied for large flat surfaces and cylindrical parts.

It is worth mentioning that all simulations were applied on C45 steel grade with the Gaussian heat distribution model. Obviously the same methods can be carried out on different materials and different heat source models.

# 8. THESES

1. Based on the numerical modelling of thermal, metallurgical and hardness analysis of single track laser transformation hardening (LTH);

   1.1. I have determined a stable process window for steady state LTH conditions presenting the appropriate laser power as a function of beam radius, and laser power as a function of scanning rate.

   1.2. I have proven that this process window can be used to determine the variation of the laser beam radius ($r_0$) with laser beam power ($P$) multiplied by the absorptivity ($A$) of the material for different laser scanning rates ($v$), avoiding melting on the surface while assuring the austenitisation temperature at a desired depth of the specimen.

2. I have developed a temperature control strategy for LTH processes using the System Interface Language (SIL) of SYSWELD FEM code. The method is to control the input laser energy to achieve a constant temperature interval, or even a constant temperature at any point of the workpiece regardless of the process state and the complexity of the geometry.

   2.1. I have proven that the temperature control strategy can be applied to overcome several difficulties concerning LTH processes such as transient states, edge problems and complex geometries.

   2.2. I have proven that even in case of non steady state conditions, the operating regions could be introduced to avoid surface melting while reaching any required

temperature, e.g. austenitisation temperature, at any desired depth using the developed temperature control strategy.

3. On the basis of the numerical modelling of the thermal phenomena and phase transformations during overlapped multi pass LTH of steels;

   3.1. I have proven that the temperature control strategy is suitable for handling the complexity of multi pass laser temperature distributions, e.g. controlling the constant peak temperature of subsequent tracks during multi pass laser applications.

   3.2. I have adapted a numerical model for the tempering phenomena during multi pass LTH by defining the tempered structure in the SYSWELD code as a “fiction phase” where its proportion is calculated by the simplified form of the frequently used Johnson Mehl Avrami formula.

   3.3. I have proven the fact that in case of multi pass LTH, numerical hardness results clearly demonstrate the tempering effects. Obviously the hardness inhomogeneity due to the tempering effect can be minimised by the application of this modelling strategy.

# PUBLISHED PAPERS RELATED TO THESES

1. Reza Rowshan, Dr. Mária Kocsis Baán, Laser transformation hardening of different steels and 3d modelling of their temperature distribution, IV. Országos Anyagtudományi Konferencia, Balatonfüred, October 2003.
2. Rowshan Reza, Kocsisné Dr. Baán Mária, Acélok edzése lézeres sugárral és elemzésük végeselem-módszerrel, Doktoranduszok Fóruma kari rendezvények, Miskolci Egyetem, 2003, pp. 219-224
3. Reza Rowshan, Dr. Mária Kocsis Baán, Laser Transformation Hardening of Steels and Their FEM Modeling, Gépészet 2004, pp.175-180
4. R. Rowshan, M. K. Baán, Finite Element Modelling of Temperature Distribution and Phase Transformation of Laser Transformation Hardening of Steels, Lane 2004, vol.2, Erlangen, Germany, pp. 859-864
5. Reza Rowshan, Dr. Mária Kocsis Baán, Laser Transformation Hardening of Different Steels and 3d Modelling of Their Temperature Distribution, Materials Science Forum Vols. 473-474 (2005) pp.399-406, Trans Tech Publication Ltd 2005.
6. R. Rowshan, M. K. Baán, Temperature Distribution and Phase Transformation Modelling in Laser Transformation Hardening of Steels, microCAD 2005, Miskolc, Hungary
7. Bitay Enikő, Rowshan Reza, Lézeres felületkezelés technológiai paramétereinek folyamatos változtatásának szimulációja, microCAD 2005, Miskolc, Hungary
8. R. Rowshan, M. K. Baán, Thermal and metallurgical modelling of laser transformation hardened steel parts, V. Országos Anyagtudományi Konferencia, Balatonfüred 2005, Conference CD proceeding.

9. R. Rowshan, M. K. Baán, Finite Element Modelling of Laser Transformation Hardening of Steels, 3rd International Conference on Thermal Process Modelling and Simulation, IFHTSE Conference 2006, Budapest, Hungary, Conference CD proceeding.
10. Reza Rowshan, Balázs Dobi, Process Control in Laser Transformation Hardening of Steels, 22nd Heat Treatment and Materials Science for Mechanical Engineering 2006, pp. 163-169, Balatonfüred, Hungary
11. R. Rowshan, M. K. Baán, Thermal and metallurgical modelling of laser transformation hardened steel parts, Materials Science Forum Vols. 537-538 (2007) pp. 599-606, Trans Tech Publication Ltd 2007.
12. R. Rowshan, M. K. Baán, Finite Element Modelling of Laser Transformation Hardening of Steels, International Journal of Microstructure and Material Properties (IJMMP), Accepted and to be published in 2007.
13. R. Rowshan, M. K. Baán, Optimal Process Control during Laser Transformation Hardening of Steels, microCAD 2007, Accepted and to be published in 2007.
14. Rowshan Reza, Kocsisné Baán Mária, Az acélok lézeres felületedzésének végeselemes modellezése, A gápipari tudományos egyesület műszaki folyóirata (GÉP), Accepted and to be published in 2007.

# REFERENCE


[1] C. Demichelis: IEEE J. Quantum Electronics, 1970, QE-6, pp.630-641.
[2] V. G. Gregson: in 'Laser materials processing', New York, NY, North Holland Publishing Co.; 1983, pp.201–233.
[3] G. R. Speich and A. Szirmae: T rans. Metall. Soc. AIME, 1969, 245 pp.1063–1074.
[4] S. Namba, P. H. Kim, S. Nakayama, and I. Ida: Jpn J. Appl. Phys., 1965, 4, pp.153–154.
[5] G. M. Rubanova and A. P. Sokolov: Sov. Phys. – T ech. Phys., 1968, 12, pp.1226–1228.
[6] V. P. Veiko, A. N. Kokora, and M. P. Libenson: Sov. Phys. Doklady, 1968, 13, pp.231–233.
[7] J. C. Ion, Laser Transformation Hardening, Surface Engineering 2002, Vol. 18 No.1, pp.14-31.
[8] Leonard R.Migliore, ed. Advanced Materials & Processes. Volume 154. August 1998, pp.H25-H29.
[9] Leonard Migliore, ed. Laser material Processing. Laser Kinetics, Inc., Mountain View, California. Theory of laser operation, pp.1-30.
[10] Leonard Migliore, ed. Laser material Processing. Excimer, 1996. pp.263-309.
[11] John C. Ion, ed. Industrial Laser Handbook. Modelling of laser material processing, pp.39-47.
[12] M. Tisza, Phisical Metallurgy of Engineers, ASM International Materials Park, Ohio and Freund Publishing House Ltd. London-Tel Aviv.
[13] H. Skrzypek: Surf. Eng., 1996, 12, pp.335–339.
[14] J. C. Ion and L. M. Anisdahl: J. Mater. Process. Technol ., 1997, 65, pp.261–267.
[15] J. Bach, R. Damascheck, E. Geissler, and H. W. Bergmann: P roc. 3rd Eur. Conf. on Laser Treatment of Materials.
[16] J. C. Ion, T. Moisio, T. F. Pedersen, B. Sorensen, and C. M. Hansson: J. Mater. Sci., 1991, 26 pp.43–48.

[17] J. Com-Nogué and E. Kerrand: Proc. Materials Processing Symp. (ICALEO ’84), (ed. J. Mazumder), pp.112–119; 1985, Toledo, Laser Institute of America.
[18] M. Roth and M. Cantello: Proc. 2nd Int. Conf. on Lasers in Manufacturing (LIM-2), (ed. M. F. Kimmitt ), IF S Publications Ltd.; Bedford, 1985, pp.119–128.
[19] A. K. Mathur and P. A. Molian: J. Eng. Mater. Technol., 1985, 107, pp.200–207.
[20] P. A. Molian: Surf. Eng., 1986, 2, pp.19–28.
[21] M. Yessik and R. P. Scherer: in ‘Source book on applications of the laser in metalworking’, (ed. E. A. Metzbower), pp.219–226; 1981, Metals Park, OH, American Society for Metals.
[22] D. N. H. Trafford, T. Bell, J. H. P. C. Megaw, and a. s. bransden: Met. Technol ., 1983, 10, pp.69–77.
[23] P. Wiesner and M. Eckstein: Weld. Int., 1987, 1, pp. 986–989.
[24] W. Amende: ‘Hardening of materials and machine components with a high power laser’, 1985, Düsseldorf, VDI Verlag.
[25] P. A. Molian and A. K. Mathur: J. Eng. Mater. Technol., 1986, 108, pp. 233–239.
[26] T. Fukuda, M. Kikuchi, A. Yamanishi, and S. Kiguchi: Indust. Heat., 1985, 52, (3 ), pp.41–43.
[27] A. Belforte, Industrial of Russian Laser Review, July 1988,pp.4-7.
[28] E. Miller and J.A. Wineman, Laser Hardening at Saginaw Steering Gear, Metals Progress, Vol.111, 1977, pp.38-43.
[29] V. Change, Paper No. 850406, SAE Technical Paper 1986, pp.3271-3286.
[30] Migliore, Laser Material Processing, Marcel Dekker Inc. NY,1996, pp.209-237.
[31] Hattacharya and F. Seaman, Laser Processing of Materials, K. Mukherjee and J. Mazumdar, Publised by AIME, 1985,pp.211-224.
[32] R. C. Gassmann, et al., Proc. Automotive Laser Applications Workshop ALAW 95, Session 6 (Laser Surface Treatment for Automotive Components).
[33] D. Holtom, Metallurgical, Vol. 53, May 1986,pp.183-184.
[34] D. Dizzi, Laser Welding, Cutting and Surface Treatment, The Welding Institute, Cambrige, 1984, pp.22-23.
[35] Y. Asaka, H. Lobayashi, and S. Arita, Proc. LAMP 87, Lasers in Materials Processing, Osaka, Japan, 1987, pp.517-522.
[36] K. Minamida, M. Kido, A. Ishbashi, S. Mogami and S. Sasaki, Pro. SPIE, The inter. Society for Optical Eng., Vol. 1601, 1990, pp.460-468.
[37] A Belev, et al., Proc. SPIE. The International Society for Optical Engineers, Bol. 3092, 1997, pp. 313-316.
[38] V. V. Diviaskii, G. A. Rainin, and A. V. Scindov, Soviet Electrical Engg., Vol. 59, 1988, pp.42-44.
[39] Rosenthal, D. The Theory of Moving Source of Heat and Its Application To Metal Treatments. Transactions of A.S.M.E, pp.849-866, 1946.
[40] J. C. Ion, PhD Thesis, University of Lulea, Sweden, 1984.
[41] N. Rykalin, A. Uglov and A. Kokora, Laser Machining and Welding, Pergamon Press, Oxford, 1978.
[42] M. F. Ashby and K. E. Easterling, Acta Metall., 32, 1935-1948, 1984.
[43] SYSWELD 2006 Reference Manual, SYSTUS Internation ESI Group.
[44] ASM Handbook,Heat treating, vol. 4,1998.
[45] R. Blondeau,Ph. Maynier, J. Dollet,Pre´vision de la durete´ et de la re´sistance des aciers au carbone et faiblement allie´s d_apre`s leur traitement thermic,Mem. Sci. Rev. Me`tallurgie 70 (12) 1973.

[46] R. Blondeau,Ph. Maynier, J. Dollet,B. Veieillard-Baron, Pre´vision de la durete´,de la re´sistance et de la limite d_e´lasticite´ des aciers au carbone et faiblement allie´s d_apre`s leur composition et leur traitement thermique. Mem. Sci. Rev. Me`tallurgie 1975.
[47] P. Scyffarth, B. Meyer, A. Scharff, Grober Atlas, Schweib-ZTU-Schaubilder, DVS-Verlag Gmblt, Düsseldorf 1992.
[48] Orlich, J., A. Rose and P. Wiest (1973), Atlas zur Wärmebehandlung von Stähle, III Zeit Temperatur Austenitisierung Schaubilder, Verlag Stahleisen MBH, Düsseldorf.
[49] Hsu, T. R., The Finite Element Method in Thermomechanics, Allen & Unwin, Inc., Winchester, MA, 1986, pp.24-76.
[50] SIL Reference Manual, SYSWORLD 2006.
[51] G. Krauss, Steel: heat treatment and processing principles, ASM international, Fifth print, 1997, pp.205-229.
[52] Gergely M., Konkoly T., Számítástechnika alkalmazása szerkezeti acélok és hökezelési technológiák kiválassztásához, OMIKK 1987, pp.69-101.
[53] J.H.Hollomon and L.D.Jaffe, Time-Temperature Relationships in Tempering Steel, Trans. AIME, Vol. 162, 1945, pp.223-249.
[54] M. Gernier, Lauralice de C.F., O. R. Crnkovic, G. E. Totten, Rapid tempering and stress relief via high speed convection heating, www.heattreating.biz/info/heat-treating/articles.htm.

# APPENDIX 1
# EXPERIMENTAL PROCEDURES

## A1.1 Introduction

All experimental procedures of LTH were took place in the *Bay Zoltan Institute of Materials Science and Technology* in Budapest.

The *Bay Zoltan* institute is equipped with "*TRUMPF*" produced "*TLC 105*" type $CO_2$ laser centre, having five beam guidance axes with maximum power of *5 kW* shown *Figure A1.1*.

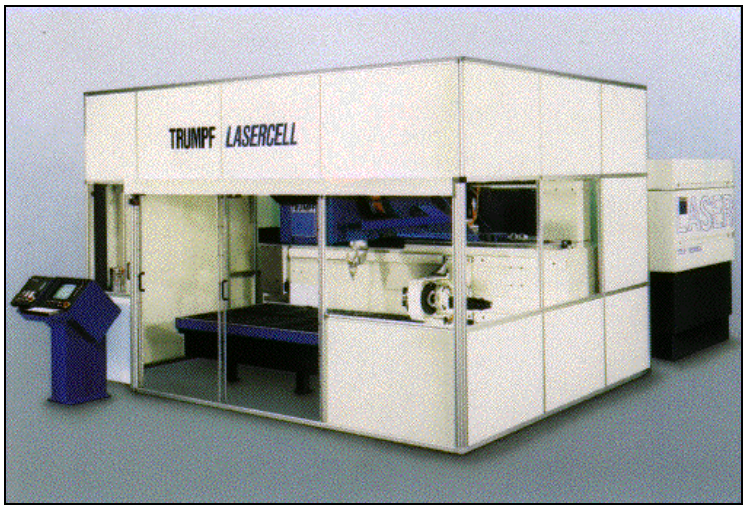


*Figure A1.1 TLC 105 $CO_2$ laser centre*

The *TRUMPF*'s system allows flat, rotationally symmetrical or any type of three-dimensional workpiece to be processed. This machine centre is controlled by CNC controller called *TASC 500* (*Trumpf Advanced Specialized Controller*).

Some important machine parameters are

- Wave length: *10.6 μm*;
- Frequency: continuous wave (*50 kHz*);
- Energy distribution of laser beam spot was measured with a device called *LASERSCOPE* and the energy distribution is illustrated in *Figure A1.2*.

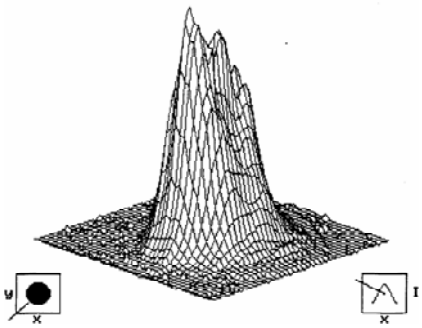

*Figure A1.2 Energy distribution of laser beam spot*

The energy distribution shows that it does not have a perfect Gaussian distribution nor a top hat one. This is due to the characteristic complex mirrors system of the laser machine head. The homogeneity of the energy distribution that affects the accuracy of the process can be changed by changing the laser source head.

In order to carry out the experiments with the laser machine the laser power in *kW*, spot diameter in *mm* and the scanning rate in *mm/min* should be setup.

Significant amount of experiments were done to investigate the LTH in more details since 1996. Our first attempts were to examine the process parameters by changing the laser power and laser spot size and scanning rates, on a steel grade to control the analytical calculations and to gather more information about the behaviour of the laser treated layers for single pass lasers. The next attempt was to investigate the process parameters changing on three different steel grades, namely C45, C60 and S100. Furthermore the overlapping phenomenon was examined by using different process parameters, steel grades, laser passes and percentage of overlapping. In the following, some of the experimental results which are related to this work will be demonstrated.

## A1.2 Single Track LTH Experiments

Different combinations of the technological parameters were applied on C45 steels as listed in Table *A1.1*.

The dimensions of the workpieces are *60×56×10 (mm)*. Three tracks or lasing passes were produced on each surface of the workpieces. The reason for producing three tracks is for the sake of control. The surface of the workpieces was coated by a graphite layer to enhance and unify the energy absorption. The laser beam started at a distance of *10 mm* from the edge of the workpiece, and travelled to a distance of *40 mm*. Each track developed by the lasing pass is at a distance of *18 mm* apart from their central axis, illustrated in *Figure A1.4*.

*Table A1.1 Laser beam parameters*

| Power [kW] | Scan rate [mm/min] |
|---|---|
| 1 | 300 |
| 1 | 600 |
| 2 | 300 |
| 2 | 600 |
| 3 | 300 |
| 3 | 600 |

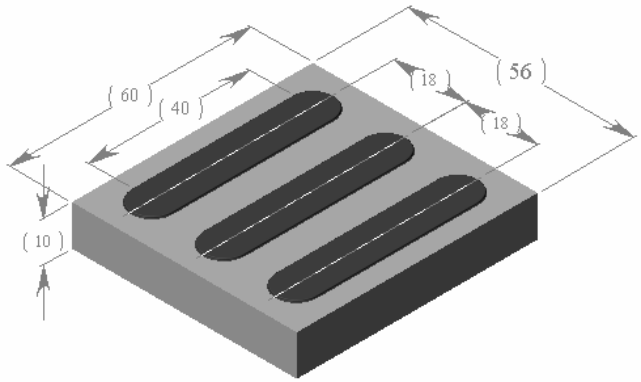


*Figure A1.4 Schematic illustration of the tracks produced on the surface*

By *Vickers* microhardness tester the hardness profiles of laser treated tracks were measured in two directions, in a horizontal direction to measure the width of the track, and a vertical direction to measure the depth of the track using pressing load of *500* g. Depending on the size of the track, the indentations were placed at distances ranging from *0.125-0.6 mm*, in order to measure the depth and width of the track respectively. *Figure A1.5* illustrates the vertical measurement of hardened zone of a C45 steel.

To compare the experimental and the modelling results (shown in section 4.7.3 *Figures 4.30-4.31*), *Figure A1.6* illustrates the microhardness results both for vertical and horizontal measurements in case of laser power of 2 kW, beam radius of 5 mm and scanning rate of 10 mm/s. Microscopic investigations were the other method we used to examine the phase transformations for all experiments.

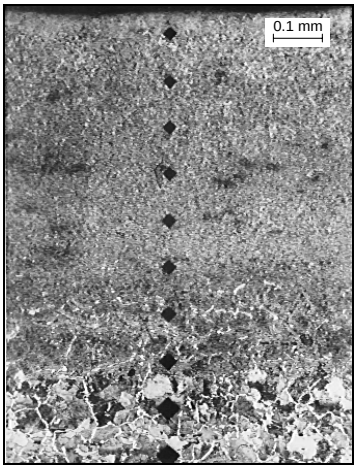


*C45 steel*

*Figure A1.5 Pattern of vertical measurement of hardness test*

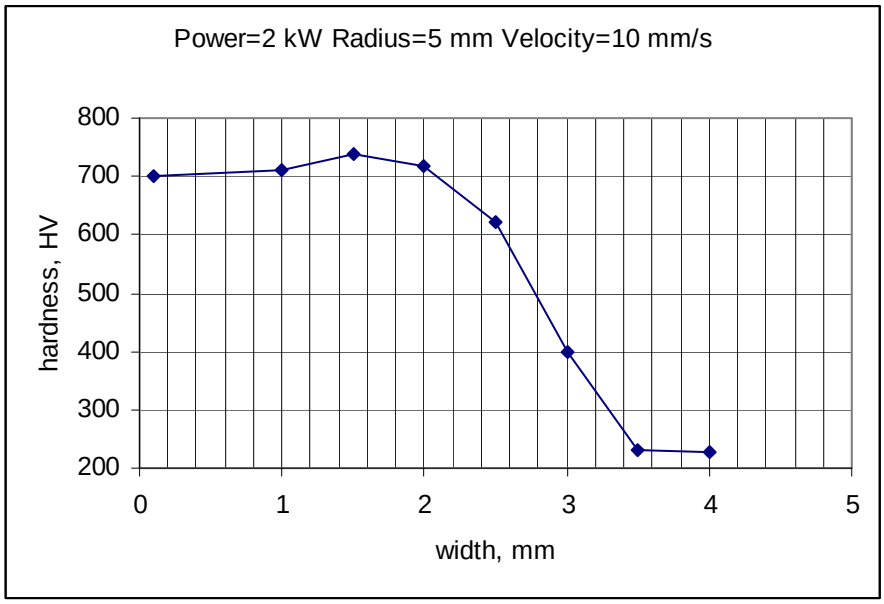


*a*)

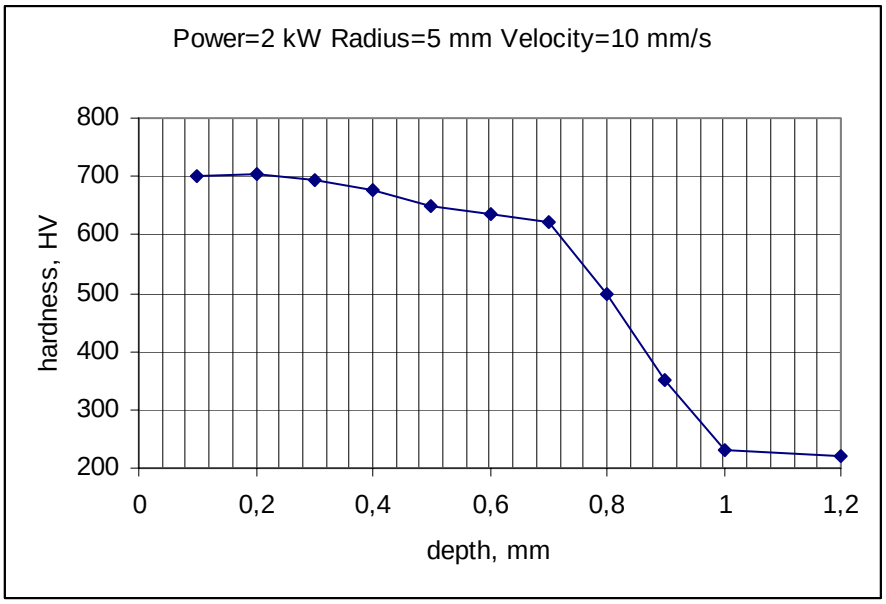


*b*)

*Figure A1.6 Hardness profiles for C45 specimens measured at a) the width and b) the depth of the hardened area*

## A1.3 Multi pass LTH Experiments

Series of experiments aimed to investigate the effect of the overlapping process in case of multi pass laser hardening has been also performed. Ten specimens were used for this purpose. Two pairs of overlapped tracks were prepared on each specimen, while the difference between the axes of the pairs was continuously decreasing. In all experiments the laser beam diameter is *10 mm* and the scanning rate is *10 mm/s*. The actual processing parameters are summarised in the *Table A1.2.*

The experimental results clearly show the effect of the tempering phenomenon discussed in Chapter 6. As mentioned and shown in *Figure A1.2* the laser heat source distribution differs from the Gaussian distribution source used during modelling. For this reason, the track dimensions and subsequently the exact overlapping dimensions is not comparable. Rather the tendency of hardness decrease of the fist treated layer due to the second laser track is the fact that can be compared to the modelling.

*Table A1.2 Experimental parameters setup of multi pass LTH*

| **specimen** | **Laser power, W** | | **Distance between the tracks, mm** |
|---|---|---|---|
| | **First track** | **Second track** | |
| 1 | 1930 | 1770 | 10 |
| 2 | 1930 | 1760 | 9 |
| 3 | 1930 | 1740 | 8 |
| 4 | 1930 | 1730 | 7 |
| 5 | 1930 | 1650 | 6 |
| 6 | 1930 | 1650 | 5 |
| 7 | 1930 | 1650 | 4 |
| 8 | 1930 | 1650 | 3 |
| 9 | 1930 | 1650 | 2 |
| 10 | 1930 | 1650 | 1 |

| First track power (W) | Second track power (W) | Laser scanning rate (mm/s) | Beam diameter (mm) | Distance between two tracks (mm) |
|---|---|---|---|---|
| 1930 | 1770 | 10 | 10 | 10 |


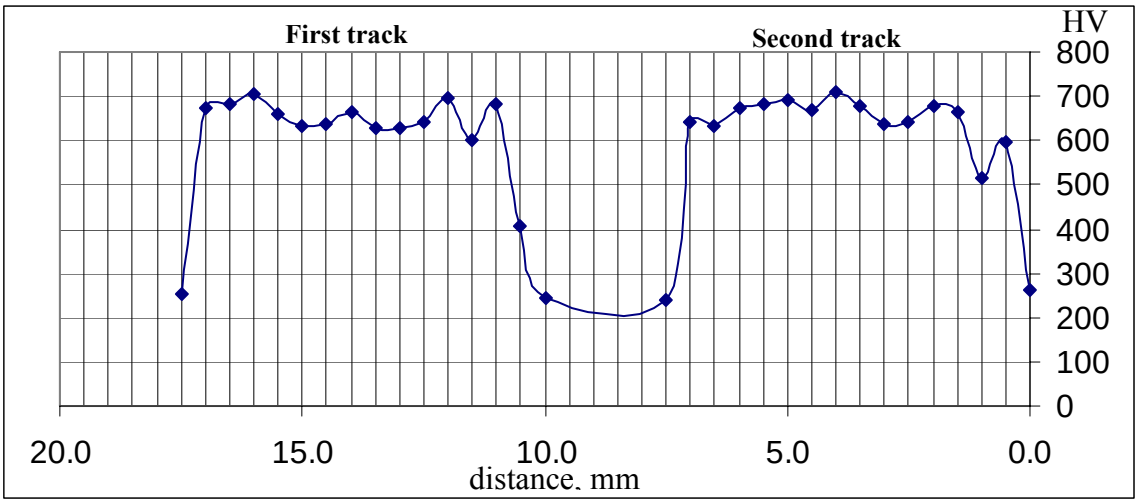


| First track power (W) | Second track power (W) | Laser scanning rate (mm/s) | Beam diameter (mm) | Distance between two tracks (mm) |
|---|---|---|---|---|
| 1930 | 1760 | 10 | 10 | 9 |


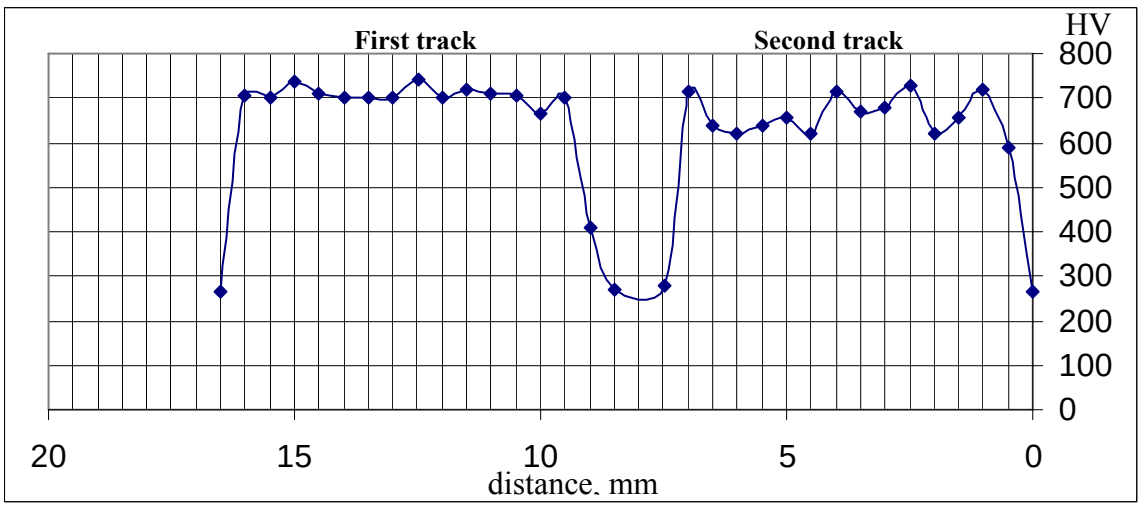

| First track power (W) | Second track power (W) | Laser scanning rate (mm/s) | Beam diameter (mm) | Distance between two tracks (mm) |
|---|---|---|---|---|
| 1930 | 1740 | 10 | 10 | 8 |

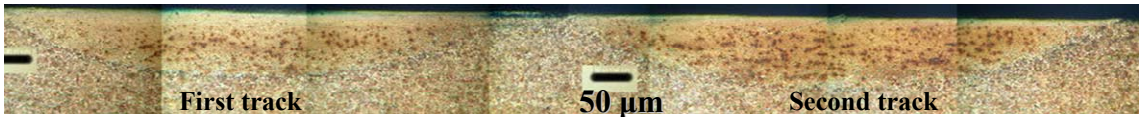


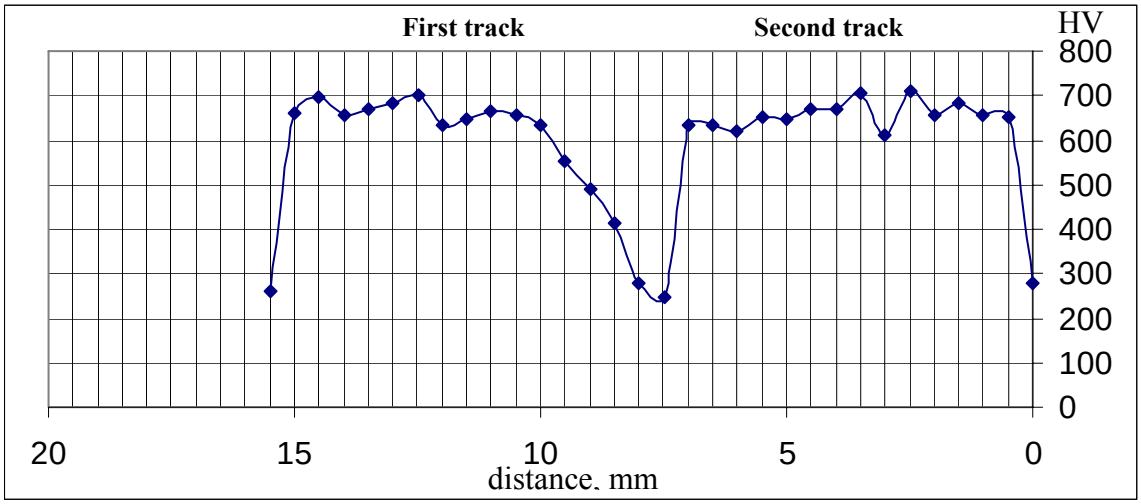


| First track power (W) | Second track power (W) | Laser scanning rate (mm/s) | Beam diameter (mm) | Distance between two tracks (mm) |
|---|---|---|---|---|
| 1930 | 1730 | 10 | 10 | 7 |


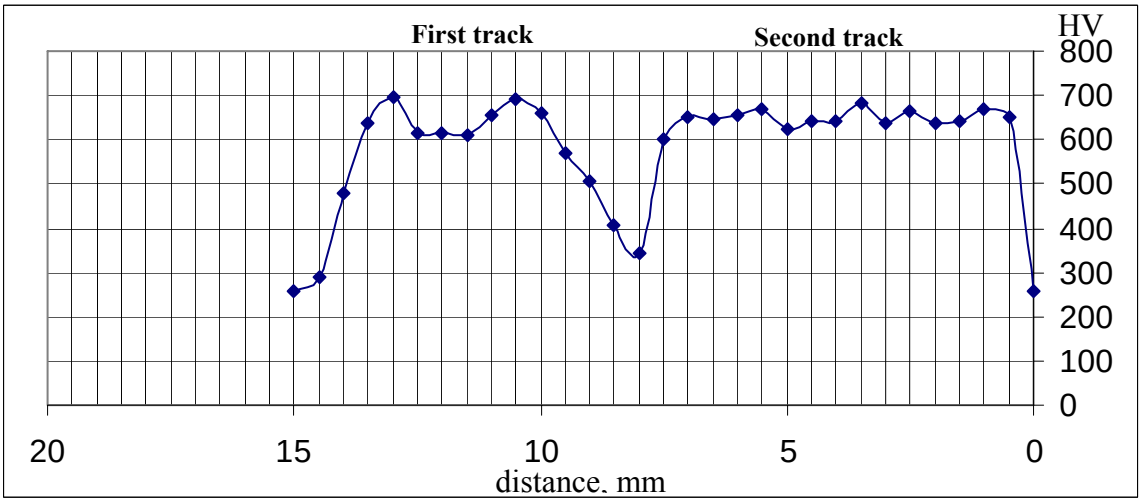

| First track power (W) | Second track power (W) | Laser scanning rate (mm/s) | Beam diameter (mm) | Distance between two tracks (mm) |
|---|---|---|---|---|
| 1930 | 1650 | 10 | 10 | 6 |

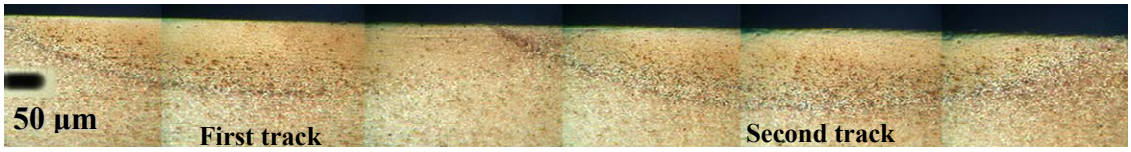


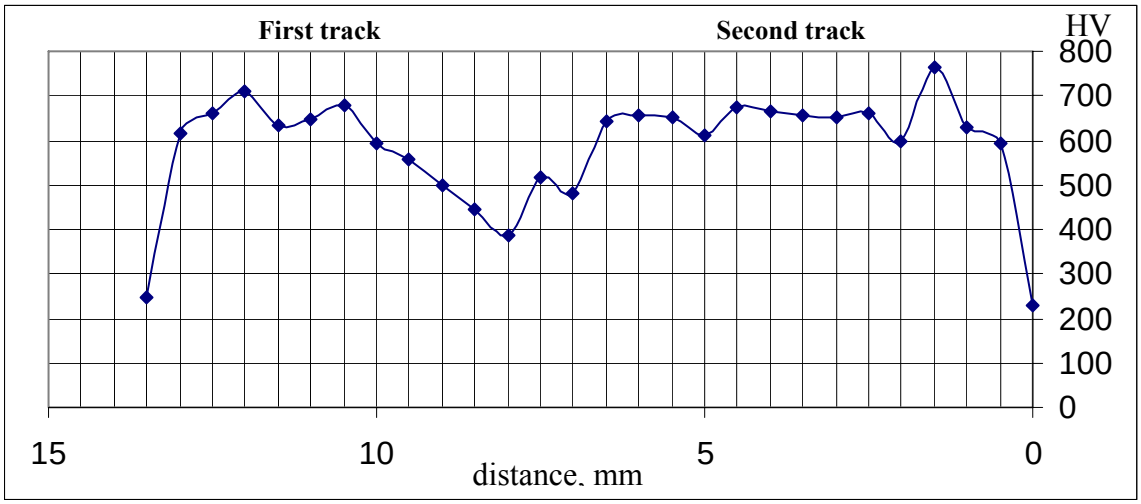


| First track power (W) | Second track power (W) | Laser scanning rate (mm/s) | Beam diameter (mm) | Distance between two tracks (mm) |
|---|---|---|---|---|
| 1930 | 1650 | 10 | 10 | 5 |

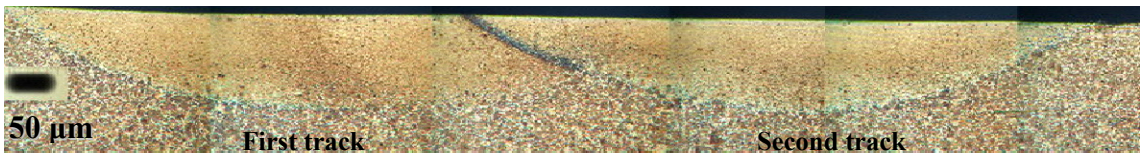


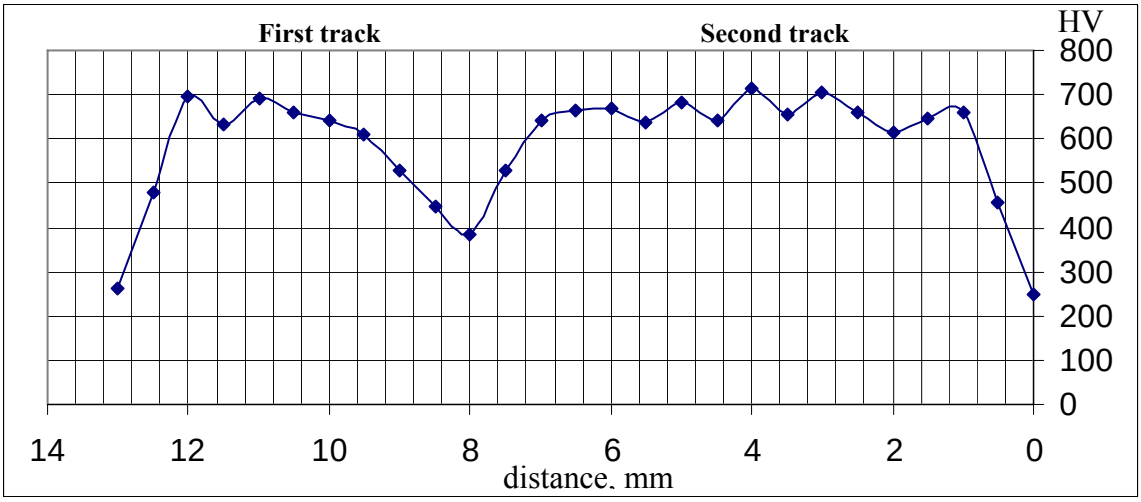

| First track power (W) | Second track power (W) | Laser scanning rate (mm/s) | Beam diameter (mm) | Distance between two tracks (mm) |
|---|---|---|---|---|
| 1930 | 1650 | 10 | 10 | 4 |


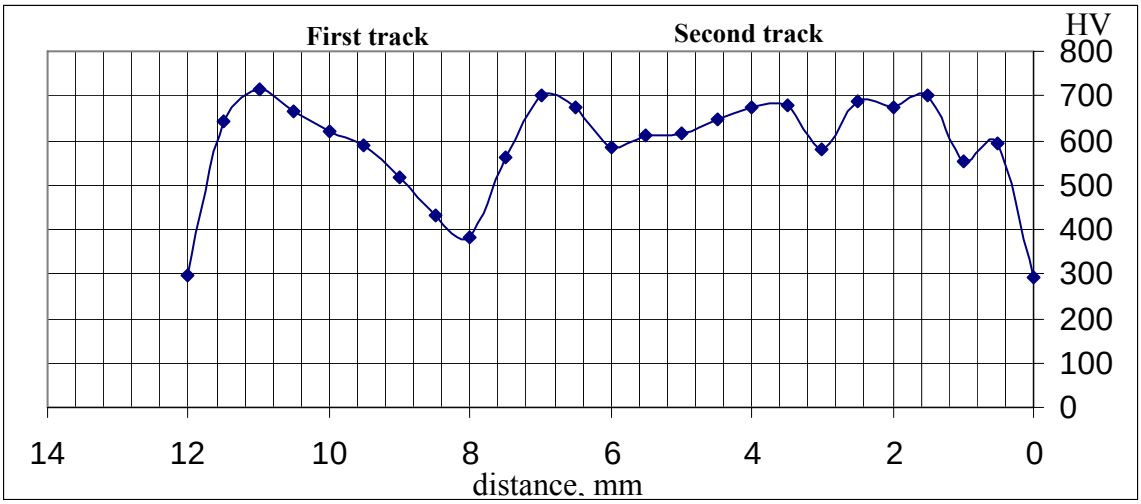


| First track power (W) | Second track power (W) | Laser scanning rate (mm/s) | Beam diameter (mm) | Distance between two tracks (mm) |
|---|---|---|---|---|
| 1930 | 1650 | 10 | 10 | 3 |

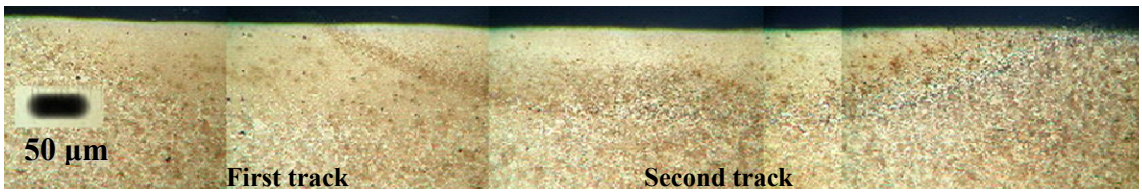


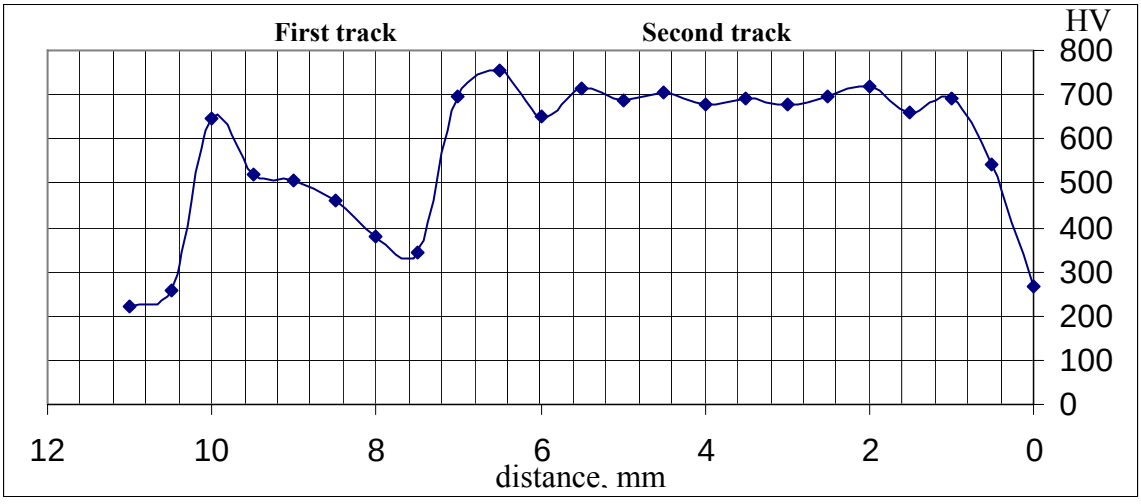

| First track power (W) | Second track power (W) | Laser scanning rate (mm/s) | Beam diameter (mm) | Distance between two tracks (mm) |
|---|---|---|---|---|
| 1930 | 1650 | 10 | 10 | 2 |

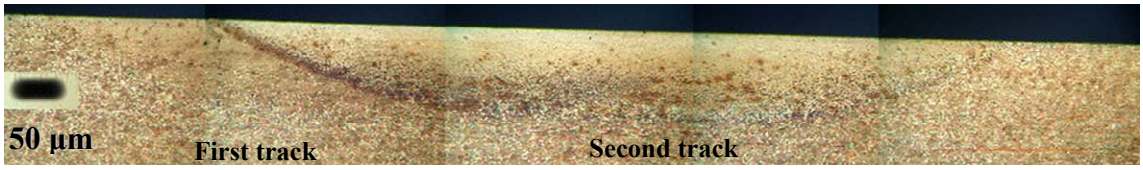


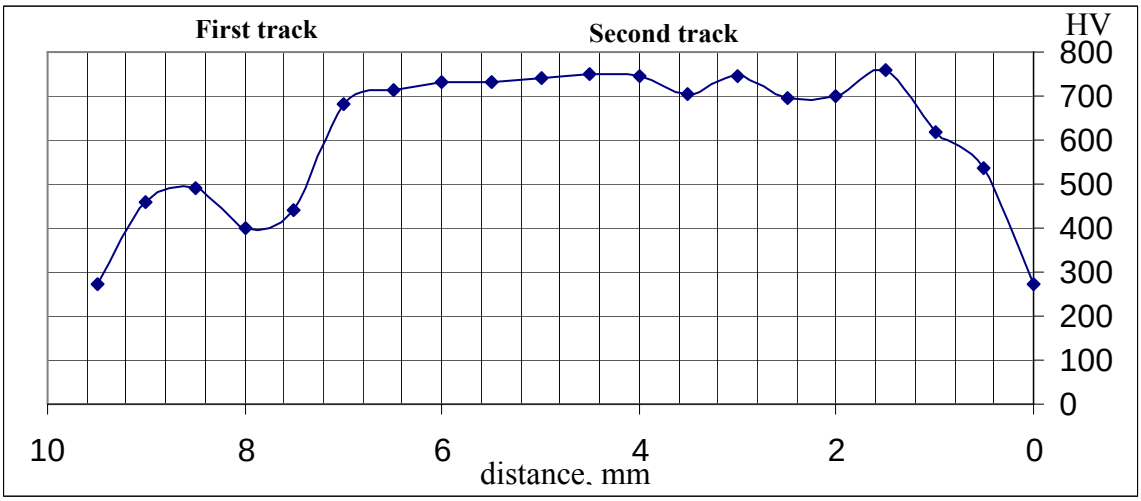


| First track power (W) | Second track power (W) | Laser scanning rate (mm/s) | Beam diameter (mm) | Distance between two tracks (mm) |
|---|---|---|---|---|
| 1930 | 1650 | 10 | 10 | 6 |

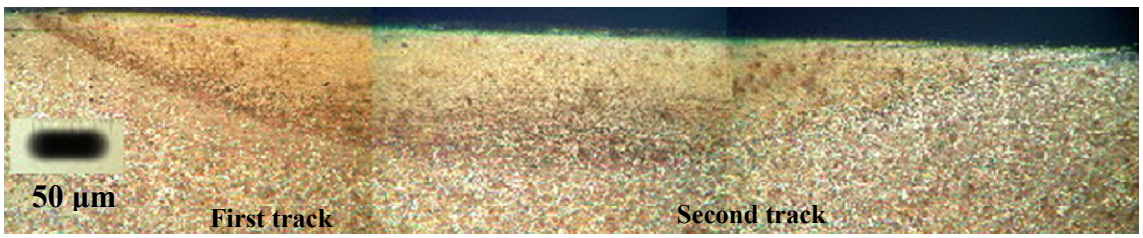


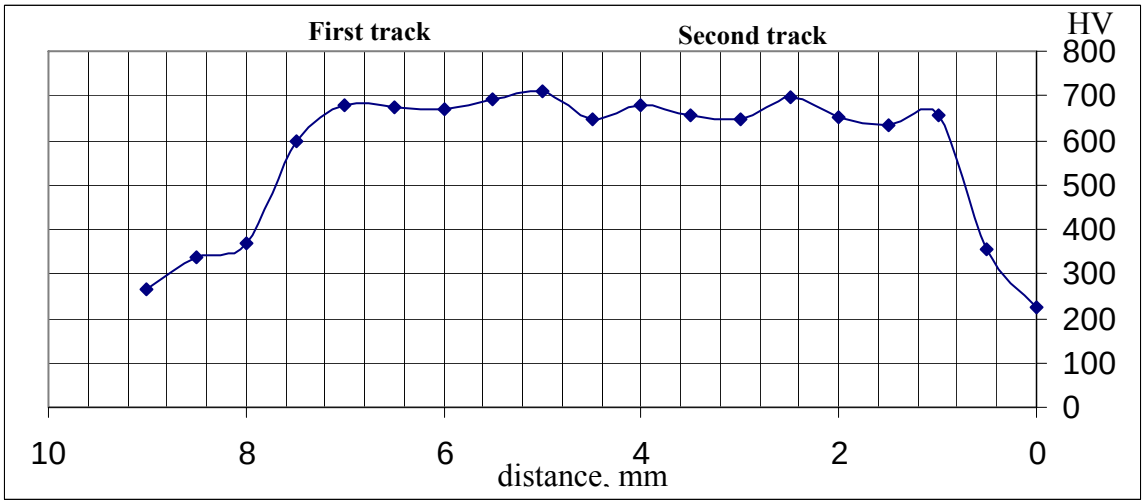

# APPENDIX 2
# PHASE TRANSFORMATIONS CALIBRATION

In this appendix the C45 steel grade phase transformation calibrations files and the METALLURGY.DAT file which is the input SYSWELD file for phase transformations calculations are demonstrated.

For austenite phase calibration the austenitisation diagram of the steel were used and for all other phase transsformations the CCT diagram was the source of the calibrations. From the CCT diagram, the cooling curves and the related phase percentages that are shown in *Table A2.1* were used for this purpose.

*Table A2.1 Cooling curves extracted form the CCT diagram*

| **CCT Calibration C45 Steel** | | | | | | | | |
|---|---|---|---|---|---|---|---|---|
| **Hardness cooling curve (HV30)** | **Identifier** | **t_700(s)** | **t_500(s)** | **t_7/5(s)** | **Cooling rate (°C/s)** | **%Ferrite /Perlite** | **%Bainite CCT** | **%Bainite PHASE** |
| | | | | | | | | |
| 685 | 1 | 1.8 | 4.8 | 3.0 | -66.7 | 0 | 0 | 0 |
| 606 | 2 | 2.0 | 6.5 | 4.5 | -44.4 | 0 | 7 | 7 |
| 473 | 3 | 2.2 | 10.0 | 7.8 | -25.6 | 0 | 13 | 13 |
| 383 | 4 | 4.5 | 16.0 | 11.5 | -17.4 | 39 | 21 | 34 |
| 363 | 5 | 5.0 | 20.0 | 15.0 | -13.3 | 50 | 40 | 80 |
| 263 | 6 | 7.0 | 32.0 | 25.0 | -8.0 | 100 | 0 | 0 |
| 262 | 7 | 14.0 | 60.0 | 46.0 | -4.3 | 100 | 0 | 0 |
| 248 | 8 | 20.0 | 80.0 | 60.0 | -3.3 | 100 | 0 | 0 |
| 235 | 9 | 28.0 | 100.0 | 72.0 | -2.8 | 100 | **0** | **0** |
| 214 | 10 | 30.0 | 140.0 | 110.0 | -1.8 | 100 | **0** | **0** |
| 211 | 11 | 38.0 | 170.0 | 132.0 | -1.5 | 100 | 0 | 0 |

## Austenite calibration file

```
PHASE
CALCULATE
 Austenite Transformation Calibration
VELOCITIES 0.01 0.1 1 10 100 1000 10000
PROPORTION FT 10
TAU FT 11
TABLE
 10 / 1  720 0  850 1
 11 / 1  720 1  1000 0.05  1200 0.001  1350 0.001
INITIAL TEMPERATURE 700
  1500 STEP 5
DRAW
FORMAT
CURVE
RETURN
deass
```

---

## Bainite calibration file

```
;                With this file, the values Tau and F
;                for the bainite transformation are calibrated
PHASE
CALCULATE
 Bainite Transformation Calibration
VELOCITIES -66.7  -44.4 -25.6   -17.4    -13.3
FVELOCITIES  0.11   0.28   0.31   0.628    1.87
PROPORTION FT 1
TAU FT 2
TABLE
 1 / 1 319 0 320 1 550 1 551 0
 2 / 1 319 1*6 320 20 550 20
INITIAL TEMPERATURE 560
  320 STEP -5
DRAW
FORMAT
LIMITS XMIN 320 XMAX 550 YMIN 0 YMAX 1
XHEADER Temperature
YHEADER B proportion
CURVE
RETURN
```

---

## Ferrite/pearlite calibration file

```
;                With this file, the values Tau and F
;                for the ferrite transformation are calibrated
PHASE
CALCULATE
 Ferrite+Pearlite Transformation Calibration
VELOCITIES -25.6 -17.4 -13.3  -8 -4.3  -2.8 -1.5
FVELOCITIES 0.01 0.86  0.925  5    2.9    2   1.1
PROPORTION FT 1
TAU FT 2
TABLE
```

```
 1 / 1 549 0 550 1 700 1 701 0
 2 / 1 549 1*6 550 15 700 15
INITIAL TEMPERATURE 720
  550 STEP -5
DRAW
FORMAT
LIMITS XMIN 550 XMAX 700 YMIN 0 YMAX 1
XHEADER Temperature
YHEADER F proportion
CURVE
RETURN
```

---

## Martensite start adjustment file

```
phase
calculate
 Martensite Calibration for C45 Steel
velocity -0.5  -1 -1.6 -4 -5.5 -7 -19 -53 -200 -1000
fvelocity 0.5   1  1.6  4  5.5  7  19  53  200  1000
proportion ft 1
tau ft 2
table
 1 / 1  0   1  325 1  326 0
 2 / 1  0  58        325 58
initial temperature 400
  -100 step -10
draw martensite
format
limit xmin= 100 xmax 500 ymin 0 ymax 1.
xheader temperature
yheader martensite
curve
;$stop
return
```

---

## Tempered martensite calibration file

```
;                With this file, the values Tau and F
;                for the Tempered Martensite transformation are calibrated
PHASE
CALCULATE
 Tempering as a function of the heating rate
VELOCITIES 700 700 700 700 700 700 700
PROPORTION FT 10
TAU FT 11
TABLE
 10 / 1 150 0 200 0.142 300 0.277 400 0.465 500 0.631 600 0.786
*     700 0.913
 11 / 1 150 100 200 50 300 1.8 400 1.5 500 1.2 600 1.2 700 1.0
INITIAL TEMPERATURE 700
  1500 STEP 5
DRAW
FORMAT
 Temperature
CURVE
RETURN
deass
```

---

## CCT curve display file

```
METALLURGY
CALCULATE NO EDITION
 CCT Calibration
FILE METALLURGY.DAT
MATERIAL 1
AUSTENITE 6
CCT VELOCITIES -66.7 -44.4 -25.6 -17.4 -13.3 -8 -4.3 -2.8 -1.5
INITIAL TEMPERATURE 830
  20 STEP -5
DRAW
ABSCISSA TIME SECONDS
PRECISION 0.01
DIAGRAM CYCLE
RETURN
```

---

## METALLURGY.DAT file

```
MATERIAL 1 PHASE 6
ENTH(1) = ENTH(2) = ENTH(3) = ENTH(4) = ENTH(5) = TABLE 3
ENTH(6)                                  = TABLE 4
KX(1) =                                 = TABLE 5
KX(2) =  KX(3) = KX(4) = KX (5)              = TABLE 6
KX(6)                                   = TABLE 7
RHO(1) = RHO(2) = RHO(3) = RHO(4)  = RHO(5)     = TABLE 8
RHO(6)                                   = TABLE 9
REACTION
 1 6  HEATING  PEQ TABLE 10  TAU TABLE 11
 2 6  HEATING  PEQ TABLE 10  TAU TABLE 11
 3 6  HEATING  PEQ TABLE 10  TAU TABLE 11
 5 6  HEATING  PEQ TABLE 10  TAU TABLE 11
 3 5  HEATING  PEQ TABLE 12  TAU TABLE 13
 6 1  COOLING  PEQ TABLE 20  TAU TABLE 21  F TABLE 22
 6 2  COOLING  PEQ TABLE 40  TAU TABLE 41  F TABLE 42
 6 3  COOLING  MS 320  KM 0.017
TABLES
 3 / 2  0 75000 483  200 177700 544  500 354900 637  700 488500 699
* 750 539700 1349  800 605100 1269  900 700900 647  1400 1027600 660
 4 / 2  0 180000 512  200 285300 541  500 454200 585  700 574200 615
* 900 700900 647  1400 1027600 660  1500 1093300 663  1525 1116600 1200
* 1550 1154500 1830  1600 1261700 2460  1650 1369000 1830
* 1675 1406800 1200 1700 1430300 680  2500 1986300 710

 5 / 1  0 0.049  200 0.044  500 0.037  700 0.032  900 0.027  950 0.0255
* 1400 0.03
 6 / 1  0 0.043  200 0.039  250 0.038  300 0.037  350 0.036  800 0.027
* 900 0.025  1400 0.03
 7 / 1  0 0.015  200 0.017  500 0.021  700 0.023  900 0.025  1400 0.03
* 1500 0.032  1525 0.042  1550 0.06  1600 0.1  1700 0.135  2500 0.27

 8 / 1  20 7815*-9  1500 7290*-9
 9 / 1  20 7990*-9  1500 7290*-9

 10 / 1  720 0  850 1
 11 / 1  720 1  1000 0.05  1200 0.001
```

```
 12 / 1 150 0 200 0.142 300 0.277 400 0.465 500 0.631 600 0.786
*     700 0.913
 13 / 1 150 100 200 50 300 1.8 400 1.5 500 1.2 600 1.2 700 1.0

 20 / 1 549 0 550 1 700 1 701 0
 21 / 1 549 1*6 550 15 700 15
 22 / 1  -25.6 0.01 -17.4 0.86 -13.3 0.925 -8 5 -6 3.5 -4.3 2.5
*     -2.8 1.5 -1.5 0.8 -1 0.6 -0.1 0.1

 40 / 1 319 0 320 1 550 1 551 0
 41 / 1 319 1*6 320 20 550 20
 42 / 1 -66.7 0.01 -44.4 0.28 -25.6 0.31 -17.4 0.628
*      -13.3 1.87
END
```

# APPENDIX 3
# SIMULATION FILES

## Single Track Modelling Files

**SIN_HT.DAT:** This file contains the initial and boundary conditions. The Gaussian heat source distribution, process parameters and its path are defined in this file.

```
NAME SIN_MESH_
SEARCH DATA 1000 ASCII
DEFINITION
 single track  10mm
OPTION THERMAL METALLURGY  SPATIAL
RESTART GEOMETRY
MATERIAL PROPERTIES
 ELEMENTS GROUPS $V1$ / MATE 1
MEDIUM
 WELDLINE / GROUPS $TRAJ1$ REFERENCE $REF1$ ELEMENTS $SE1$ START $SN1$ --
ARRIVAL $EN1$ VELOCITY 10.000000 TINF 0.000000
CONSTRAINTS
 ELEMENTS GROUPS $CONVECTION$ / KT 1 VARIABLE 1
LOAD
1
 ELEMENTS GROUPS $CONVECTION$ / TT 20.
 ELEMENTS GROUPS $D5$ / QR 1 VARIABLE -10000 TRAJECTORY 1
TABLE
 1 / FORTRAN
      function f(t)
c  radiative losses : f = sig * e * (t + to)(t**2 + to**2)
      e = 0.8
      sig = 5.67*-8
```

```
      to = 20.
      to = 20. + 273.15
      t1  = t + 273.15
      a = t1 * t1
      b = to * to
      c = a + b
      d = t1 + to
      d = d * c
      d = d * e
      d = d * sig
c  convective losses = 25 W/m2
      f = d + 25.
c  change to W/mm2
      d = 1*-6
      f = f * d
      return
      END
 10000 /  FORTRAN
      FUNCTION F(X)
C   F   = Q0 * exp( - R^2 / R0^2 ) with
C   R^2 = ( XX-X0 )^2 + ( YY-Y0-VY*T )^2
      DIMENSION X(4)
C Input
      XX = X(1)   ; X Coordinate
      YY = X(2)   ; Y Coordinate
      ZZ = X(3)   ; Z Coordinate (not used)
      TT = X(4)   ; Time
C Variables
      Q0 = 23    ; Maximal source intensity
      R0 = 5     ; Gaussian parameter
      X0 = 0     ; X initial location of source center
      Y0 = 0     ; Y initial location of source center
      Z0 = 0    ; Z initial location of source center
      VY = 0    ; Source displacement velocity
      AY = 0     ; Angle of torch [deg.]
C Constant
      M1 = -1
C
      PIDEG = ATAN(1.)
      PIDEG = PIDEG / 45.
      AY = AY * PIDEG
C Transformation of global to local coordinates
      XD   = XX - X0
      YD   = VY * TT
      YD   = YD + Y0
      ZD   = ZZ - Z0
C Source rotation about Y axis
      SA   = SIN( AY )
      SA   = - SA
      CA   = COS( AY )
      A1   = XD * CA
      A2   = ZD * SA
      XL   = A1 + A2
      YL   = YY - YD
      A1   = ZD * CA
      A2   = XD * SA
      ZL   = A1 - A2
C R^2 computation
      A1   = XL * XL
      A2   = YL * YL
```

```
      R2   = A1 + A2
C R0^2 computation
      R02  = R0 * R0
C F computation
      A    = R2 / R02
      A    = M1 * A
      A    = EXP( A )
      F    = Q0 * A
      RETURN
      END
RETURN
NAME SIN_
SAVE DATA 1000
MEDIUM
EXTRACT MEDIUM
-------------------------------------------------
```

**SIN_HT_C.DAT:** file containing the solver options, simulation time steps and the iteration methods.

```
MEDIUM
; Time Step 1
TRANSIENT NON-LINEAR ARCHIVATE
BEHAVIOUR METALLURGY 6 FILE SIN_METALLURGY.DAT
ALGORITHM BFGS IMPLICIT 1 ITERATION 20
PRECISION ABSOLUTE FORCE 0.01 DISPLACEMENT 0.1 ENERGY 10*-20
METHOD SYMMETRICAL TEST 0  SPARSE
STEP DTMINI 0.001 DTMAXI 5000. EPSF 10*+20 EPSD 50. FACC 0.5 FACP 1.5 FORCE
INITIAL CONDITIONS
 NODES / TT 20.00
 ELEMENTS GROUPS $V1$ / P 1. 0. 0. 0. 0. 0.
TIME INITIAL 0.
 1.000000 STEP 0.010000 / STORE 1
RETURN
; Save as Files DATAyyyy.TIT, TRANyyyy.TIT And HISTyyyy.TIT
NAME SIN_
SAVE DATA TRAN HIST 1000
; File TRANyyyy.TIT And HISTyyyy.TIT
ASSIGN 25 SIN_HIST1000.TIT
ASSIGN 19 SIN_TRAN1000.TIT
TRANSIENT NON-LINEAR ARCHIVATE
BEHAVIOUR METALLURGY 6 FILE SIN_METALLURGY.DAT
ALGORITHM BFGS IMPLICIT 1 ITERATION 20
PRECISION ABSOLUTE FORCE 0.01 DISPLACEMENT 0.1 ENERGY 10*-20
METHOD SYMMETRICAL TEST 0 SPARSE
STEP DTMINI 0.001 DTMAXI 20.000000 EPSF 10*+20 EPSD 50. FACC 0.5 FACP 1.1 --
FORCE
INITIAL CONDITIONS RESTART CARD LAST
TIME INITIAL RESTART
   6.000000 STEP 0.050000 / STORE 1
RETURN
TRANSIENT NON-LINEAR ARCHIVATE
BEHAVIOUR METALLURGY 6 FILE SIN_METALLURGY.DAT
ALGORITHM BFGS IMPLICIT 1 ITERATION 20
PRECISION ABSOLUTE FORCE 0.01 DISPLACEMENT 0.1 ENERGY 10*-20
METHOD SYMMETRICAL TEST 0 SPARSE
STEP DTMINI 0.001 DTMAXI 5000. EPSF 10*+20 EPSD 50. FACC 0.5 FACP 2.0 FORCE
INITIAL CONDITIONS RESTART CARD LAST
TIME INITIAL RESTART
```

```
   1000.000000 STEP 0.100000 / STORE 1
RETURN
; File POST
GROUP SUPPRESS NAME ELEMENTS_POST
$GROUP CREATE NAME ELEMENTS_POST
ELEMENTS DIMENSION 3
RETURN
CONVERSION TRANSIENT
NAME SIN_V_POST1000.fdb
ELEMENTS GROUP $ELEMENTS_POST$
RETURN
NAME SIN_V_
SAVE DATA 1000
DEASSIGN 19
Rebuild File TRAN
NAME SIN_
SEARCH DATA 1000 ; (Standard)
ASSIGN 25 SIN_HIST1000.TIT
TRANSIENT NON-LINEAR REBUILD
BEHAVIOUR METALLURGY 6 FILE SIN_METALLURGY.DAT
METHOD ITERATIVE
CARD ###(List)###
RETURN
Save
SAVE DATA TRAN ###(Output files number)###
```

---

**Hardness.DAT**: This file containing the steel composition and the parameters needed for hardness calculation.

```
SEARCH DATA 1000
ASSIGN 19 TRAN1000.TIT
; Hardness calculation 1. track
HARDNESS EXTRACT -1
COMPOSITION C 0.45 SI 0.4 MN 0.65 NI 0.4 CR 0.4 MO 0.1
PHASE 6
FORMULE MARTENSITE 3
FORMULE BAINITE 2
FORMULE FERRITE 1 5 4
units seconds
VALUE INITIAL MARTENSITE 400 BAINITE 300
ELEMENTS GROUPS $V1$ GAUSS
CARD 0 TO 61 STORE
RETURN
```

---

## Single Track Modelling Files with SIL, Temperature Control Strategy

**T0.DAT**: The initial calculation file at time 0.001s needed as the initial step for further calculations.

```
SEARCH DATA 20
DEFINITION
 CONSTANT TEMPERATURE
OPTION THERMAL METALLURGY  SPATIAL
RESTART GEOMETRY
```

```
MATERIAL PROPERTIES
 ELEMENTS GROUPS $V1$ / MATE 1
MEDIUM
 WELDLINE / GROUPS $TR1$ REFERENCE $REF$ ELEMENTS $SE1$ START $SN1$ ARRIVAL --
$EN1$ VELOCITY 10.000000 TINF 0.000000
CONSTRAINTS
 ELEMENTS GROUPS $D1$ $D2$ $D3$ $D4$ $D5$ / KT 1 VARIABLE 1
LOAD
1
 ELEMENTS GROUPS $D1$ $D2$ $D3$ $D4$ $D5$ / TT 20.
 ELEMENTS GROUPS $D5$ / QR 1 VARIABLE -10000 TRAJECTORY 1
TABLE
 1 / FORTRAN
      function f(t)
c  radiative losses : f = sig * e * (t + to)(t**2 + to**2)
      e = 0.8
      sig = 5.67*-8
      to = 20.
      to = 20. + 273.15
      t1  = t + 273.15
      a = t1 * t1
      b = to * to
      c = a + b
      d = t1 + to
      d = d * c
      d = d * e
      d = d * sig
c  convective losses = 25 W/m2
      f = d + 25.
c  change to W/mm2
      d = 1*-6
      f = f * d
      return
      END
 10000 /  FORTRAN
      FUNCTION F(X)
C   F   = Q0 * exp( - R^2 / R0^2 ) with
C   R^2 = ( XX-X0 )^2 + ( YY-Y0-VY*T )^2
      DIMENSION X(4)
C Input
      XX = X(1)   ; X Coordinate
      YY = X(2)   ; Y Coordinate
      ZZ = X(3)   ; Z Coordinate (not used)
      TT = X(4)   ; Time
C Variables
      Q0 = 50    ; Maximal source intensity
      R0 = 5    ; Gaussian parameter
      X0 = 0    ; X initial location of source center
      Y0 = 0    ; Y initial location of source center
      Z0 = 0   ; Z initial location of source center
      VY = 0   ; Source displacement velocity
      AY = 0    ; Angle of torch [deg.]
C Constant
      M1 = -1
      PIDEG = ATAN(1.)
      PIDEG = PIDEG / 45.
      AY = AY * PIDEG
C Transformation of global to local coordinates
      XD   = XX - X0
      YD   = VY * TT
```

```
      YD   = YD + Y0
      ZD   = ZZ - Z0
C Source rotation about Y axis
      SA   = SIN( AY )
      SA   = - SA
      CA   = COS( AY )
      A1   = XD * CA
      A2   = ZD * SA
      XL   = A1 + A2
      YL   = YY - YD
      A1   = ZD * CA
      A2   = XD * SA
      ZL   = A1 - A2
C R^2 computation
      A1   = XL * XL
      A2   = YL * YL
      R2   = A1 + A2
C R0^2 computation
      R02  = R0 * R0
C F computation
      A    = R2 / R02
      A    = M1 * A
      A    = EXP( A )
      F    = Q0 * A
      RETURN
      END
RETURN
MEDIUM
EXTRACT MEDIUM
MEDIUM
TRAN NON LINEAR
BEHAVIOUR METALLURGY 6 FILE METALLURGY.DAT
METHOD SYMMETRICAL TEST 0  OPTIMISE
ALGORITHM BFGS IMPLICIT 1 ITERATION 20
PRECISION ABSOLUTE FORCE 1*-8 DISPLACEMENT 1*-1
INITIAL CONDITIONS
 NODES / TT 20.00
 ELEMENTS GROUPS $V1$ / P 1. 0. 0. 0. 0. 0.
TIME INITIAL 0.
 0.001 / STORE 1
RETURN
Save DATA TRAN 1000
--------------------------------------------------
```

**tc.cmd**: this is the SIL file. The time interval, time step and temperature interval are set in this file. The SIL file for melting limit is applied to all nodes. For austenitisation limit it is applied only to that group of nodes that is situated at a distance of 0.12mm below the surface. That is why there are some differences in the two files.

### *SIL for melting limit*

```
variable c$,nf;
variable nfile,power,n_nodes,temp[3],i,tmax,n_elem,nbc,q1;
variable lmap,ncards,ttt,i_card,t_init,t_stop,t_step,i_store,t_card;
list param$,textval$,map;
nf=open_file("SOURCE.TXT","continued");
nfile=1000;
power=50.;
tconst=1395;
```

```
i_card=1; t_init=0;
t_card=0.1; t_step=0.1; i_store=1;
t_stop=6.;
write_file(nf,"time = %6.3f",t_init,"   QR = %10.5f\n",power);
label1:
initialize_list(map);
initialize_list(param$);
initialize_list(textval$);
param$ = file_parameter("T1.PAR");
//textval$ #= real_systus_conversion(power);
sprintf(c$,"%f",power);   textval$ #= c$;
sprintf(c$,"%d",i_card);  textval$ #= c$;
sprintf(c$,"%f",t_init);  textval$ #= c$;
sprintf(c$,"%f",t_card);  textval$ #= c$;
sprintf(c$,"%f",t_step);  textval$ #= c$;
sprintf(c$,"%d",i_store); textval$ #= c$;
file_instanciation("T1.PAR",param$,textval$,"T1.DAT");
systus_file("T1.DAT");
sprintf(c$,"ASSIGN 19 TRAN%d.TIT BINARY",nfile);
systus(c$);
map = tran_maps(1);
lmap = length(map);
ncards = map[lmap];
n_nodes=code_systus("nmax");
tmax=-10000;
for (i=1;i<=n_nodes;i=i+1)
 {
   n_elem=int_node_ext_number(i);
   temp=trans_node_displacement(ncards,n_elem);
   if (tmax < temp[1])tmax=temp[1];
 };
tmax ?;
if(abs(tmax-tconst) < 10.)goto label2;
if(tmax > tconst)ttt=tmax; else ttt=tconst;
q1=power;
power =(((tconst-tmax)/ttt)+1.)*q1;
power ?;
goto label1;
label2 :
i_card=ncards; t_init=time_map(ncards);
write_file(nf,"time = %6.3f",t_init,"   QR = %10.5f\n",power);
t_card=t_init+t_step;
if(t_card<=t_stop)goto label1;
close_file(nf);
return();
```

### *SIL for austenitisation limit*

```
variable c$,nf;
variable nfile,power,n_nodes,temp[3],i,tmax,nbc,q1;
variable lmap,ncards,ttt,i_card,t_init,t_stop,t_step,i_store,t_card;
variable meth$,prop$,comm$,issu,icol;
list param$,textval$,map;
list n_elem;
nf=open_file("SOURCE_r1.TXT","continued");
nfile=1000;
power=50.;
tconst=930;
i_card=1; t_init=0;
t_card=0.1; t_step=0.1; i_store=1;
```

```
t_stop=6.;
write_file(nf,"time = %6.3f",t_init,"   QR = %10.5f\n",power);
label1:
initialize_list(map);
initialize_list(param$);
initialize_list(textval$);
initialize_list(n_elem);
param$ = file_parameter("T1.PAR");
//textval$ #= real_systus_conversion(power);
sprintf(c$,"%f",power);   textval$ #= c$;
sprintf(c$,"%d",i_card);  textval$ #= c$;
sprintf(c$,"%f",t_init);  textval$ #= c$;
sprintf(c$,"%f",t_card);  textval$ #= c$;
sprintf(c$,"%f",t_step);  textval$ #= c$;
sprintf(c$,"%d",i_store); textval$ #= c$;
file_instanciation("T1.PAR",param$,textval$,"T1.DAT");
systus_file("T1.DAT");
sprintf(c$,"ASSIGN 19 TRAN%d.TIT BINARY",nfile);
systus(c$);
map = tran_maps(1);
lmap = length(map);
ncards = map[lmap];
//n_nodes=code_systus("nmax");
extract_group("DEP12",0,1,n_nodes,n_elem,meth$,prop$,comm$,issu,icol);
n_elem?;
tmax=-10000;
for (i=1;i<=n_nodes;i=i+1)
 {
//   n_elem=int_node_ext_number(i);
   temp=trans_node_displacement(ncards,n_elem[i]);
   if (tmax < temp[1])tmax=temp[1];
 };
tmax ?;
if(abs(tmax-tconst) < 10.)goto label2;
if(tmax > tconst)ttt=tmax; else ttt=tconst;
q1=power;
power =(((tconst-tmax)/ttt)+1.)*q1;
power ?;
goto label1;
label2 :
i_card=ncards; t_init=time_map(ncards);
write_file(nf,"time = %6.3f",t_init,"   QR = %10.5f\n",power);
t_card=t_init+t_step;
if(t_card<=t_stop)goto label1;
close_file(nf);
return();
```

---

**T1.PAR**: This file contains all thermal initial and boundary conditions. Heat source shape is modelled here and the value of heat flux density, process time and the time step are recalled from the previous SIL file. This file iterates the process until obtaining the required temperature set in SIL.

```
SEARCH DATA 20
DEFINITION
 CONSTANT TEMPERATURE
OPTION THERMAL METALLURGY  SPATIAL
RESTART GEOMETRY
MATERIAL PROPERTIES
```

```
 ELEMENTS GROUPS $V1$ / MATE 1
MEDIUM
 WELDLINE / GROUPS $TR1$ REFERENCE $REF$ ELEMENTS $SE1$ START $SN1$ ARRIVAL --
$EN1$ VELOCITY 10.000000 TINF 0.000000
CONSTRAINTS
 ELEMENTS GROUPS $D1$ $D2$ $D3$ $D4$ $D5$ / KT 1 VARIABLE 1
LOAD
1
 ELEMENTS GROUPS $D1$ $D2$ $D3$ $D4$ $D5$ / TT 20.
 ELEMENTS GROUPS $D5$ / QR 1 VARIABLE -10000 TRAJECTORY 1
TABLE
 1 / FORTRAN
      function f(t)
c  radiative losses : f = sig * e * (t + to)(t**2 + to**2)
      e = 0.8
      sig = 5.67*-8
      to = 20.
      to = 20. + 273.15
      t1  = t + 273.15
      a = t1 * t1
      b = to * to
      c = a + b
      d = t1 + to
      d = d * c
      d = d * e
      d = d * sig
c  convective losses = 25 W/m2
      f = d + 25.
c  change to W/mm2
      d = 1*-6
      f = f * d
      return
      END
 10000 /  FORTRAN
      FUNCTION F(X)
C   F   = Q0 * exp( - R^2 / R0^2 ) with
C   R^2 = ( XX-X0 )^2 + ( YY-Y0-VY*T )^2
      DIMENSION X(4)
C Input
      XX = X(1)   ; X Coordinate
      YY = X(2)   ; Y Coordinate
      ZZ = X(3)   ; Z Coordinate (not used)
      TT = X(4)   ; Time
C Variables
      Q0 = @par1@    ; Maximal source intensity
      R0 = 5    ; Gaussian parameter
      X0 = 0    ; X initial location of source center
      Y0 = 0    ; Y initial location of source center
      Z0 = 0   ; Z initial location of source center
      VY = 0   ; Source displacement velocity
      AY = 0    ; Angle of torch [deg.]
C Constant
      M1 = -1
      PIDEG = ATAN(1.)
      PIDEG = PIDEG / 45.
      AY = AY * PIDEG
C Transformation of global to local coordinates
      XD   = XX - X0
      YD   = VY * TT
      YD   = YD + Y0
```

```
      ZD   = ZZ - Z0
C Source rotation about Y axis
      SA   = SIN( AY )
      SA   = - SA
      CA   = COS( AY )
      A1   = XD * CA
      A2   = ZD * SA
      XL   = A1 + A2
      YL   = YY - YD
      A1   = ZD * CA
      A2   = XD * SA
      ZL   = A1 - A2
C R^2 computation
      A1   = XL * XL
      A2   = YL * YL
      R2   = A1 + A2
C R0^2 computation
      R02  = R0 * R0
C F computation
      A    = R2 / R02
      A    = M1 * A
      A    = EXP( A )
      F    = Q0 * A
      RETURN
      END
RETURN
MEDIUM
EXTRACT MEDIUM
MEDIUM;
Time Step 0
assi 19 TRAN1000.TIT
TRANSIENT NON-LINEAR
BEHAVIOUR METALLURGY 6 FILE METALLURGY.DAT
METHOD SYMMETRICAL TEST 0  OPTIMISE
ALGORITHM BFGS IMPLICIT 1 ITERATION 30
PRECISION ABSOLUTE FORCE 1*-8 DISPLACEMENT 1*-1
initial conditions restart card @par2@
time initial @par3@
 @par4@  step @par5@ / store @par6@
return
-------------------------------------------------
```

**T_COOL.DAT**: This file contains the calculation of the simulations for the cooling process. In this case the load is removed from the surface and the SIL program is switched off.

```
SEARCH DATA 1000
DEFINITION
 CONSTANT TEMPERATURE
OPTION THERMAL METALLURGY  SPATIAL
RESTART GEOMETRY
MATERIAL PROPERTIES
 ELEMENTS GROUPS $V1$ / MATE 1
CONSTRAINTS
 ELEMENTS GROUPS $D1$ $D2$ $D3$ $D4$ $D5$ / KT 1 VARIABLE 1
LOAD
1
 ELEMENTS GROUPS $D1$ $D2$ $D3$ $D4$ $D5$ / TT 20.
TABLE
 1 / FORTRAN
```

```
      function f(t)
c  radiative losses : f = sig * e * (t + to)(t**2 + to**2)
      e = 0.8
      sig = 5.67*-8
      to = 20.
      to = 20. + 273.15
      t1  = t + 273.15
      a = t1 * t1
      b = to * to
      c = a + b
      d = t1 + to
      d = d * c
      d = d * e
      d = d * sig
c  convective losses = 25 W/m2
      f = d + 25.
c  change to W/mm2
      d = 1*-6
      f = f * d
      return
      END
 10000 /  FORTRAN
      FUNCTION F(X)
C   F   = Q0 * [(R1 - R)/(R1 - R0)]
      DIMENSION X(4)
C Input
      XX = X(1)   ; X Coordinate
      YY = X(2)   ; Y Coordinate
      ZZ = X(3)   ; Z Coordinate (not used)
      TT = X(4)   ; Time
C Variables
      Q0 = 50    ; Maximal source intensity
      R0 = 2     ; Inner Radius
      R1 = 5     ; Outer Radius
      XX2   = XX * XX
      YY2   = YY * YY
      RR2   = XX2 + YY2
      RR    = SQRT (RR2)
      F = 0
      IF (RR.GE.R1) RETURN
      F = Q0
      IF (RR.LE.R0) RETURN
      P1    = R1 - RR
      P2    = R1 - R0
      F     = P1/P2
      F     = F * Q0
      RETURN
      END
RETURN
ASSI 19 TRAN1000.TIT
TRAN NON LINEAR
BEHAVIOUR METALLURGY 6 FILE METALLURGY.DAT
METHOD SYMMETRICAL TEST 0  OPTIMISE
ALGORITHM BFGS IMPLICIT 1 ITERATION 20
PRECISION ABSOLUTE FORCE 1*-8 DISPLACEMENT 1*-1
INITIAL CONDITIONS RESTART CARD 61
TIME INITIAL RESTART
   30 step 1 / STORE 1
   50 step 5 / STORE 1
   100 step 10 / STORE 1
```

```
   1000 step 100 / STORE 1
RETURN
Save DATA 1000
-------------------------------------------------
```

**HARDNESS_ALL:DAT**: this file calculates hardness distribution.

```
SEARCH DATA 1000
ASSIGN 19 TRAN1000.TIT
Hardness calculation 1. track
HARDNESS EXTRACT -1
COMPOSITION C 0.45 SI 0.4 MN 0.65 NI 0.4 CR 0.4 MO 0.1
PHASE 6
FORMULE MARTENSITE 3
FORMULE BAINITE 2
FORMULE FERRITE 1 5 4
units seconds
VALUE INITIAL MARTENSITE 400 BAINITE 300
ELEMENTS GROUPS $V1$ GAUSS
CARD 0 TO 61 STORE
RETURN
save data tran 3000 ascii sele
ELEM GROUP $V1$
CARD 0 TO 61 STORE
RETURN
SEARCH DATA tran 3000 ascii
save data tran 3000
delete data tran 3000 ascii
```

# Two Overlapped Laser Tracks Modelling Files with SIL, Temperature Control Strategy

**T0.DAT:** Initial file.

```
SEARCH DATA 12
DEFINITION
 CONSTANT TEMPERATURE
OPTION THERMAL METALLURGY  SPATIAL
RESTART GEOMETRY
MATERIAL PROPERTIES
 ELEMENTS GROUPS $V1$ / MATE 1
MEDIUM
 WELDLINE / GROUPS $TR1$ REFERENCE $REF$ ELEMENTS $SE1$ START $SN1$ --
ARRIVAL $EN1$ VELOCITY 10.000000 TINF 0.000000
CONSTRAINTS
 ELEMENTS GROUPS $D1$ $D2$ $D3$ $D4$ $D5$ $D6$ / KT 1 VARIABLE 1
LOAD
1
 ELEMENTS GROUPS $D1$ $D2$ $D3$ $D4$ $D5$ $D6$ / TT 20.
 ELEMENTS GROUPS $D5$ / QR 1 VARIABLE -10000 TRAJECTORY 1
TABLE
 1 / FORTRAN
      function f(t)
c  radiative losses : f = sig * e * (t + to)(t**2 + to**2)
      e = 0.8
      sig = 5.67*-8
      to = 20.
      to = 20. + 273.15
```

```
      t1  = t + 273.15
      a = t1 * t1
      b = to * to
      c = a + b
      d = t1 + to
      d = d * c
      d = d * e
      d = d * sig
c  convective losses = 25 W/m2
      f = d + 25.
c  change to W/mm2
      d = 1*-6
      f = f * d
      return
      END
 10000 /  FORTRAN
      FUNCTION F(X)
C   F   = Q0 * exp( - R^2 / R0^2 ) with
C   R^2 = ( XX-X0 )^2 + ( YY-Y0-VY*T )^2
      DIMENSION X(4)
C Input
      XX = X(1)   ; X Coordinate
      YY = X(2)   ; Y Coordinate
      ZZ = X(3)   ; Z Coordinate (not used)
      TT = X(4)   ; Time
C Variables
      Q0 = 20    ; Maximal source intensity
      R0 = 5     ; Gaussian parameter
      X0 = 0     ; X initial location of source center
      Y0 = 0     ; Y initial location of source center
      Z0 = 0   ; Z initial location of source center
      VY = 0   ; Source displacement velocity
      AY = 0     ; Angle of torch [deg.]
C Constant
      M1 = -1
      PIDEG = ATAN(1.)
      PIDEG = PIDEG / 45.
      AY = AY * PIDEG
C Transformation of global to local coordinates
      XD   = XX - X0
      YD   = VY * TT
      YD   = YD + Y0
      ZD   = ZZ - Z0
C Source rotation about Y axis
      SA   = SIN( AY )
      SA   = - SA
      CA   = COS( AY )
      A1   = XD * CA
      A2   = ZD * SA
      XL   = A1 + A2
      YL   = YY - YD
      A1   = ZD * CA
      A2   = XD * SA
      ZL   = A1 - A2
C R^2 computation
      A1   = XL * XL
      A2   = YL * YL
      R2   = A1 + A2
C R0^2 computation
      R02  = R0 * R0
```

```
C F computation
      A    = R2 / R02
      A    = M1 * A
      A    = EXP( A )
      F    = Q0 * A
      RETURN
      END
RETURN
MEDIUM
EXTRACT MEDIUM
MEDIUM
TRAN NON LINEAR
BEHAVIOUR METALLURGY 6 FILE METALLURGY.DAT
METHOD SYMMETRICAL TEST 0  OPTIMISE
ALGORITHM BFGS IMPLICIT 1 ITERATION 20
PRECISION ABSOLUTE FORCE 1*-8 DISPLACEMENT 1*-1
INITIAL CONDITIONS
 NODES / TT 20.00
 ELEMENTS GROUPS $V1$ / P 1. 0. 0. 0. 0. 0.
TIME INITIAL 0.
 0.001 / STORE 1
RETURN
Save DATA TRAN 1000
-------------------------------------------------
```

**tc.cmd**: First track SIL file.

```
variable c$,nf;
variable nfile,power,n_nodes,temp[3],i,tmax,n_elem,nbc,q1;
variable lmap,ncards,ttt,i_card,t_init,t_stop,t_step,i_store,t_card;
list param$,textval$,map;
nf=open_file("SOURCE.TXT","continued");
nfile=1000;
power=20.;
tconst=1395;
i_card=1; t_init=0;
t_card=0.1; t_step=0.1; i_store=1;
t_stop=4.;
write_file(nf,"time = %6.3f",t_init,"    QR = %10.5f\n",power);
label1:
initialize_list(map);
initialize_list(param$);
initialize_list(textval$);
param$ = file_parameter("T1.PAR");
//textval$ #= real_systus_conversion(power);
sprintf(c$,"%f",power);   textval$ #= c$;
sprintf(c$,"%d",i_card);  textval$ #= c$;
sprintf(c$,"%f",t_init);  textval$ #= c$;
sprintf(c$,"%f",t_card);  textval$ #= c$;
sprintf(c$,"%f",t_step);  textval$ #= c$;
sprintf(c$,"%d",i_store); textval$ #= c$;
file_instanciation("T1.PAR",param$,textval$,"T1.DAT");
systus_file("T1.DAT");
sprintf(c$,"ASSIGN 19 TRAN%d.TIT BINARY",nfile);
systus(c$);
map = tran_maps(1);
lmap = length(map);
ncards = map[lmap];
n_nodes=code_systus("nmax");
tmax=-10000;
```

```
for (i=1;i<=n_nodes;i=i+1)
 {
  n_elem=int_node_ext_number(i);
  temp=trans_node_displacement(ncards,n_elem);
  if (tmax < temp[1])tmax=temp[1];
 };
tmax ?;
if(abs(tmax-tconst) < 10.)goto label2;
if(tmax > tconst)ttt=tmax; else ttt=tconst;
q1=power;
power =(((tconst-tmax)/ttt)+1.)*q1;
power ?;
goto label1;
label2 :
i_card=ncards; t_init=time_map(ncards);
write_file(nf,"time = %6.3f",t_init,"   QR = %10.5f\n",power);
t_card=t_init+t_step;
if(t_card<=t_stop)goto label1;
close_file(nf);
return();
-----------------------------------------------------
```

**T1.PAR**: First track running file.

```
SEARCH DATA 12
DEFINITION
 CONSTANT TEMPERATURE
OPTION THERMAL METALLURGY  SPATIAL
RESTART GEOMETRY
MATERIAL PROPERTIES
 ELEMENTS GROUPS $V1$ / MATE 1
MEDIUM
 WELDLINE / GROUPS $TR1$ REFERENCE $REF$ ELEMENTS $SE1$ START $SN1$ --
ARRIVAL $EN1$ VELOCITY 10.000000 TINF 0.000000
CONSTRAINTS
 ELEMENTS GROUPS $D1$ $D2$ $D3$ $D4$ $D5$ $D6$ / KT 1 VARIABLE 1
LOAD
1
 ELEMENTS GROUPS $D1$ $D2$ $D3$ $D4$ $D5$ $D6$ / TT 20.
 ELEMENTS GROUPS $D5$ / QR 1 VARIABLE -10000 TRAJECTORY 1
TABLE
 1 / FORTRAN
      function f(t)
c  radiative losses : f = sig * e * (t + to)(t**2 + to**2)
      e = 0.8
      sig = 5.67*-8
      to = 20.
      to = 20. + 273.15
      t1  = t + 273.15
      a = t1 * t1
      b = to * to
      c = a + b
      d = t1 + to
      d = d * c
      d = d * e
      d = d * sig
c  convective losses = 25 W/m2
      f = d + 25.
c  change to W/mm2
      d = 1*-6
```

```
      f = f * d
      return
      END
 10000 /  FORTRAN
      FUNCTION F(X)
C   F   = Q0 * exp( - R^2 / R0^2 ) with
C   R^2 = ( XX-X0 )^2 + ( YY-Y0-VY*T )^2
      DIMENSION X(4)
C Input
      XX = X(1)   ; X Coordinate
      YY = X(2)   ; Y Coordinate
      ZZ = X(3)   ; Z Coordinate (not used)
      TT = X(4)   ; Time
C Variables
      Q0 = @par1@    ; Maximal source intensity
      R0 = 5    ; Gaussian parameter
      X0 = 0    ; X initial location of source center
      Y0 = 0    ; Y initial location of source center
      Z0 = 0   ; Z initial location of source center
      VY = 0   ; Source displacement velocity
      AY = 0    ; Angle of torch [deg.]
C Constant
      M1 = -1
      PIDEG = ATAN(1.)
      PIDEG = PIDEG / 45.
      AY = AY * PIDEG
C Transformation of global to local coordinates
      XD   = XX - X0
      YD   = VY * TT
      YD   = YD + Y0
      ZD   = ZZ - Z0
C Source rotation about Y axis
      SA   = SIN( AY )
      SA   = - SA
      CA   = COS( AY )
      A1   = XD * CA
      A2   = ZD * SA
      XL   = A1 + A2
      YL   = YY - YD
      A1   = ZD * CA
      A2   = XD * SA
      ZL   = A1 - A2
C R^2 computation
      A1   = XL * XL
      A2   = YL * YL
      R2   = A1 + A2
C R0^2 computation
      R02  = R0 * R0
C F computation
      A    = R2 / R02
      A    = M1 * A
      A    = EXP( A )
      F    = Q0 * A
      RETURN
      END
RETURN
MEDIUM
EXTRACT MEDIUM
MEDIUM
; Time Step 0
```

```
assi 19 TRAN1000.TIT
TRANSIENT NON-LINEAR
BEHAVIOUR METALLURGY 6 FILE METALLURGY.DAT
METHOD SYMMETRICAL TEST 0  OPTIMISE
ALGORITHM BFGS IMPLICIT 1 ITERATION 20
PRECISION ABSOLUTE FORCE 1*-8 DISPLACEMENT 1*-1
initial conditions restart card @par2@
time initial @par3@
 @par4@  step @par5@ / store @par6@
return
---------------------------------------------------
```

**Tc_mod2.cmd**: Second track SIL file (melting limit).

```
variable c$,nf;
variable nfile,power,n_nodes,temp[3],i,tmax,n_elem,nbc,q1;
variable lmap,ncards,ttt,i_card,t_init,t_stop,t_step,i_store,t_card;
list param$,textval$,map;
nf=open_file("SOURCE2.TXT","continued");
nfile=1000;
power=50.;
tconst=1395;
i_card=45; t_init=6;
t_step=0.1; i_store=1; t_card=t_init+t_step;
t_stop=10;
write_file(nf,"time = %6.3f",t_init,"   QR = %10.5f\n",power);
label1:
initialize_list(map);
initialize_list(param$);
initialize_list(textval$);
param$ = file_parameter("T2.PAR");
//textval$ #= real_systus_conversion(power);
sprintf(c$,"%f",power);   textval$ #= c$; // par1
sprintf(c$,"%d",i_card);  textval$ #= c$; // par2
sprintf(c$,"%f",t_init);  textval$ #= c$; // par3
sprintf(c$,"%f",t_card);  textval$ #= c$; // par4
sprintf(c$,"%f",t_step);  textval$ #= c$; // par5
sprintf(c$,"%d",i_store); textval$ #= c$; // par6
file_instanciation("T2.PAR",param$,textval$,"T2.DAT");
systus_file("T2.DAT");
sprintf(c$,"ASSIGN 19 TRAN%d.TIT BINARY",nfile);
systus(c$);
map = tran_maps(1);
lmap = length(map);
ncards = map[lmap];
n_nodes=code_systus("nmax");
tmax=-10000;
for (i=1;i<=n_nodes;i=i+1)
 {
  n_elem=int_node_ext_number(i);
  temp=trans_node_displacement(ncards,n_elem);
  if (tmax < temp[1])tmax=temp[1];
 };
tmax ?;
if(abs(tmax-tconst) < 10.)goto label2;
if(tmax > tconst)ttt=tmax; else ttt=tconst;
q1=power;
power =(((tconst-tmax)/ttt)+1.)*q1;
power ?;
goto label1;
```

```
label2 :
i_card=ncards; t_init=time_map(ncards);
write_file(nf,"time = %6.3f",t_init,"   QR = %10.5f\n",power);
t_card=t_init+t_step;
if(t_card<=t_stop)goto label1;
close_file(nf);
return();
-------------------------------------------------
```

**T2.PAR**: Second track running file (melting limit).

```
SEARCH DATA 1000
DEFINITION
 CONSTANT TEMPERATURE
OPTION THERMAL METALLURGY  SPATIAL
RESTART GEOMETRY
MATERIAL PROPERTIES
 ELEMENTS GROUPS $V1$ / MATE 1
MEDIUM
 WELDLINE / GROUPS $TR02$ REFERENCE $REF$ ELEMENTS $SE02$ START $SN02$ --
ARRIVAL $EN02$ VELOCITY 10.000000 TINF 6.000000
CONSTRAINTS
 ELEMENTS GROUPS $D1$ $D2$ $D3$ $D4$ $D5$ $D6$ / KT 1 VARIABLE 1
LOAD
1
 ELEMENTS GROUPS $D1$ $D2$ $D3$ $D4$ $D5$ $D6$ / TT 20.
 ELEMENTS GROUPS $D5$ / QR 1 VARIABLE -10000 TRAJECTORY 1
TABLE
 1 / FORTRAN
      function f(t)
c  radiative losses : f = sig * e * (t + to)(t**2 + to**2)
      e = 0.8
      sig = 5.67*-8
      to = 20.
      to = 20. + 273.15
      t1  = t + 273.15
      a = t1 * t1
      b = to * to
      c = a + b
      d = t1 + to
      d = d * c
      d = d * e
      d = d * sig
c  convective losses = 25 W/m2
      f = d + 25.
c  change to W/mm2
      d = 1*-6
      f = f * d
      return
      END
 10000 /  FORTRAN
      FUNCTION F(X)
C   F   = Q0 * exp( - R^2 / R0^2 ) with
C   R^2 = ( XX-X0 )^2 + ( YY-Y0-VY*T )^2
      DIMENSION X(4)
C Input
      XX = X(1)   ; X Coordinate
      YY = X(2)   ; Y Coordinate
      ZZ = X(3)   ; Z Coordinate (not used)
      TT = X(4)   ; Time
```

```
C Variables
      Q0 = @par1@    ; Maximal source intensity
      R0 = 5    ; Gaussian parameter
      X0 = 0    ; X initial location of source center
      Y0 = 0    ; Y initial location of source center
      Z0 = 0   ; Z initial location of source center
      VY = 0   ; Source displacement velocity
      AY = 0    ; Angle of torch [deg.]
C Constant
      M1 = -1
      PIDEG = ATAN(1.)
      PIDEG = PIDEG / 45.
      AY = AY * PIDEG
C Transformation of global to local coordinates
      XD   = XX - X0
      YD   = VY * TT
      YD   = YD + Y0
      ZD   = ZZ - Z0
C Source rotation about Y axis
      SA   = SIN( AY )
      SA   = - SA
      CA   = COS( AY )
      A1   = XD * CA
      A2   = ZD * SA
      XL   = A1 + A2
      YL   = YY - YD
      A1   = ZD * CA
      A2   = XD * SA
      ZL   = A1 - A2
C R^2 computation
      A1   = XL * XL
      A2   = YL * YL
      R2   = A1 + A2
C R0^2 computation
      R02  = R0 * R0
C F computation
      A    = R2 / R02
      A    = M1 * A
      A    = EXP( A )
      F    = Q0 * A
      RETURN
      END
RETURN
MEDIUM
EXTRACT MEDIUM
MEDIUM
; SECOND TRACK 6 TO 10
assi 19 TRAN1000.TIT
TRANSIENT NON-LINEAR
BEHAVIOUR METALLURGY 6 FILE METALLURGY.DAT
METHOD SYMMETRICAL TEST 0  OPTIMISE
ALGORITHM BFGS IMPLICIT 1 ITERATION 30
PRECISION ABSOLUTE FORCE 1*-8 DISPLACEMENT 1*-1
initial conditions restart card @par2@
time initial @par3@
 @par4@  step @par5@ / store @par6@
return
-----------------------------------------------------
```

**HARDNESS_ALL.DAT**: Hardness calculations file of the whole process.

```
SEARCH DATA 1000
ASSIGN 19 TRAN1000.TIT
Hardness calculation 1. track AND COOLING
HARDNESS EXTRACT -1
COMPOSITION C 0.45 SI 0.4 MN 0.65 NI 0.4 CR 0.4 MO 0.1
PHASE 6
FORMULE MARTENSITE 3
FORMULE BAINITE 2
FORMULE FERRITE 1 5 4
units seconds
VALUE INITIAL MARTENSITE 400 BAINITE 300
ELEMENTS GROUPS $V1$ GAUSS
CARD 0 TO 45 STORE
RETURN
; Hardness calculation 2. track AND COOLING
HARDNESS EXTRACT -1
COMPOSITION C 0.45 SI 0.4 MN 0.65 NI 0.4 CR 0.4 MO 0.1
PHASE 6
FORMULE MARTENSITE 3
FORMULE BAINITE 2
FORMULE FERRITE 1 5 4
units seconds
VALUE INITIAL CARD 45
ELEMENTS GROUPS $V1$ GAUSS
CARD 45 TO 202 STORE
RETURN
save data tran 3000 ascii sele
ELEM GROUP $V1$
card 45 124 202
retu
SEARCH DATA tran 3000 ascii
save data tran 3000
delete data tran 3000 ascii
```